AFRL-VS-HA-TR-2005-1206

# Calibration of the $M_S$:$m_b$ Discriminant at the International Monitoring System Array NVAR (PS-47)

Jessie L. Bonner
Ileana M. Tibuleac
David G. Harkrider
Robert H. Shumway
Eugene Herrin
Sara A. Russell
David Russell
Delaine T. Reiter
Robert Herrmann

Weston Geophysical
57 Bedford Street, Suite 102
Lexington, MA 02420

Final Report

September 2005



AIR FORCE RESEARCH LABORATORY
Space Vehicles Directorate
29 Randolph Road
AIR FORCE MATERIEL COMMAND
Hanscom AFB, MA 01731-3010

This technical report has been reviewed and is approved for publication.

AFRL-VS-HA-TR-2005-1206

/signed/

ROBERT J. RAISTRICK
Contract Manager

/signed/

ROBERT BELAND, Chief
Battlespace Surveillance Innovation Center

This report has been reviewed by the ESC Public Affairs Office (PA) and is releasable to the National Technical Information Service (NTIS).

Qualified requestors may obtain additional copies form the Defense Technical Information Center (DTIC). All others should apply to the National Technical Information Service.

If your address has changed, if you with to be removed from the mailing list, or if the addressee is no longer employed by your organization, please notify AFRL/VSIM, 29 Randolph Rd., Hanscom AFB, MA 01731-3010. This will assist us in maintaining a current mailing list.

Do not return copies of this report unless contractual obligations or notices on a specific document require that it be returned.

Using Government drawings, specifications, or other data included in this document for any purpose other than Government procurement does not in any way obligate the U.S. Government. The fact that the Government formulated or supplied the drawings, specifications, or other data does not license the holder or any other person or corporation; or convey any rights or permission to manufacture, use, or sell any patented invention that may relate to them.

This report is published in the interest of scientific and technical information exchange and its publication does not constitute the Government's approval or disapproval of its ideas or findings.

| REPORT DOCUMENTATION PAGE | | | Form Approved OMB No. 0704-0188 |
|---|---|---|---|



| 1. AGENCY USE ONLY (*Leave blank*) | 2. REPORT DATE | 3. REPORT TYPE AND DATES COVERED |
|---|---|---|
| | 25 September 2005 | Final Report ( 27 Sept. 2001 – 25 Sept. 2005) |

4. TITLE AND SUBTITLE

Calibration of the $M_S$:$m_b$ Discriminant at the International Monitoring System Array NVAR (PS-47)

5. FUNDING NUMBERS
Contract No.: DTRA01-01-C-0080
Program Element No.: 810000
Project No.: DTRA
Task No.: OT Work Unit No.: AI

6. AUTHOR(S)
Jessie L. Bonner, Ileana M. Tibuleac, David G. Harkrider, Robert H. Shumway, Eugene Herrin, Sara A. Russell, David Russell, Delaine T. Reiter, and Robert Herrmann

7. PERFORMING ORGANIZATION NAME(S) AND ADDRESS(ES)

Weston Geophysical
57 Bedford Street, Suite 102
Lexington, MA 02420

8. PERFORMING ORGANIZATION REPORT NUMBER

WG-1112-2005-01

9. SPONSORING/MONITORING AGENCY NAME(S) AND ADDRESS(ES)
Air Force Research Laboratory
AFRL/VSBYE
29 Randolph Road
Hanscom AFB, MA 01731

Contract Manager: Robert Raistrick

10. SPONSORING/MONITORING AGENCY REPORT NUMBER

AFRL-VS-HA-TR-2005-1206

11. SUPPLEMENTARY NOTES

12a. DISTRIBUTION/AVAILABILITY STATEMENT
Approved for public release; distribution unlimited.

12b. DISTRIBUTION CODE

## 13. ABSTRACT (*Maximum 200 words*)

Surface wave magnitude ($M_s$) estimation for small events recorded at near-regional distances will often require a magnitude scale designed for Rayleigh waves with periods between 5 and 25 seconds. We have completed several studies aimed at examining the usefulness of existing and new formulas at estimating surface wave magnitudes at periods not restricted to approximately 20 seconds.

In Chapter 1, we show that 7-second surface waves can be used to estimate magnitudes for Nevada Test Site explosions and earthquakes using a modified version of the Marshall and Basham (1971) formula. Body wave magnitudes for recent earthquakes were estimated by calibrating the new NVAR array to the Denny *et al.* (1987) $m_b$ as shown in Chapter 2. New methods of measuring local and near-regional amplitudes for body wave magnitude estimation are also discussed in Chapter 3.

Additionally, the Russell surface-wave magnitude formula (2005) and the $M_s$(VMAX) measurement technique provide a new method for estimating surface-wave magnitudes as described in Chapter 4. There are several benefits to the new method. First, the technique allows for time domain measurements of surface wave amplitudes, giving an analyst the ability to visually confirm that the pick is correct and is an actual surface wave. Also, it allows for surface wave magnitudes to be measured at local and regional distances where traditional 20-second magnitudes cannot be used. And these magnitudes are not biased with respect to teleseismic estimates using the same $M_s$(VMAX) measurement technique. Additionally, the application of narrow-band Butterworth filtering techniques appropriately handles Airy phase phenomena that prior to this study, had to be accounted for using Marshall and Basham's (1972) empirical corrections. Finally, because the method is variable period and not restricted to near 20-seconds period, the analyst is allowed to measure $M_s$ where the signal is largest. The new method has been successfully tested on three research datasets, and the results suggest that the method can be used to screen out a large percentage of small earthquakes at $m_b < 5$. Thus, we are currently implementing the technique for operational testing and examining the usefulness of the same technique on Love waves (Chapter 5).

| 14. SUBJECT TERMS | 15. NUMBER OF PAGES |
|---|---|
| surface wave magnitude, seismic moment, discrimination, body wave magnitude scales | 103 |
| | 16. PRICE CODE |

| 17. SECURITY CLASSIFICATION OF REPORT | 18. SECURITY CLASSIFICATION OF THIS PAGE | 19. SECURITY CLASSIFICATION OF ABSTRACT | 20. LIMITATION OF ABSTRACT |
|---|---|---|---|
| Unclassified | Unclassified | Unclassified | UL |

## Table of Contents

# CHAPTER 1: ESTIMATING $M_S$ FROM SHORT-PERIOD (< 10 SEC) RAYLEIGH WAVES FOR EARTHQUAKES AND EXPLOSIONS AT THE NEVADA TEST SITE

*Jessie L. Bonner,[1] David G. Harkrider,[1] Eugene Herrin,[2] Robert H. Shumway,[3] Sara A. Russell,[1] Ileana Tibuleac,[1] and Delaine T. Reiter,[1]*

Weston Geophysical Corporation,[1] Southern Methodist University,[2]
University of California, Davis[3]

## ABSTRACT

Surface wave magnitude ($M_S$) estimation for small events recorded at near-regional distances will often require a magnitude scale designed for Rayleigh waves with periods less than 10 seconds. We have examined the performance of applying two previously published $M_S$ scales on 7-second Rayleigh waves recorded at distances less than 500 km. First, we modified the Marshall and Basham (1972) $M_S$ scale, originally defined for periods greater than 10 seconds, to estimate surface wave magnitudes for short-period Rayleigh waves from earthquakes and explosions on or near the Nevada Test Site (NTS). We refer to this modification as $\overset{M+B}{M_s}(7)$, and we have used short-period, high-quality dispersion curves to determine empirical path corrections for the 7-second Rayleigh waves. We have also examined the performance of the Rezapour and Pearce (1998) formula, developed using theoretical distance corrections and surface wave observations with periods greater than 10 seconds, for 7-second Rayleigh waves ($\overset{R+P}{M_s}(7)$) as recorded from the same dataset. The results demonstrate that both formulas can be used to estimate $M_S$ for nuclear explosions and earthquakes over a wider magnitude distribution than is possible using conventional techniques developed for 20 second Rayleigh waves. These $M_S(7)$ values scale consistently with other $M_S$ studies at regional and teleseismic distances with the variance described by a constant offset; however, the offset for the $\overset{M+B}{M_s}(7)$ estimates is over one magnitude unit nearer the teleseismic values than the $\overset{R+P}{M_s}(7)$ estimates. Using our technique, it is possible to employ a near-regional single-station or sparse network to estimate surface wave magnitudes, thus allowing quantification of the size of both small earthquakes and explosions. Finally, we used a jackknife technique to determine the false alarm rates for the $\overset{M+B}{M_s}(7)$-$m_b$ discriminant for this region, and found that the probability of misclassifying an earthquake as an explosion is 10% while the probability of classifying an explosion as an earthquake was determined to be 1.2%. The misclassification probabilities are slightly higher for the $\overset{R+P}{M_s}(7)$ estimates. Our future research will be aimed at examining the transportability of these methods.

## INTRODUCTION

One of the most robust methods for discriminating between explosions and earthquakes is the relative difference between the body wave ($m_b$) and surface wave ($M_s$) magnitude for a seismic event. For a given $m_b$, earthquakes often generate substantially more surface wave energy than explosions and thus are characterized by a larger surface wave magnitude. $M_s$ scales include those defined for Rayleigh waves with periods near 20 seconds recorded at teleseismic distances (Gutenberg, 1945; von Seggern, 1977; Yacoub, 1983) as well as scales developed for variable periods at both regional and teleseismic distances (e.g. the Prague formula of Vanek *et al.*, 1962; Evernden, 1971; Basham, 1971; Marshall and Basham, 1972; Rezapour and Pearce, 1998). The predominance of $M_s$ measurements determined for explosion sources using these formulae are for events with $m_b$ greater than 4.5; thus, there is uncertainty in the $M_s$-$m_b$ discriminant performance for explosions with smaller $m_b$, corresponding to yields of less than approximately 20 kilotons.

None of these aforementioned studies have attempted to determine if magnitudes obtained from surface waves recorded at near-regional distances and periods less than 10 seconds can be used to accurately characterize the size of a seismic source. The answer to this question is essential in determining our ability to discriminate lower yield events in the $3.5 < m_b < 4.5$ range. Levshin and Ritzwoller (2001) suggest this problem is difficult to answer because structural variations that alter short-period surface wave amplitudes by as much as 50% have scales that cannot be resolved with current 3-D models, thus rendering path corrections difficult to determine. Also, short-period surface waves are more sensitive to high-frequency asymmetries in the shot cavity (Zhao and Harkrider, 1991) and spall (Taylor and Randall, 1989; Day and McLaughlin, 1991). The fact remains, however, that at regional distances, surface wave trains are not well dispersed and are often characterized by a pulse-like shape with dominant periods ranging from 5 to 12 seconds. Thus, it is difficult, and for small events often impossible, to determine an $M_s$ as it was originally defined for 20-second Rayleigh waves. Either a path-corrected, spectral magnitude (e.g. Stevens and McLaughlin, 2001; Stevens and Murhpy, 2001) or an $M_s$ scale that can incorporate these shorter periods is required to examine the performance of the $M_s$-$m_b$ discriminant for small events recorded at regional distances.

The purpose of this paper is to present the results of applying two established and popular $M_s$ formulas, both developed using surface waves with periods between 10 and 20 seconds, on seven (7) second, near-regional, Rayleigh-wave data. First, we modified the Marshall and Basham (1972) $M_s$ scale, originally defined for periods greater than 10 seconds, to estimate surface wave magnitudes for 7 second Rayleigh waves. We refer to this modification as $\overset{M+B}{M}_s(7)$. We based our decision to use 7 second Rayleigh waves on observations that this period (1) represents an average of the dominant energy for surface waves recorded at near-regional distances near the Nevada Test Site (NTS) and (2) is far enough from Airy phase phenomena so that path corrections can be estimated. We have applied our $\overset{M+B}{M}_s(7)$ to 158 NTS explosions and 40 earthquakes recorded at near-regional distances (< 1000 km). We have also applied the Rezapour and Pearce (1998) formula to this dataset and refer to this estimate as $\overset{R+P}{M}_s(7)$. Finally, we used estimates from both of these scales to examine the $M_s(7)$-$m_b$ discriminants for the western United States (WUS).

## DATA

The data are vertical-component, digital broadband seismograms from NTS explosions and WUS earthquakes recorded on the four stations of the Lawrence Livermore Regional Seismic network (henceforth referred to as LNN). The LNN network consists of seismic stations at Landers, California (LAC), Mina, Nevada (MNV), Elko, Nevada (ELK) and Kanab, Utah (KNB), and has been in operation since the 1960's (Figure 1.1). The data recorded at these stations originally consisted of analog seismograms, which were subsequently digitized by Lawrence Livermore National Laboratory (LLNL). The analog instruments were replaced in July 1979 by digital systems that have been in almost continuous operation since, resulting in an extensive record of the testing conducted at the Nevada Test Site (NTS). In December 1998, an International Monitoring System (IMS) station, NV31 (Figure 1.1), was collocated with MNV, and we have included data from this station for this research. Although, there are additional stations in the region for which data are available, we chose not to use them since one of our research goals was to examine how well a regional surface wave magnitude scale can perform using sparse data. This is an important aspect of the research since small yield events will be recorded on relatively few regional stations.

We have estimated surface wave magnitudes for NTS explosions that occurred between December 1968 and September 1992. The primary research focus was on the 198 NTS explosions (Yang *et al.*, 2000) that were detonated after August 1979, for which digital data are available from the LNN stations. Sixty-one (61) of these events have no LNN data available, are plagued by untimely data dropouts and glitches, or are too small for measurable surface wave energy. We also analyzed 21 events prior to July 1979 that were digitized from analog records in order to compare these results with previous $M_s$ studies for NTS events completed by Yacoub (1983), Marshall *et al.*, (1979), and Stevens and Murphy (2001). Thus, this paper presents the results of our analyses of 158 NTS explosions: including 51 events from Pahute Mesa, 13 from Rainier Mesa, and 94 explosions from the Yucca Flats. We have also tabulated the location of the events relative to the water table and the lithology in which the event was detonated.

We also estimated the $M_s$ and $m_b$ magnitudes for 40 earthquakes whose locations are shown in Figure 1.1. The earthquake data consisted of LNN seismograms for events tabulated in Patton (2001; Table A.1) that were within 2 degrees of the NTS. This allowed us to maintain similar azimuthal coverage and propagation paths for the NTS explosions in our dataset. The Patton (2001) earthquake database has no events beyond 1994, thus we also downloaded data recorded at station NV31 for events between January 1999 and June 2002. This earthquake dataset, while not as extensive as our explosion database, has $m_b(Pn)$ (Patton, 2001) values ranging from 2.98 to 5.84 and depths ranging from 0 to 17 km.

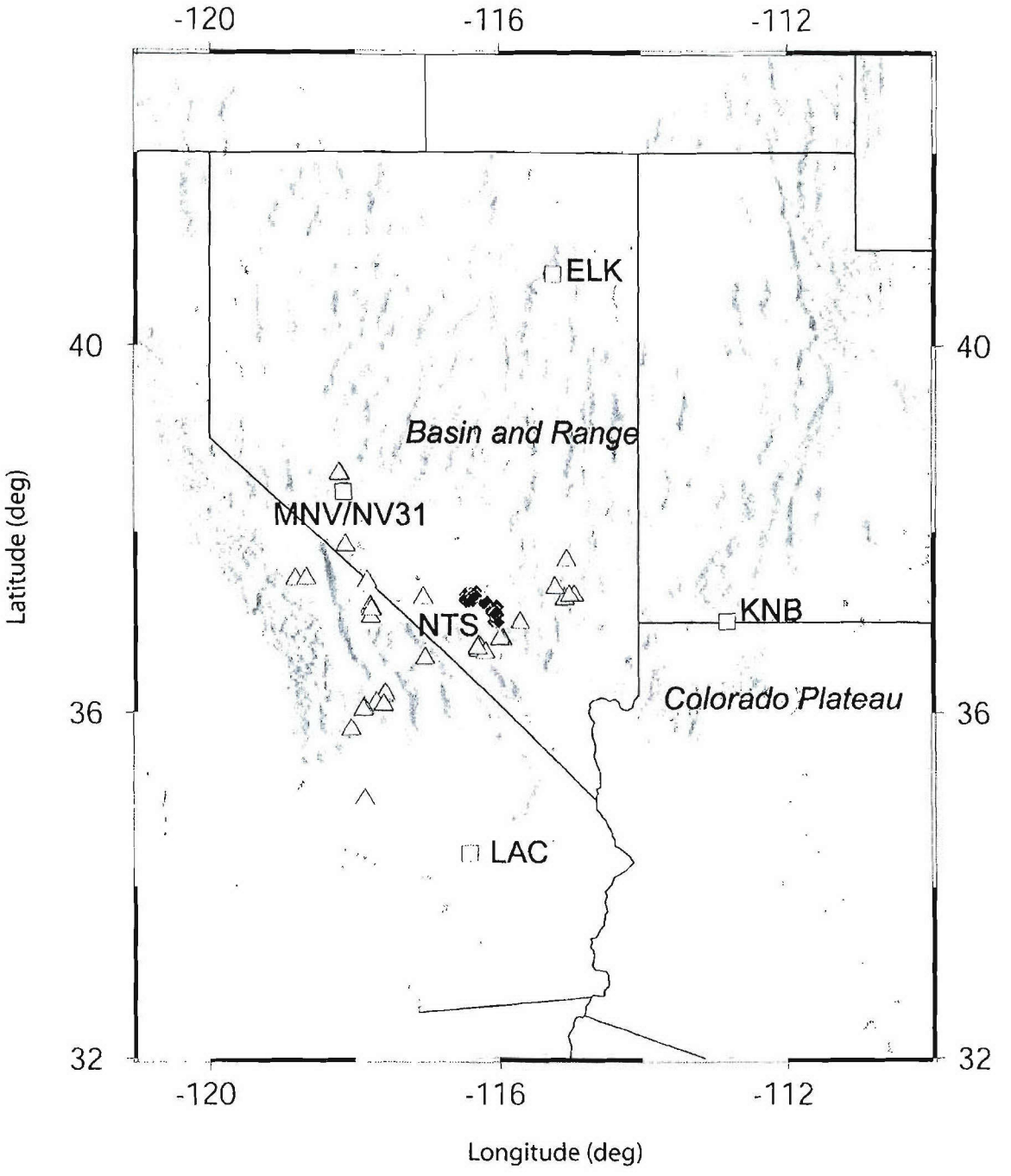


**Figure 1.1. The locations of the four LNN stations (white squares), as well as earthquakes (white triangles) and explosions (black diamonds on the NTS) used in this study.**

## METHODOLOGY

Examples of near-regional, fundamental-mode surface waves recorded at MNV from five different source regions of the WUS are shown in Figure 1.2. These surface waves have been

extracted from the MNV vertical broadband components through phase-matched filtering (Herrin and Goforth, 1977). All five of these events are in the $3.7 < m_b < 4.1$ range, and none of the events have Rayleigh-wave periods greater than 12 seconds. The largest amplitude for the events occurs at periods between 6 seconds (Mammoth Lake earthquake) and 9 seconds (Little Skull Mountain earthquake). Denny *et al.* (1987) showed some success at obtaining regional $M_s$ for similar earthquakes and explosions in this region and expressed the need for accurate path corrections to maximize the $M_s$-$m_b$ discriminant performance. This paper differs from their methodology in three ways: (1) we obtain the path corrections directly from observed dispersion curves instead of from regional velocity models; (2) we use a processing technique developed to positively identify small amplitude, fundamental-mode Rayleigh wave motion; and (3) we calculate the $M_s$ for Rayleigh waves of 7-seconds period as opposed to variable periods. We are not aware of other $M_s$ scales that have been developed and tested for 7-second Rayleigh waves at near-regional distances and calibrated using conventional $M_s$ estimates.

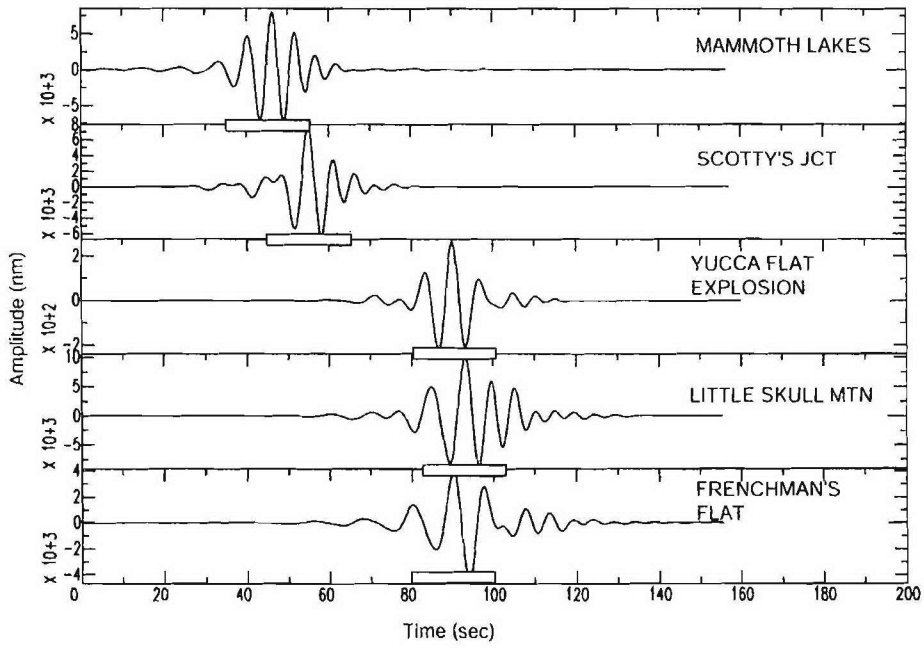


**Figure 1.2. Examples of near-regional, fundamental mode Rayleigh waves extracted from events near Mammoth Lakes, California, Scotty's Junction, Nevada, Yucca Flats on the Nevada Test Site (NTS), Little Skull Mountain (NTS), and Frenchman's Flat (NTS). The events are earthquakes with the exception of the Yucca Flats explosion. None of these events ($3.7 < m_b < 4.1$) exhibit surface wave periods greater than 12 seconds; the maximum amplitudes occur at periods between 5 and 9 seconds. The bar plotted below each seismogram corresponds to a length of 20 seconds.**

## $m_b$ Estimation

For our examination of the $M_s$-$m_b$ discriminant performance for small events in the WUS, we required both regional $m_b$ and $M_s$ magnitude scales. Fortunately, an $m_b$ scale has already been developed and tested for the WUS. The Denny *et al.* (1987; 1989) body wave magnitude formula (referred to henceforth as the DTV $m_b$) was specifically developed for the WUS using an extensive database of earthquakes and nuclear explosions at or near the Nevada Test Site. They defined their $m_b$ scale for *Pn* arrivals as:

$$m_b(Pn) = \log_{10}(A) + 2.4*\log_{10}(d) - 3.95 + C \qquad (1.1)$$

where A is peak-to-peak amplitude in nm, d is the distance in km, and C is a station constant empirically determined to be -0.02 for MNV, -0.13 for ELK, -0.19 for KNB, and +0.33 for LAC (Denny *et al.*, 1989). Subsequently, Tibuleac (Chapter 4 of this Annual Scientific Report) showed the constant at NV31 was approximately equal to the MNV constant. The amplitude measurements were made on simulated short-period Worldwide Standard Seismographic Network (WWSSN) response seismograms. This magnitude scale was correlated to the yield of the NTS explosions, and therefore does not have a network bias problem for small magnitude events. All $m_b$s presented in this study are $m_b(Pn)$s estimated using Equation 1.1. For most of the NTS explosions, we used the $m_b(Pn)$ determined by Vergino and Mensing (1989), and we used the $m_b(Pn)$ determined by Patton (2001) for most of the WUS earthquakes. For events in which no $m_b(Pn)$ was published, we used Equation 1.1 to calculate an average network $m_b(Pn)$ using the available LNN stations.

## Surface Wave Processing

Near-regional surface waves in the WUS have their largest amplitudes occurring at periods between 5 and 9 seconds (Figure 1.2), and these amplitudes can often be 6 to 10 dB larger than the amplitudes measured at 20 seconds period. We have shown (Tibuleac *et al.*, 2002) that for NTS events recorded at MNV, the energy in 20- second Rayleigh waves subsides below background noise levels at approximately $m_b = 4.3 \pm 0.2$. Therefore, $M_s$ scales that consider surface waves between 5 and 9 seconds will be applicable to lower $m_b$ values. It is important to note that caution must be used to ensure that the measured signals are, in fact, Rayleigh waves and not microseisms, higher-mode energy, or Love wave contamination.

We employ a surface wave processing routine that is designed to help positively identify small amplitude, fundamental-mode, Rayleigh-wave motion. The method is applied to all explosions with $m_b < 4.0$ (and for earthquakes with $m_b < 3.5$), since the signal-to-noise ratio (SNR) for larger events is great enough that amplitude measurements can be made by bandpass filtering the velocity records and measuring the amplitudes in a group velocity window indicative of 7-second Rayleigh waves in the WUS. For explosions with $m_b < 4.0$, we first use the multiple filter analysis technique (Dziewonski *et al.*, 1969) to generate a group velocity dispersion curve for each event-to-station path. We then overlay the theoretical fundamental- and first-higher mode dispersion curves predicted for the path from the Stevens *et. al.* (2001) global shear-wave model. We require at least 70% overlap (similar to Stevens and McLaughlin, 2001) in the observed dispersion, plus error in the 5 to 10 second period band with the predicted fundamental mode dispersion from the Stevens *et al.* (2001) model. If the event passes the

dispersion test, we then determine if the signal has retrograde elliptical particle motion and a back azimuth that is within ± 30 degrees of the true back azimuth. We have followed the methods of Chael (1997) and Selby (2001) to determine the back azimuth that corresponds to the largest positive value, indicative of retrograde elliptical motion, in a covariance matrix formed by the Hilbert-transformed vertical component and the two horizontal components. If a given event passes the dispersion, back azimuth, and particle motion tests, we have positively identified fundamental-mode Rayleigh waves for the event of interest. It is critical that the event pass all three tests since microseisms may occur in the correct group velocity window and possess retrograde elliptical motion with the correct back azimuth. However, our experience with these rare situations has shown that we will not observe the 70% overlap between the observed and predicted dispersion curve in the entire 5 to 10 second band.

Once identified as fundamental-mode Rayleigh waves, we employ a phase match filter (PMF) technique (Herrin and Goforth, 1977) to extract the Rayleigh waves from the complex wavetrain. We use the observed group velocity dispersion curve for the event and an iterative approach (Herrmann, 2002) to find and apply a filter that has approximately the same phase as the Rayleigh-wave signal of interest. This technique improves the signal-to-noise ratio for the extracted surface waves. We then perform a bandpass filter around a center period of 7 seconds on the PMF-extracted signal. From this filtered data, the maximum zero-to-peak amplitude is measured, and this amplitude is then used to estimate $M_s(7)$.

**Surface Wave Magnitude Estimation**

$M_s(7)$ from Marshall and Basham (1972). Marshall and Basham (1972) reformulated the Prague formula (Vanek *et al.*, 1962) as:

$$M_s = \log_{10}(A) + B'(\Delta) + P(T) \qquad (1.2)$$

where A is the Rayleigh wave amplitude (zero-to-peak in nm), $B'(\Delta)$ is an attenuation correction as a function of distance ($\Delta$) in degrees, and P(T) is a path correction as a function of period T. There is an additional term of $0.008h$ (Bath, 1952), where $h$ is the depth of the event, that can be included in Equation 1.2. Because depth is often difficult to determine for near-regional events, we did not apply a depth correction to the explosion and earthquake data in order to examine the discriminant performance assuming a surface focus. The distance corrections $B'(\Delta)$ (Table 1.1) used for this study are proportional to $0.8 \log_{10}(\Delta)$, as Basham (1971) showed this relation to be valid for earthquakes and explosions with an 8-14 second period at regional distances.

The path corrections listed in Table 2 of Marshall and Basham (1972) are not applicable to periods less than 10 seconds; however, Figure 1.2 of this paper shows that path corrections are needed for periods as low as 5 seconds. The path correction P(T) is estimated from the amplitude of a group velocity (U) dispersion curve predicted by the method of stationary phase (Ewing *et al.*, 1957) with the expression $\frac{U}{T^{3/2}\sqrt{\frac{dU}{dT}}}$. The P(T) corrections are normalized to a 20 second period in order to compare the short-period results with conventional $M_s$ measurements.

**Table 1.1. B'(Δ) Corrections for Near-Regional Distances.**

| Distance (degrees) | B'(Δ) |
|---|---|
| 0.5 | 0.10 |
| 1.0 | 0.20 |
| 1.5 | 0.29 |
| 2.0 | 0.37 |
| 2.5 | 0.44 |
| 3.0 | 0.52 |
| 3.5 | 0.58 |
| 4.0 | 0.64 |
| 4.5 | 0.70 |
| 5.0 | 0.75 |

To generate the P(T) corrections, we used multiple filter analyses to generate group velocity dispersion curves for paths from NTS to MNV, ELK, KNB, and LAC. We averaged the dispersion curves for 8 NTS explosions with large Rayleigh-wave SNR ($m_b > 5.2$) between 5 and 20 seconds, and the results are shown in Figure 1.3. We based our decision to make our surface wave measurements at a period of 7 seconds on two observations. First, as shown in Figure 1.2, a period of 7 seconds represents an average of the dominant periods for surface waves recorded at near-regional distances in the WUS. Additionally, Figure 1.3 shows there is an inverse Airy phase (or a group velocity maximum) observable on the dispersion curves near approximately 9 seconds period, and it is best to retreat from the complications associated with this phenomenon when making amplitude measurements. As determined from expression $\frac{U}{T^{3/2}\sqrt{\frac{dU}{dT}}}$, the P(T) corrections will become infinite at each Airy phase. We determined the P(7) corrections for each path, and the results are listed in Table 1.2. The P(7) corrections for paths to MNV, ELK, and LAC are essentially the same since these paths are all located within the southern Basin and Range tectonic province (Figure 1). The different dispersion curve for the path from NTS to KNB is caused by the thickening of the crust near the station associated with the transition from the Basin and Range to the Colorado Plateau (Keller *et al.*, 1976). We refer to our surface wave estimates for 7-second Rayleigh waves using Equation 1.2 and empirically calibrated path corrections as $\overset{M+B}{M_s}(7)$.

<u>$M_S$(7) from Rezapour and Pearce (1998).</u> Using the entire dataset from the International Seismic Center, Rezapour and Pearce (1998) developed a distance independent $M_s$ defined as:

$$M_s = \log\frac{A}{T} + \frac{1}{3}\log_{10}(\Delta) + \frac{1}{2}\log_{10}(\sin(\Delta)) + 0.0046\Delta + 2.370 \qquad (1.3)$$

where A is the zero to peak amplitude in nm, T is the period in seconds, and Δ is the distance in degrees. Unlike the Marshall and Basham (1972) formula that used empirical distance and path

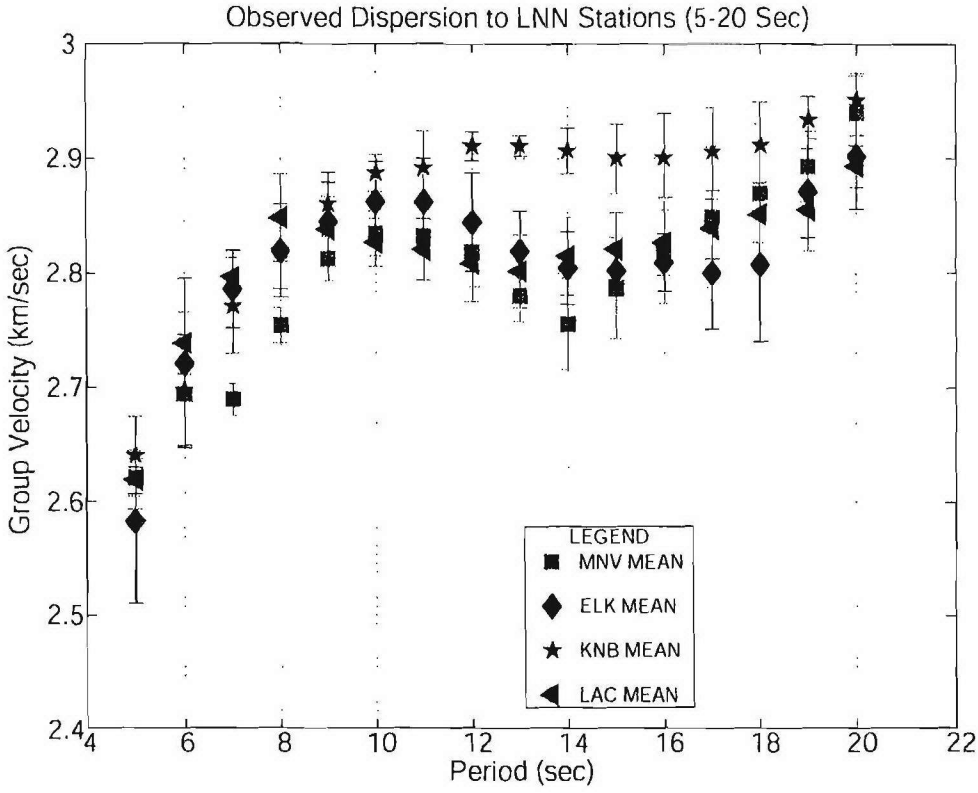


**Figure 1.3. Average Rayleigh-wave group velocity dispersion curves obtained from the multiple filter analyses and phase match filtering of 8 NTS explosions with paths to MNV, ELK, KNB, and LAC. The dispersion curves were used to determine path corrections (P(T)). The vertical lines through the dispersion data points represent one standard deviation.**

**Table 1.2. P(T) corrections.**

| Station | P(T) |
|---|---|
| MNV/NV31 | -0.79 |
| ELK | -0.79 |
| KNB | -0.56 |
| LAC | -0.73 |

corrections (Equation 1.2), the Rezapour and Pearce (1998) equation was developed using theoretical aspects of dispersion and geometrical spreading. The formula was adopted by the prototype International Data Center in 1998 for calculating surface wave magnitudes at distances between 20 and 100 degrees; however, it is now used by the International Data Centre to determine an $M_S$ for all surface waves recorded at distances less than 100 degrees (Stevens and McLaughlin, 2001). We note that the original Rezapour and Pearce (1998) paper presents no

application of their formula at periods less than 10 seconds and at distances less than 20 degrees. For this study, we applied Equation 3 to short-period, near-regional data to determine $\overset{R+P}{M_s}(7)$ estimates for the same dataset as used for the modified Marshall and Basham (1972) formula.

## RESULTS

### NTS Explosions

We measured the amplitude for 7-second period Rayleigh waves for 158 NTS events recorded at MNV, ELK, KNB, and LAC and estimated both $\overset{M+B}{M_s}(7)$ and $\overset{R+P}{M_s}(7)$ for each event. The results are compiled in Table 1.3 and are shown in Figures 4-7. Figure 1.4 examines the variability in both $M_s(7)$ estimates by comparing the MNV values to the $M_s(7)$ estimated at ELK (top), KNB (middle), and LAC (bottom). When we consider the effects that tectonic release can have on explosion magnitudes as well as the fact that small-scale structural variations have a magnified effect on shorter-period surface waves, we believe that the scatter in the data is tolerable. In all six cases, the correlation coefficient is at least 0.98. For all comparisons, we note that the slopes for the best least squares fit to the data are slightly smaller than unity (0.90 to 0.95) resulting in positive y-intercepts. The MNV $M_s(7)$ estimates are on average 0.15 m.u. less than the LAC values. It is very hard to pinpoint the source of this bias. However, two possible explanations include inadequate path corrections, P(T), or differences between the attenuation model used in Equations 1.2 (Basham, 1971 for 8-14 second surface waves) and 3 (Rezapour and Pearce, 1998) and the actual attenuation of 7-second surface waves in the WUS. We note that for events with an $\overset{M+B}{M_s}(7) < 3.5$, the MNV estimates are on average smaller than the KNB estimates, while at greater magnitudes the KNB estimates are smaller. The reason for this difference is thought to be a spectral hole that occurs on the KNB data between 6 and 7 seconds period that is more prevalent for the larger magnitude events. Even with the presence of the spectral hole near 7 seconds, we note that the maximum difference between the KNB and MNV estimates above $\overset{M+B}{M_s}(7) = 3.5$ is -0.4 m.u. with the average difference being less than –0.1 m.u. The results of these comparisons show that single-station (e.g. MNV) $\overset{M+B}{M_s}(7)$ and $\overset{R+P}{M_s}(7)$ estimates for NTS explosions are reliable (one standard deviation $< \pm 0.2$ m.u.) in the WUS when only sparse data are available.

We present a comparison of the network-averaged $\overset{M+B}{M_s}(7)$ and $\overset{R+P}{M_s}(7)$ for all measured NTS events versus the DTV network $m_b(Pn)$ in Figure 1.5. Pahute Mesa, Rainier Mesa, and Yucca Flats events were analyzed and are presented as circles, stars, and triangles, respectively. We also denote the location of the water table, relative to each event, as either a solid symbol (events that were detonated above the water table) or an open symbol (events detonated below the water table). We regressed the $\overset{M+B}{M_s}(7)$ and $\overset{R+P}{M_s}(7)$ versus the DTV $m_b(Pn)$, and the resulting equations and standard deviations for each NTS test area are shown.

## Table 1.3. Results

| Date | Name | $m_b$ | $M_s$ M+B | std | $M_s$ R+P | std | # | A | W | L |
|---|---|---|---|---|---|---|---|---|---|---|
| 1968354 | Benham | 6.49 | 5.66 | 0.12 | 6.87 | 0.17 | 3 | P | B | T |
| 1969302 | Calabash | 5.5 | 4.44 | 0.09 | 5.72 | 0.04 | 2 | Y | B | T |
| 1970085 | Handley | 6.57 | 5.61 | 0.10 | 6.85 | 0.14 | 4 | P | B | T |
| 1970146 | Flask | 5.47 | 4.17 | 0.15 | 5.41 | 0.11 | 4 | Y | A | T |
| 1970351 | Carpetbag | 5.79 | 4.68 | 0.11 | 5.92 | 0.14 | 4 | Y | B | T |
| 1972265 | Osocurro | 5.6 | 4.47 | 0.06 | 5.68 | 0.16 | 3 | Y | B | T |
| 1972270 | Delphinium | 4.54 | 2.64 | 0.14 | 3.85 | 0.14 | 3 | Y | A | A |
| 1973116 | Starwort | 5.49 | 4.03 | 0.10 | 5.26 | 0.05 | 4 | Y | B | T |
| 1973157 | Alemendro | 6.23 | 5.07 | 0.20 | 6.35 | 0.23 | 3 | P | B | R |
| 1974191 | Escabosa | 5.54 | 4.49 | 0.01 | 5.69 | 0.15 | 2 | Y | B | T |
| 1975059 | Topgallant | 5.7 | 4.48 | 0.13 | 5.72 | 0.04 | 4 | Y | B | T |
| 1975154 | Stilton | 6.03 | 4.62 | 0.10 | 5.85 | 0.18 | 4 | P | B | R |
| 1975154 | Mizzen | 5.66 | 4.45 | 0.10 | 5.69 | 0.08 | 4 | Y | B | T |
| 1975170 | Mast | 6.24 | 5.03 | 0.15 | 6.26 | 0.19 | 4 | P | B | R |
| 1975324 | Inlet | 6.01 | 4.90 | 0.16 | 6.14 | 0.22 | 4 | P | B | R |
| 1975354 | Chiberta | 5.76 | 4.60 | 0.15 | 5.83 | 0.09 | 4 | Y | B | T |
| 1976035 | Keelson | 5.61 | 4.31 | 0.18 | 5.55 | 0.16 | 4 | Y | B | T |
| 1976035 | Esrom | 5.69 | 4.53 | 0.10 | 5.76 | 0.07 | 3 | Y | B | T |
| 1976045 | Cheshire | 6.13 | 5.03 | 0.12 | 6.26 | 0.17 | 4 | P | B | R |
| 1976069 | Estuary | 6.09 | 5.13 | 0.19 | 6.36 | 0.25 | 4 | P | B | R |
| 1976077 | Strait | 5.87 | 4.87 | 0.13 | 6.08 | 0.08 | 3 | Y | B | T |
| 1979215 | Burzet | 4.78 | 2.89 | 0.06 | 4.10 | 0.17 | 3 | Y | A | A |
| 1979220 | Offshore | 4.85 | 3.18 | 0.10 | 4.39 | 0.20 | 3 | Y | A | T |
| 1979241 | Nessel | 4.93 | 3.14 | 0.17 | 4.37 | 0.23 | 4 | Y | A | A |
| 1979249 | Hearts | 5.83 | 4.43 | 0.07 | 5.67 | 0.15 | 4 | Y | B | T |
| 1979269 | Sheepshead | 5.73 | 4.25 | 0.10 | 5.48 | 0.18 | 4 | P | A | T |
| 1980059 | Tarko | 4.43 | 2.69 | 0.17 | 3.91 | 0.11 | 3 | Y | A | A |
| 1980094 | Liptauer | 4.9 | 2.95 | 0.22 | 4.19 | 0.28 | 4 | Y | A | A |
| 1980107 | Pyramid | 5.45 | 4.05 | 0.24 | 5.29 | 0.30 | 4 | Y | B | T |
| 1980117 | Colwick | 5.66 | 4.30 | 0.14 | 5.53 | 0.22 | 4 | P | B | R |
| 1980123 | Canfield | 4.38 | 2.58 | 0.10 | 3.81 | 0.05 | 3 | Y | A | T |
| 1980164 | Kash | 5.61 | 4.41 | 0.11 | 5.62 | 0.20 | 3 | P | B | R |
| 1980176 | Huron King | 4.2 | 2.28 | 0.12 | 3.50 | 0.19 | 3 | Y | A | A |
| 1980207 | Tafi | 5.8 | 4.38 | 0.09 | 5.62 | 0.18 | 4 | P | B | T |
| 1980213 | Verdello | 4.12 | 2.50 | 0.10 | 3.77 | 0.13 | 2 | Y | A | A |
| 1980269 | Bonarda | 4.5 | 2.44 | 0.09 | 3.68 | 0.09 | 4 | Y | A | T |
| 1980298 | Dutchess | 4.43 | 2.82 | 0.13 | 4.06 | 0.11 | 4 | Y | A | T |
| 1980305 | Miners Iron | 4.65 | 3.02 | 0.16 | 4.25 | 0.21 | 4 | R | A | T |

| | | | | | | | | | | |
|---|---|---|---|---|---|---|---|---|---|---|
| 1980319 | Dauphin | 4.39 | 2.72 | 0.05 | 3.96 | 0.14 | 4 | Y | A | T |
| 1980352 | Serpa | 5.26 | 3.77 | 0.11 | 5.01 | 0.17 | 4 | P | A | T |
| 1981015 | Baseball | 5.56 | 4.15 | 0.11 | 5.39 | 0.18 | 4 | Y | B | T |
| 1981149 | Aligote | 4.19 | 2.52 | 0.20 | 3.75 | 0.10 | 3 | Y | A | T |
| 1981157 | Harzer | 5.62 | 4.15 | 0.14 | 5.39 | 0.19 | 4 | P | A | T |
| 1981191 | Niza | 4.18 | 2.43 | 0.12 | 3.66 | 0.04 | 4 | Y | A | T |
| 1981239 | Islay | 3.96 | 2.08 | 0.08 | 3.39 | 0.06 | 2 | Y | A | T |
| 1981247 | Trebbiano | 3.98 | 1.87 | 0.16 | 3.10 | 0.18 | 4 | Y | A | T |
| 1981274 | Paliza | 5.12 | 3.69 | 0.37 | 4.93 | 0.40 | 4 | Y | A | T |
| 1981315 | Tilci | 4.9 | 3.16 | 0.06 | 4.40 | 0.16 | 4 | Y | A | A |
| 1981316 | Rousanne | 5.38 | 3.92 | 0.12 | 5.16 | 0.17 | 4 | Y | B | T |
| 1981337 | Akavi | 4.7 | 2.97 | 0.18 | 4.21 | 0.14 | 4 | Y | A | T |
| 1981350 | Caboc | 4.53 | 2.55 | 0.09 | 3.79 | 0.10 | 4 | Y | A | T |
| 1982028 | Jornada | 5.76 | 4.43 | 0.09 | 5.67 | 0.16 | 4 | Y | B | T |
| 1982043 | Molbo | 5.48 | 4.09 | 0.14 | 5.33 | 0.19 | 4 | P | B | R |
| 1982043 | Hosta | 5.76 | 4.18 | 0.13 | 5.42 | 0.17 | 4 | P | A | R |
| 1982107 | Tenaja | 4.49 | 2.72 | 0.10 | 3.95 | 0.16 | 4 | Y | A | T |
| 1982115 | Gibne | 5.47 | 4.11 | 0.11 | 5.35 | 0.18 | 4 | P | A | T |
| 1982126 | Kryddost | 4.19 | 2.15 | 0.12 | 3.46 | 0.14 | 2 | Y | A | T |
| 1982127 | Bouschet | 5.66 | 4.04 | 0.12 | 5.28 | 0.19 | 4 | Y | B | T |
| 1982167 | Kesti | 4.01 | 2.19 | 0.23 | 3.43 | 0.25 | 3 | Y | A | T |
| 1982175 | Nebbiolo | 5.73 | 4.26 | 0.17 | 5.50 | 0.25 | 4 | P | A | R |
| 1982210 | Monterey | 4.68 | 2.56 | 0.15 | 3.80 | 0.17 | 4 | Y | A | T |
| 1982217 | Atrisco | 5.82 | 4.49 | 0.15 | 5.73 | 0.21 | 4 | Y | B | T |
| 1982266 | Frisco | 4.76 | 3.08 | 0.03 | 4.32 | 0.15 | 3 | Y | A | T |
| 1982266 | Huron Landing | 4.88 | 3.12 | 0.08 | 4.35 | 0.12 | 3 | R | A | T |
| 1982316 | Seyval | 4.18 | 2.35 | 0.22 | 3.56 | 0.05 | 2 | Y | A | A |
| 1982344 | Manteca | 4.72 | 2.82 | 0.14 | 4.06 | 0.22 | 4 | Y | A | A |
| 1983085 | Cabra | 5.36 | 3.90 | 0.18 | 5.13 | 0.26 | 3 | P | A | R |
| 1983104 | Turquoise | 5.64 | 4.04 | 0.09 | 5.28 | 0.15 | 4 | Y | B | T |
| 1983112 | Armada | 4.15 | 2.37 | 0.05 | 3.59 | 0.06 | 3 | Y | A | T |
| 1983125 | Crowdie | 4.37 | 2.35 | 0.08 | 3.64 | 0.05 | 3 | Y | A | A |
| 1983146 | Fahada | 4.52 | 3.02 | 0.16 | 4.26 | 0.22 | 4 | Y | A | T |
| 1983160 | Danablu | 4.73 | 2.63 | 0.11 | 3.90 | 0.07 | 2 | Y | A | A |
| 1983215 | Laban | 4.48 | 2.17 | 0.07 | 3.48 | 0.08 | 2 | Y | A | A |
| 1983223 | Sabado | 4.17 | 2.34 | 0.12 | 3.63 | 0.08 | 3 | Y | A | T |
| 1983239 | Jarlsberg | 3.87 | 2.07 | 0.25 | 3.35 | 0.21 | 2 | Y | _ | _ |
| 1983244 | Chancellor | 5.52 | 4.02 | 0.17 | 5.31 | 0.16 | 3 | P | A | R |
| 1983264 | MidniteZ | 4.04 | 2.53 | 0.18 | 3.77 | 0.17 | 4 | R | A | T |
| 1983265 | Techado | 4.2 | 2.25 | 0.11 | 3.49 | 0.14 | 4 | Y | B | T |
| 1983350 | Romano | 4.97 | 3.57 | 0.12 | 4.79 | 0.18 | 3 | Y | A | T |
| 1984031 | Gorbea | 4.51 | 2.62 | 0.08 | 3.85 | 0.09 | 4 | Y | A | T |
| 1984061 | Tortugas | 5.82 | 4.35 | 0.11 | 5.56 | 0.19 | 3 | Y | B | T |
| 1984091 | Agrini | 4.35 | 2.79 | 0.01 | 3.96 | 0.11 | 2 | Y | A | A |

| | | | | | | | | | | |
|---|---|---|---|---|---|---|---|---|---|---|
| 1984122 | Mundo | 5.47 | 4.12 | 0.02 | 5.32 | 0.14 | 2 | Y | B | T |
| 1984152 | Caprock | 5.61 | 4.37 | 0.19 | 5.58 | 0.22 | 3 | Y | B | T |
| 1984207 | Kappeli | 5.62 | 4.20 | 0.13 | 5.41 | 0.24 | 3 | P | A | R |
| 1984215 | Correo | 4.57 | 2.73 | 0.12 | 3.97 | 0.19 | 4 | Y | A | T |
| 1984243 | Dolcetto | 4.49 | 2.98 | 0.11 | 4.19 | 0.12 | 3 | Y | A | T |
| 1984257 | Breton | 4.98 | 3.44 | 0.05 | 4.68 | 0.13 | 4 | Y | A | T |
| 1984276 | Vermejo | 4.28 | 2.39 | 0.11 | 3.59 | 0.04 | 2 | Y | _ | _ |
| 1984315 | Villita | 3.9 | 2.56 | 0.21 | 3.80 | 0.11 | 4 | Y | A | A |
| 1984344 | Egmont | 5.51 | 4.10 | 0.09 | 5.34 | 0.18 | 4 | P | A | T |
| 1984350 | Tierra | 5.64 | 4.09 | 0.17 | 5.33 | 0.24 | 4 | P | A | R |
| 1985074 | Vaughn | 4.42 | 2.88 | 0.08 | 4.17 | 0.11 | 3 | Y | A | T |
| 1985082 | Cottage | 5.19 | 3.91 | 0.00 | 5.23 | 0.00 | 1 | Y | A | T |
| 1985096 | Misty Rain | 4.7 | 3.18 | 0.12 | 4.42 | 0.21 | 4 | R | A | T |
| 1985122 | Towanda | 5.63 | 4.27 | 0.15 | 5.51 | 0.23 | 4 | P | B | T |
| 1985163 | Salut | 5.62 | 4.17 | 0.14 | 5.41 | 0.16 | 4 | P | A | R |
| 1985177 | Maribo | 4.32 | 2.45 | 0.10 | 3.69 | 0.12 | 4 | Y | A | T |
| 1985206 | Serena | 5.48 | 4.24 | 0.16 | 5.52 | 0.13 | 3 | P | A | R |
| 1985270 | Ponil | 4.49 | 3.04 | 0.15 | 4.27 | 0.13 | 4 | Y | A | T |
| 1985282 | Diamond Beech | 4.01 | 2.12 | 0.08 | 3.36 | 0.12 | 4 | R | A | T |
| 1985289 | Roquefort | 4.62 | 2.90 | 0.15 | 4.14 | 0.06 | 4 | Y | A | T |
| 1985339 | Kinibito | 5.6 | 4.10 | 0.13 | 5.32 | 0.19 | 3 | Y | B | T |
| 1985362 | Goldstone | 5.45 | 4.11 | 0.14 | 5.35 | 0.07 | 4 | P | A | R |
| 1986081 | Glencoe | 5.41 | 3.61 | 0.06 | 4.83 | 0.14 | 3 | Y | B | T |
| 1986100 | Mighty Oak | 4.93 | 3.26 | 0.06 | 4.46 | 0.22 | 2 | R | A | T |
| 1986112 | Jefferson | 5.48 | 4.21 | 0.04 | 5.43 | 0.12 | 3 | P | A | R |
| 1986141 | Panamint | 3.78 | 2.14 | 0.05 | 3.36 | 0.08 | 3 | Y | A | A |
| 1986156 | Tajo | 5.29 | 3.93 | 0.00 | 5.25 | 0.00 | 1 | Y | A | T |
| 1986176 | Darwin | 5.58 | 4.18 | 0.11 | 5.39 | 0.21 | 3 | P | A | T |
| 1986198 | Cybar | 5.57 | 4.24 | 0.06 | 5.47 | 0.15 | 3 | P | A | R |
| 1986205 | Cornucopia | 4.3 | 2.56 | 0.14 | 3.78 | 0.11 | 3 | Y | A | A |
| 1986247 | Galveston | 3.71 | 2.24 | 0.09 | 3.51 | 0.05 | 2 | P | A | R |
| 1986273 | Labquark | 5.54 | 4.20 | 0.13 | 5.50 | 0.13 | 2 | P | A | R |
| 1986289 | Belmont | 5.56 | 4.25 | 0.07 | 5.48 | 0.15 | 3 | P | A | T |
| 1986318 | Gascon | 5.58 | 4.21 | 0.00 | 5.53 | 0.00 | 1 | Y | B | T |
| 1986347 | Bodie | 5.52 | 4.30 | 0.00 | 5.61 | 0.00 | 1 | P | A | T |
| 1987042 | Tornero | 4.24 | 2.19 | 0.13 | 3.42 | 0.08 | 3 | Y | A | T |
| 1987077 | Middle Note | 4.22 | 2.51 | 0.20 | 3.72 | 0.04 | 2 | R | A | T |
| 1987108 | Delamar | 5.51 | 4.12 | 0.08 | 5.35 | 0.14 | 3 | P | A | T |
| 1987120 | Hardin | 5.54 | 4.22 | 0.06 | 5.44 | 0.17 | 3 | P | A | T |
| 1987169 | Brie | 4.15 | 1.96 | 0.11 | 3.20 | 0.20 | 3 | Y | A | T |
| 1987225 | Tahoka | 5.72 | 4.35 | 0.00 | 5.67 | 0.00 | 1 | Y | B | T |
| 1987267 | Lockney | 5.61 | 4.31 | 0.12 | 5.62 | 0.13 | 2 | P | A | A |
| 1987336 | Mission Cyber | 3.99 | 2.21 | 0.06 | 3.43 | 0.16 | 4 | R | A | T |
| 1988046 | Kernville | 5.48 | 4.10 | 0.20 | 5.31 | 0.26 | 3 | P | A | T |

| | | | | | | | | | | |
|---|---|---|---|---|---|---|---|---|---|---|
| 1988134 | Schellbourne | 4.77 | 3.12 | 0.07 | 4.33 | 0.12 | 3 | P | A | A |
| 1988142 | Laredo | 4.27 | 2.48 | 0.18 | 3.72 | 0.24 | 4 | Y | _ | _ |
| 1988154 | Comstock | 5.58 | 4.03 | 0.06 | 5.23 | 0.10 | 2 | P | B | T |
| 1988189 | Alamo | 5.78 | 4.21 | 0.19 | 5.44 | 0.32 | 3 | P | B | R |
| 1988230 | Kearsarge | 5.64 | 4.25 | 0.24 | 5.49 | 0.30 | 4 | P | A | T |
| 1988243 | Bullfrog | 5.04 | 3.38 | 0.04 | 4.62 | 0.09 | 4 | Y | A | T |
| 1988287 | Dalhart | 5.67 | 4.43 | 0.13 | 5.67 | 0.17 | 4 | Y | B | T |
| 1988345 | Misty Echo | 4.79 | 3.37 | 0.25 | 4.66 | 0.23 | 3 | R | A | T |
| 1989041 | Texarkana | 5.32 | 3.77 | 0.02 | 5.00 | 0.13 | 3 | Y | _ | _ |
| 1989055 | Kawich-Red | 4.41 | 2.65 | 0.17 | 3.89 | 0.04 | 3 | Y | A | T |
| 1989068 | Ingot | 4.86 | 3.14 | 0.25 | 4.37 | 0.38 | 3 | Y | A | T |
| 1989135 | Palisade-1 | 4.55 | 2.49 | 0.08 | 3.72 | 0.08 | 3 | Y | A | T |
| 1989146 | Tulia | 3.7 | 2.08 | 0.11 | 3.32 | 0.02 | 3 | Y | A | T |
| 1989173 | Contact | 5.43 | 3.94 | 0.07 | 5.17 | 0.19 | 3 | P | A | T |
| 1989178 | Amarillo | 5.03 | 3.30 | 0.24 | 4.53 | 0.24 | 3 | P | B | R |
| 1989257 | Disko Elm | 4.04 | 2.28 | 0.20 | 3.52 | 0.18 | 4 | R | A | T |
| 1989304 | Hornitos | 5.83 | 4.19 | 0.13 | 5.42 | 0.20 | 4 | P | _ | _ |
| 1989342 | Barnwell | 5.56 | 4.05 | 0.13 | 5.29 | 0.17 | 4 | P | A | T |
| 1990069 | Metropolis | 5.16 | 3.47 | 0.12 | 4.71 | 0.18 | 4 | Y | A | T |
| 1990164 | Bullion | 5.96 | 4.57 | 0.15 | 5.80 | 0.21 | 4 | P | _ | _ |
| 1990172 | Austin | 4.21 | 2.59 | 0.14 | 3.83 | 0.12 | 4 | Y | A | T |
| 1990206 | Mineral Quarry | 4.53 | 2.91 | 0.20 | 4.15 | 0.21 | 4 | R | A | T |
| 1990318 | Houston | 5.46 | 3.91 | 0.15 | 5.15 | 0.22 | 4 | P | A | T |
| 1991067 | Coso-Bronze | 4.51 | 2.50 | 0.28 | 3.71 | 0.20 | 3 | Y | A | T |
| 1991094 | Bexar | 5.65 | 4.22 | 0.12 | 5.44 | 0.22 | 3 | P | _ | _ |
| 1991257 | Hoya | 5.69 | 4.31 | 0.13 | 5.52 | 0.24 | 3 | P | _ | _ |
| 1991262 | Distant Zenith | 4.09 | 2.49 | 0.17 | 3.70 | 0.13 | 3 | R | A | T |
| 1991291 | Lubbock | 5.16 | 3.33 | 0.05 | 4.55 | 0.13 | 3 | Y | A | T |
| 1991330 | Bristol | 4.79 | 3.13 | 0.13 | 4.34 | 0.17 | 3 | Y | A | T |
| 1992086 | Junction | 5.81 | 4.17 | 0.13 | 5.38 | 0.19 | 3 | P | _ | _ |
| 1992175 | Galena-Yellow | 4.13 | 2.30 | 0.19 | 3.52 | 0.16 | 3 | Y | _ | _ |
| 1992262 | Hunters-Trophy | 4.16 | 2.55 | 0.11 | 3.76 | 0.03 | 3 | R | A | T |

Table Explanation:

*Date* is the year and Julian day for the explosion, *Name* is the explosion code name, and $m_b$ is the DTV $m_b(Pn)$ for the event. For each Marshall and Basham (1972) (*M+B*) and Rezapour and Pearce (1998) (*R+P*) estimated $M_s(7)$, there is a standard deviation (*std*) for # stations. *A*, *W*, and *L* are test area (P=Pahute; R=Rainer; Y=Yucca), water table location relative to the explosion (A=above and B=below), and lithology (A=alluvium, T=Tuff and R=Rhyolite), respectively.

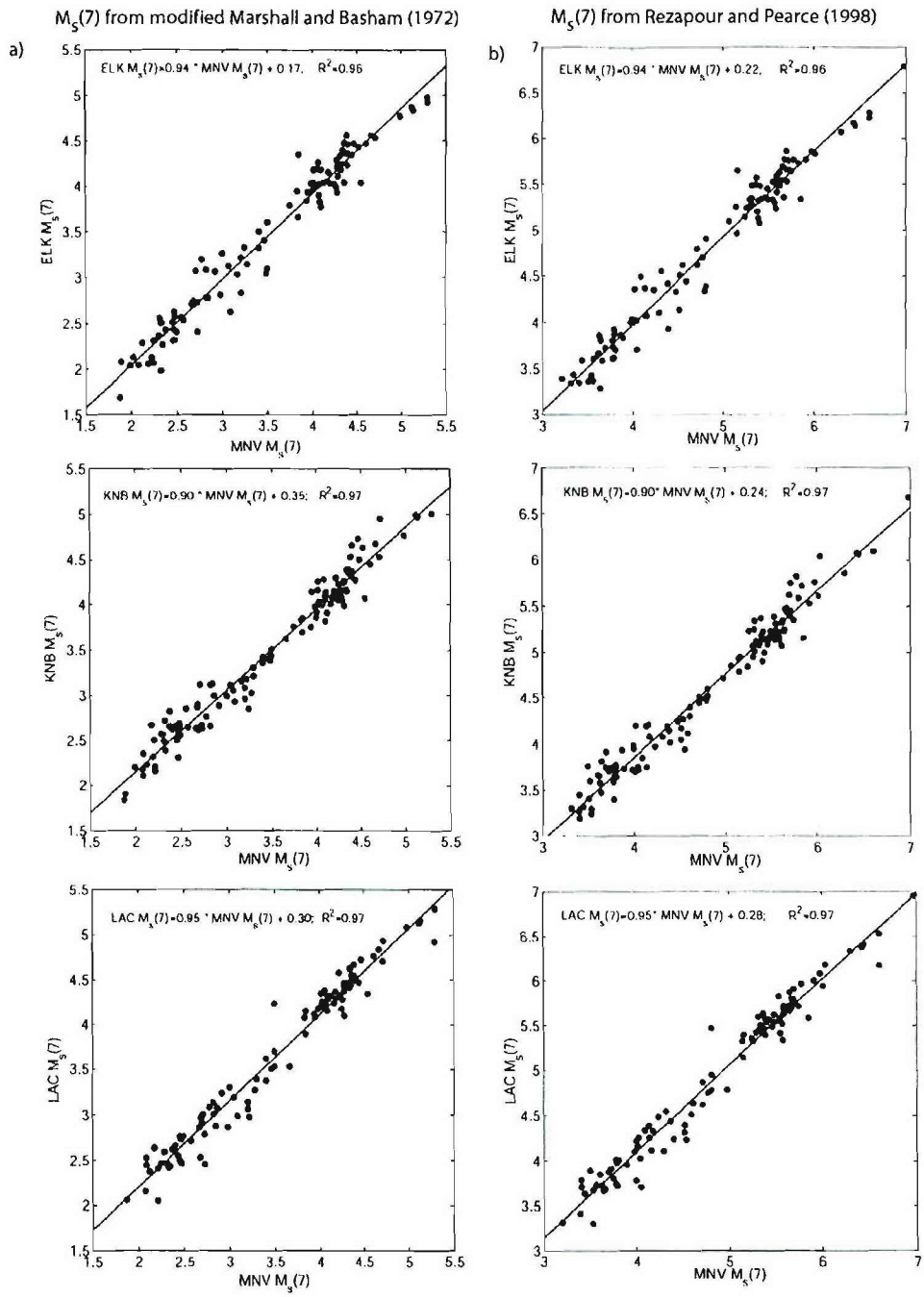


**Figure 1.4. Comparison of a) $M_S^{M+B}(7)$ and b) $M_S^{R+P}(7)$ estimates at MNV versus the measurements at ELK (top), KNB (middle), and LAC (bottom). The best least square fit to the data is shown as the solid line running through the data points, and the squared correlation coefficients ($R^2$) are also given.**

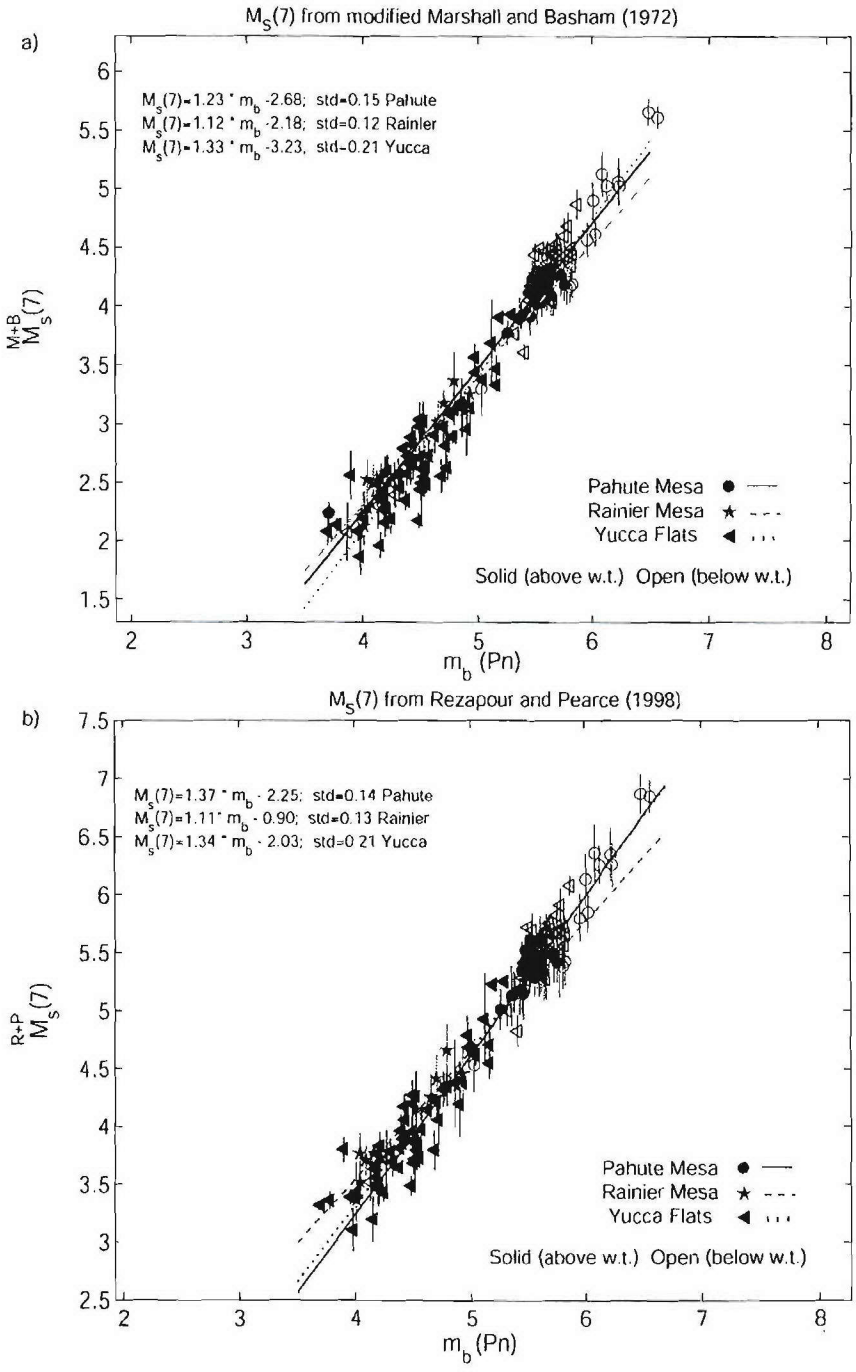


**Figure 1.5. Network-averaged a) $M_s^{M+B}(7)$ and b) $M_s^{R+P}(7)$ for 158 NTS events at Pahute Mesa, Rainier Mesa, and Yucca Flats regressed against $m_b(Pn)$. The best-fitting regression lines are plotted as solid (Pahute), dashed (Rainier), and dotted (Yucca) lines. Solid symbols indicate events above the water table (w.t.) with open symbols showing events below the water table. The vertical lines represent one standard deviation for the $M_s$ estimate.**

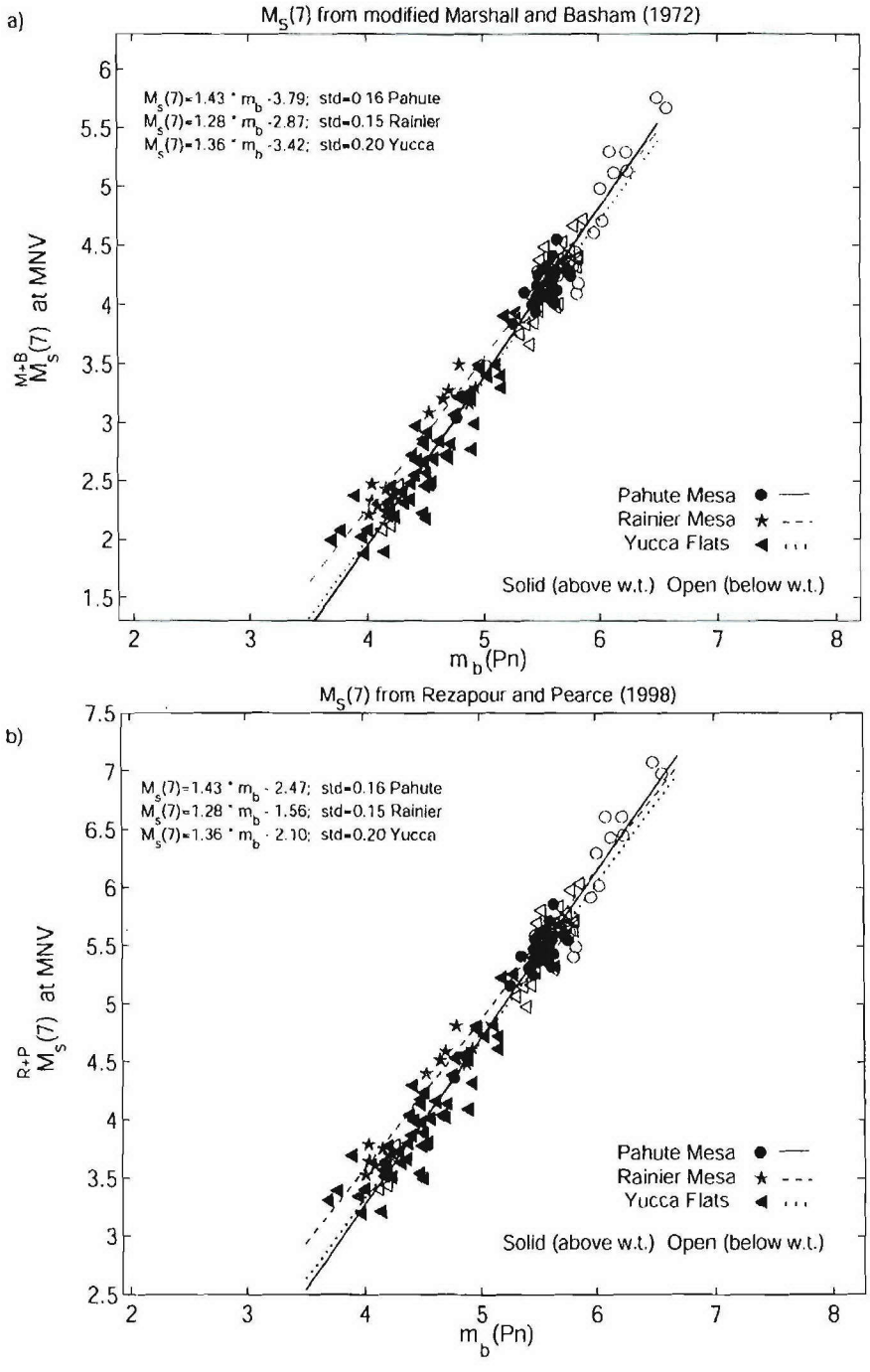


**Figure 1.6. MNV single-station a) $M_s^{M+B}(7)$ and b) $M_s^{R+P}(7)$ for NTS events at Pahute Mesa, Rainier Mesa, and Yucca Flats regressed against $m_b(Pn)$.**

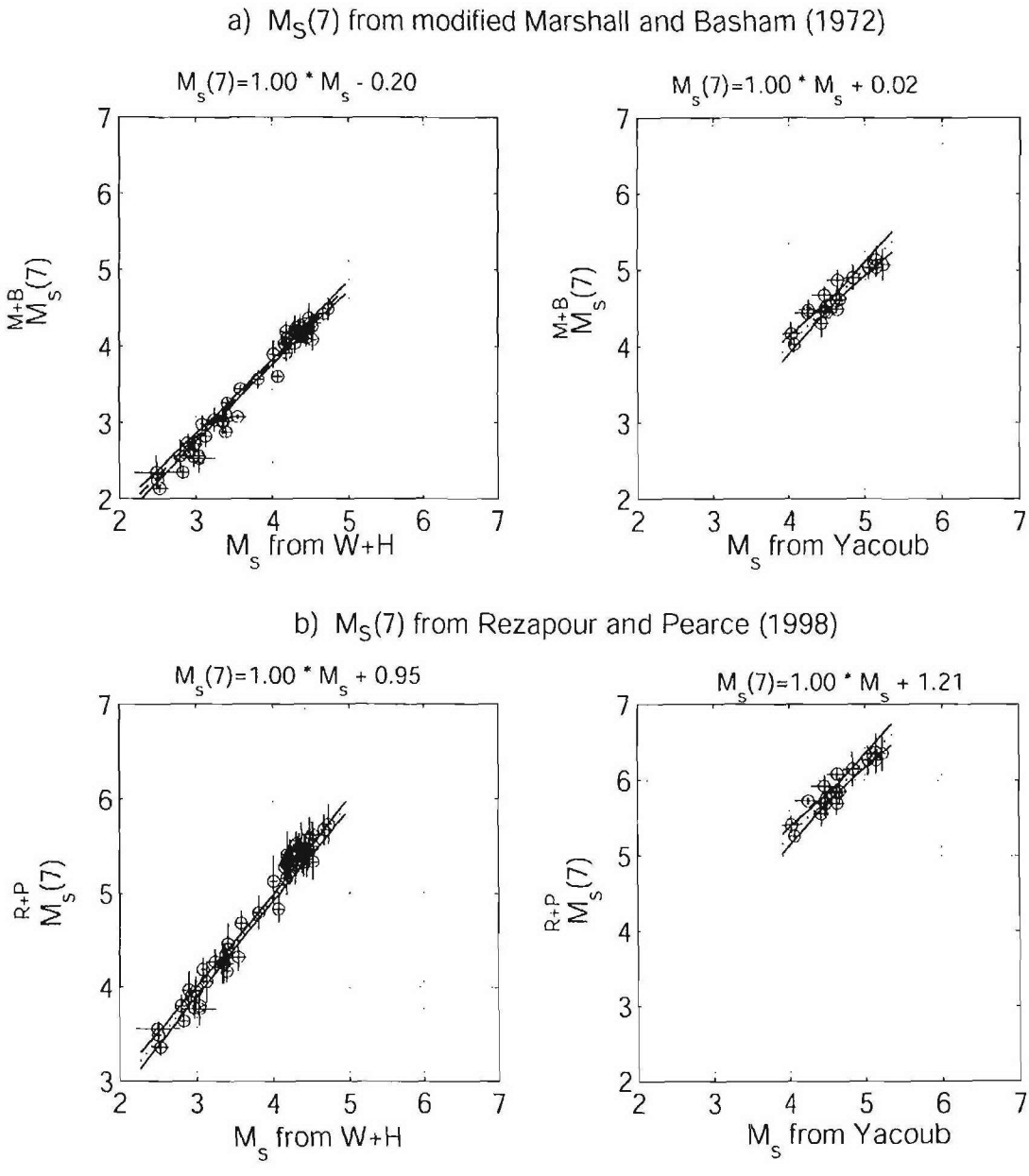


**Figure 1.7. A comparison of our a) $M_s^{M+B}(7)$ and b) $M_s^{R+P}(7)$ estimates for NTS with the Woods and Harkrider (1995) indirect estimates (W+H; left) and Yacoub (1983; right). The best-fitting regression line, with a fixed slope = 1.0, is given by the dotted line running through the data points, and it is surrounded by the pointwise 95% confidence intervals plotted as two solid lines.**

The purpose of this paper is not to examine scaling laws or coupling factors for the areas of the Nevada Test Site, and the reader is referred to Woods and Harkrider (1995) and Patton (1991) for further details concerning these topics. However, our results generally agree with Woods and Harkrider (1995), who suggested that there are different scaling relationships between Pahute Mesa and Yucca Flats events. The primary goals of our paper are to present the applicability of the $M_S(7)$ scale, and to highlight the fact that using the short-period data allows us to estimate surface wave magnitudes for 45 explosions with $m_b < 4.5$, as compared to one in the original Marshall and Basham (1972) paper, two in the Rezapour and Pearce (1998) paper, and less than ten in Stevens and McLaughlin (2001). In addition, we have determined $M_S(7)$ measurements for 9 events with $3.7 < m_b < 4.0$.

For the purpose of regional application of an $M_S(7)$ magnitude scale, it is unlikely that a network similar to LNN will be available for monitoring most nuclear test sites. Thus, we examined the relationship between single-station MNV $\overset{M+B}{M_s}(7)$ and $\overset{R+P}{M_s}(7)$ estimates and DTV $m_b(Pn)$ and present the results in Figure 1.6. For this analysis, we note that the regression results for the Yucca Flats events do not change significantly for the single-station $\overset{M+B}{M_s}(7)$ and $\overset{R+P}{M_s}(7)$, while there are differences for the results for Pahute Mesa and Rainier Mesa. In general, the "clouds" formed by the single-station $\overset{M+B}{M_s}(7)$ and $\overset{R+P}{M_s}(7)$ measurements do not change significantly from the results using network averages.

## Comparison of the Near-Regional $M_S(7)$ and Teleseismic $M_S$

Of course, estimating near-regional $M_S(7)$ values for NTS events that can be calibrated to conventional $M_S$ scales is of primary importance to our research as well. We compared our $\overset{M+B}{M_s}(7)$ and $\overset{R+P}{M_s}(7)$ estimates taken directly from the near-regional surface waves with the $M_S$ measurements obtained from a modeling technique derived by Woods and Harkrider (1995). Their indirect method of estimating $M_S$ consisted of modeling the surface waves recorded at regional distances, and then propagating the regional synthetics to distances of 40 degrees. At 40 degrees, the synthetics showed significant 20 second surface wave energy and the authors used a modified von Seggern (1977) formula to measure $M_S$ from the synthetics. Figure 1.7 shows the comparison of our $\overset{M+B}{M_s}(7)$ and $\overset{R+P}{M_s}(7)$ with $\pm$ 1$\sigma$ plotted as the horizontal lines and the Woods and Harkrider (1995) indirect method (W+H) with $\pm$ 1$\sigma$ plotted as vertical lines. We performed a fixed-slope (slope=1) linear regression to compare the $M_S(7)$ values with the Woods and Harkrider (1995) values and found a strong correlation. The offset shows that the $\overset{M+B}{M_s}(7)$ and $\overset{R+P}{M_s}(7)$ estimates are 0.20 m.u. lower and 0.95 m.u. higher, respectively, than the Woods and Harkrider (1995) estimates. Woods and Harkrider (1995) showed their measurements also correlated very well with conventional NTS $M_S$ values from Basham (1969), Marshall and Basham (1972), Basham and Horner (1973), von Seggern (1973), Marshall *et al.* (1979), and Yacoub (1983) with considerable variance in the offsets. We also compared the performance of $\overset{M+B}{M_s}(7)$ and $\overset{R+P}{M_s}(7)$ with Yacoub (1983). The results for the comparison with Yacoub (1983) are

shown also in Figure 1.7 and indicate similar scaling relationships based on the fixed-slope regression analysis. In this case, our $\overset{M+B}{M_s}(7)$ and $\overset{R+P}{M_s}(7)$ values are offset from Yacoub's (1983) estimates by approximately +0.02 m.u. and +1.21 m.u., respectively. Differences in these absolute estimates result from the use of different $M_S$ definitions, especially in the attenuation factors; however, these comparisons do show that our estimates are scaling similarly to other measurements of NTS surface wave magnitudes.

The properties of Rayleigh wave propagation make it difficult to develop a single expression that gives consistent $M_S$ values at both regional and teleseismic distances. Figure 1.8 presents the comparison of near-regional $M_S$ estimates (i.e. $\overset{M+B}{M_s}(7)$ and $\overset{R+P}{M_s}(7)$) with far-regional and teleseismic estimates of $M_S$ using the same formulas (i.e. Marshall and Basham (1972) and Rezapour and Pearce (1998) formulas, respectively). Marshall *et al.* (1979) used the Marshall and Basham (1972) $M_S$ formula for far-regional and teleseismic distance recordings of NTS events for Rayleigh waves with periods greater than 14 seconds. We determined that the near-regional $\overset{M+B}{M_s}(7)$ estimates have a similar scaling relationship when using a fixed slope (slope = 1.00) regression analysis, but are consistently 0.35 m.u. higher than Marshall *et al.* (1979) for the 5 events in their dataset for which we had LNN data to analyze. We note that most of our near-regional estimates have better azimuthal coverage than Marshall *et al.* (1979) who mainly used Canadian data and thus may have strong azimuthal biases. This could be a possible source for the bias. Another source could be the attenuation terms; however, we do not have data at a wide enough distance range in this study to verify the appropriateness of Basham (1971) as the correct attenuation model. We observed that the $\overset{R+P}{M_s}(7)$ estimates are on average 1.6 m.u. larger than the Marshall *et al.* (1979) teleseismic $M_S$ values.

The Rezapour and Pearce (1998) formula has not been tested significantly at near-regional distances and short-periods until this paper, and our results suggest there are considerable differences between the short-period, near-regional magnitudes and teleseismic magnitude estimates for NTS events. We regressed our $\overset{R+P}{M_s}(7)$ estimates versus far regional and teleseismic $M_S$ estimates (Figure 1.8) determined by Stevens and Murphy (2001) using the Rezapour and Pearce (1998) formula. We note consistent scaling between the two estimates, however, there is an offset of +1.46 m.u. We note much better agreement between the Stevens and Murphy (2001) teleseismic $M_S$ values and the 7-second modified Marshall and Basham (1972) estimates. Thus, we believe path corrections will be required for correct application of the Rezapour and Pearce (1992) formula at near-regional distances and periods less than 10 seconds.

**Earthquakes**

We measured the amplitude for 7-second period Rayleigh waves for 40 earthquakes (Figure 1.1) within 2 degrees of the NTS as recorded at MNV (or the collocated NV31), ELK, KNB, and LAC and estimated a $\overset{M+B}{M_s}(7)$ and $\overset{R+P}{M_s}(7)$ for each event. The results are compiled in Table 1.4 and are presented in Figures 9 and 10 in addition to the explosion analyses. In Figure 1.9, we present a comparison of the $\overset{M+B}{M_s}(7)$ and $\overset{R+P}{M_s}(7)$ estimates for both earthquakes and

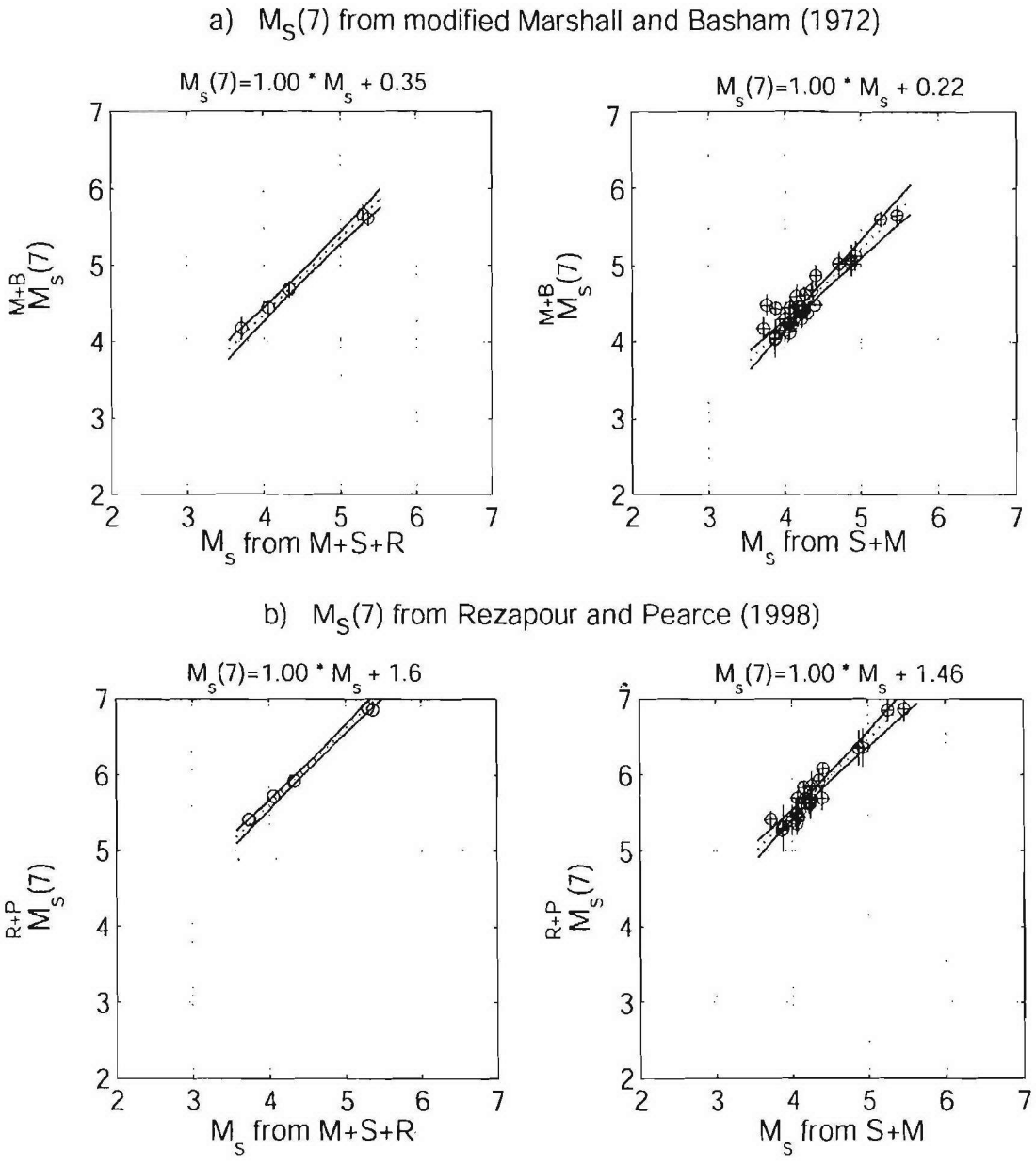


**Figure 1.8. A comparison of our a) $\overset{M+B}{M}_s(7)$ and b) $\overset{R+P}{M}_s(7)$ estimates for NTS with the Marshall *et al.* (1979) estimates (M+S+R; left) and Stevens and Murphy (2001) estimates (S+M; right).**

## Table 1.4. Earthquake Information

| yymmdd | hhmmss | Lat | Long | Depth | $m_b$ | $M_s(7)$ M+B | STD | $M_s(7)$ R+P | STD | # |
|---|---|---|---|---|---|---|---|---|---|---|
| 19790812 | 113119 | 37.26 | 115.08 | 5 | 3.18 | 2.33 | 0.24 | 3.47 | 0.47 | 3 |
| 19791225 | 141710 | 37.27 | 117.06 | 5 | 3.67 | 2.95 | 0.13 | 4.07 | 0.19 | 4 |
| 19800115 | 202822 | 36.18 | 117.60 | 8 | 3.63 | 2.64 | 0.20 | 3.74 | 0.17 | 4 |
| 19800225 | 234332 | 36.20 | 117.58 | 5 | 3.86 | 2.73 | 0.18 | 3.83 | 0.22 | 4 |
| 19800527 | 145057 | 37.48 | 118.81 | 13 | 5.79 | 5.40 | 0.14 | 6.47 | 0.27 | 4 |
| 19811201 | 161850 | 38.62 | 118.19 | 11 | 4.02 | 3.41 | 0.10 | 4.25 | 0.35 | 3 |
| 19811219 | 205652 | 38.63 | 118.21 | 17 | 4.12 | 3.20 | 0.37 | 4.16 | 0.29 | 4 |
| 19820124 | 154407 | 37.45 | 117.83 | 5 | 4.09 | 2.82 | 0.08 | 3.90 | 0.31 | 4 |
| 19820316 | 84700 | 36.60 | 117.03 | 6 | 3.48 | 2.80 | 0.18 | 3.92 | 0.20 | 4 |
| 19820512 | 192924 | 37.27 | 115.08 | 10 | 3.49 | 2.46 | 0.30 | 3.65 | 0.44 | 4 |
| 19820706 | 21043 | 37.69 | 115.05 | 3 | 4.3 | 2.97 | 0.22 | 4.26 | 0.23 | 3 |
| 19820924 | 74024 | 37.85 | 118.12 | 5 | 4.99 | 4.09 | 0.14 | 5.14 | 0.34 | 4 |
| 19830604 | 113740 | 37.39 | 115.21 | 6 | 3.44 | 2.36 | 0.18 | 3.54 | 0.27 | 4 |
| 19840802 | 110134 | 37.30 | 114.94 | 5 | 3.49 | 2.14 | 0.28 | 3.33 | 0.35 | 4 |
| 19841123 | 180825 | 37.48 | 118.66 | 5 | 5.54 | 5.15 | 0.40 | 6.14 | 0.42 | 3 |
| 19851210 | 61025 | 37.30 | 115.01 | 5 | 3.7 | 2.85 | 0.07 | 3.99 | 0.19 | 3 |
| 19920629 | 103102 | 36.69 | 116.24 | 5 | 4.66 | 3.71 | 0.13 | 4.73 | 0.29 | 2 |
| 19920629 | 155239 | 36.71 | 116.29 | 7.94 | 3.89 | 2.36 | 0.12 | 3.38 | 0.54 | 2 |
| 19920629 | 170116 | 36.74 | 116.29 | 7.62 | 3.81 | 2.49 | 0.16 | 3.51 | 0.26 | 2 |
| 19920630 | 160624 | 36.72 | 116.26 | 5 | 3.5 | 2.24 | 0.05 | 3.26 | 0.37 | 2 |
| 19920705 | 65412 | 36.69 | 116.28 | 5 | 4.38 | 2.92 | 0.19 | 3.94 | 0.23 | 2 |
| 19920705 | 84838 | 36.67 | 116.19 | 11.11 | 3.05 | 1.99 | 0.26 | 3.02 | 0.15 | 2 |
| 19930517 | 232049 | 37.17 | 117.78 | 6 | 5.84 | 5.67 | 0.34 | 6.70 | 0.45 | 3 |
| 19930518 | 10306 | 37.15 | 117.76 | 2 | 4.9 | 3.81 | 0.23 | 4.91 | 0.22 | 4 |
| 19930518 | 234853 | 37.06 | 117.78 | 3 | 4.93 | 3.94 | 0.14 | 5.04 | 0.32 | 4 |
| 19930519 | 141322 | 37.14 | 117.77 | 0 | 5.21 | 3.94 | 0.15 | 5.03 | 0.20 | 4 |
| 19930520 | 201414 | 36.10 | 117.70 | 0 | 4.32 | 3.52 | 0.14 | 4.80 | 0.19 | 2 |
| 19990125 | 185207 | 36.82 | 115.96 | 5 | 4.17 | 3.19 | 0 | 4.51 | 0 | 1 |
| 19990125 | 195154 | 36.81 | 115.96 | 5 | 2.98 | 2.40 | 0 | 3.72 | 0 | 1 |
| 19990127 | 104423 | 36.82 | 115.99 | 5 | 4.48 | 3.33 | 0 | 4.64 | 0 | 1 |
| 20000228 | 230842 | 36.07 | 117.60 | 0 | 3.87 | 3.08 | 0 | 4.40 | 0 | 1 |
| 20000229 | 220805 | 36.08 | 117.60 | 0 | 3.7 | 2.83 | 0 | 4.15 | 0 | 1 |
| 20000302 | 150034 | 36.08 | 117.60 | 0 | 3.68 | 2.63 | 0 | 3.95 | 0 | 1 |
| 20010517 | 215357 | 35.80 | 118.05 | 9 | 3.6 | 2.73 | 0 | 4.04 | 0 | 1 |
| 20010517 | 225645 | 35.80 | 118.05 | 8 | 3.64 | 2.88 | 0 | 4.20 | 0 | 1 |
| 20010717 | 120726 | 36.01 | 117.86 | 7 | 4.94 | 4.19 | 0 | 5.51 | 0 | 1 |
| 20010717 | 122518 | 36.04 | 117.87 | 5 | 3.74 | 2.97 | 0 | 4.29 | 0 | 1 |
| 20010717 | 125959 | 36.02 | 117.88 | 0 | 4.22 | 3.84 | 0 | 5.16 | 0 | 1 |
| 20020324 | 100407 | 37.00 | 115.70 | 10 | 3.77 | 2.55 | 0 | 3.88 | 0 | 1 |
| 20020614 | 124044 | 36.72 | 116.30 | 5 | 3.81 | 3.50 | 0.22 | 4.81 | 0.24 | 2 |

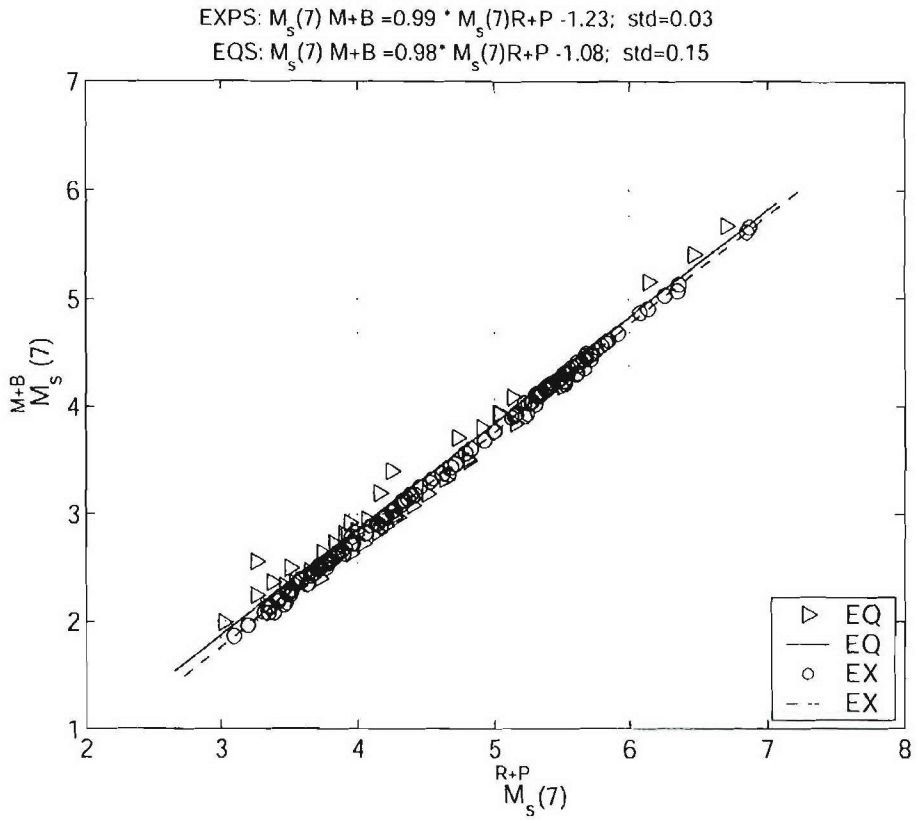


**Figure 1.9.** $\overset{M+B}{M_s}(7)$ **versus** $\overset{R+P}{M_s}(7)$ **estimates for all earthquakes and explosions considered in this study.**

explosions. We find that to obtain an $\overset{M+B}{M_s}(7)$ estimate from a $\overset{R+P}{M_s}(7)$ magnitude, we must subtract 1.23 m.u. for explosions and 1.08 m.u for earthquakes; however, the scatter in the earthquake data is 0.2 m.u larger than for the explosion estimates. In Figure 1.10, we regressed the $\overset{M+B}{M_s}(7)$ and $\overset{R+P}{M_s}(7)$ versus DTV $m_b$ for both populations. The best-fitting regression lines are plotted and labeled in the figure together with 95% confidence intervals. Although the slopes for each line are different, we do not have enough earthquakes with $m_b > 4.5$ to fully constrain this section of the regression analyses. We also note that the standard deviation for the earthquake data for both plots is a factor of two larger than that of the explosions, which could possibly be related to depth effects on 7-second period, Rayleigh-wave generation. We compared our earthquake regression results (slope=1.1, y-intercept=1.4, std=0.31) with the original Marshall and Basham (1972) results for North American earthquakes recorded at far-regional and teleseismic distances at periods greater than 14 seconds (slope=1.2, y-intercept=1.4, std=0.23). We note similar slopes and y-intercepts; however, the differences in the standard deviation are caused by near-source and receiver complexities that affect 7 second Rayleigh waves more drastically than surface waves with periods greater than 14 seconds. However, this discrepancy is countered by the ability of our method to estimate $M_s$ for earthquakes with $m_b$ as small as 3 and explosions with $m_b$ as small as 3.7 (as compared to 3.8 and 4.5, respectively, for Marshall and Basham (1972)).

**Discriminant Analysis**

The final objective of this paper is to examine the performance of the modified Marshall and Basham (1972) and Rezapour and Pearce (1998) $M_s(7)$-$m_b$ discriminants for earthquakes and explosions. The populations plotted in Figure 1.10 suggest that $M_s$ and $m_b$ will be fitted well by linear regressions, with approximately equal slopes assumed for the earthquake and explosion populations. Although, we did observe slightly different slopes in the regression analyses for the two populations, we believe that this is due to inadequate sampling of earthquakes at $m_b$ magnitudes greater than 4.5. Our dataset does not present any evidence that the two populations are converging at smaller magnitudes, although other $M_s$-$m_b$ studies (Stevens and McLaughlin, 2001) suggest that convergence does occur. Furthermore, it seems sensible to regard the $M_s$ values as dependent variables, observed conditionally on fixed values for $m_b$, which are more accurately determined in the WUS when the DTV $m_b$ (Denny *et al.*, 1987; 1989) formula is applied. This yields the following regression model:

$$M_s = \alpha_i + \beta m_b + e \qquad (1.4)$$

i=1,2 where the intercepts $\alpha_1$ and $\alpha_2$ correspond to the earthquake (Q) and explosion (X) populations respectively. Under this approach, the errors (e) are assumed to be independent and identically distributed normal variables.

For determining the optimal discriminant functions, the parallel regression assumption with independent normal errors seems more sensible than the usual assumption of bivariate normality used to get the classification function. Hence, we proceed to use the linear function following from the conditional regression approach to discrimination. This leads to a discriminant function of the form:

$$d = M_s - \frac{1}{2}(\alpha_1 + \alpha_2) - \beta m_b. \qquad (1.5)$$

With equal prior probabilities, we classify an event of unknown origin as an earthquake if d>0 and as an explosion otherwise. Estimating the parameters $\alpha_1$, $\alpha_2$, and $\beta$ for the two $M_s$ populations led to the values given in Table 1.5.

The classification criterion in the equal slope case is then applied with the values estimated from the data. We note first the result of applying the discriminant function, $d$, directly, as shown in Figure 1.11. Note the four misclassified earthquakes in the $M_s^{M+B}(7)$-$m_b$ plot and the six misclassified earthquakes in the $M_s^{R+P}(7)$-$m_b$ case. To estimate the performance of the discriminant function (Equation 5), we used a jackknifing technique where the observation to be classified is held out during the estimation of the slope and intercept procedure and then the discriminant function is applied to the observation to be classified using the estimated parameters. The results are shown in Table 1.6 and we note that the modified Marshall and Basham $M_s^{M+B}(7)$ values perform better. For the $M_s^{M+B}(7)$ case, we misclassified 4 earthquakes as

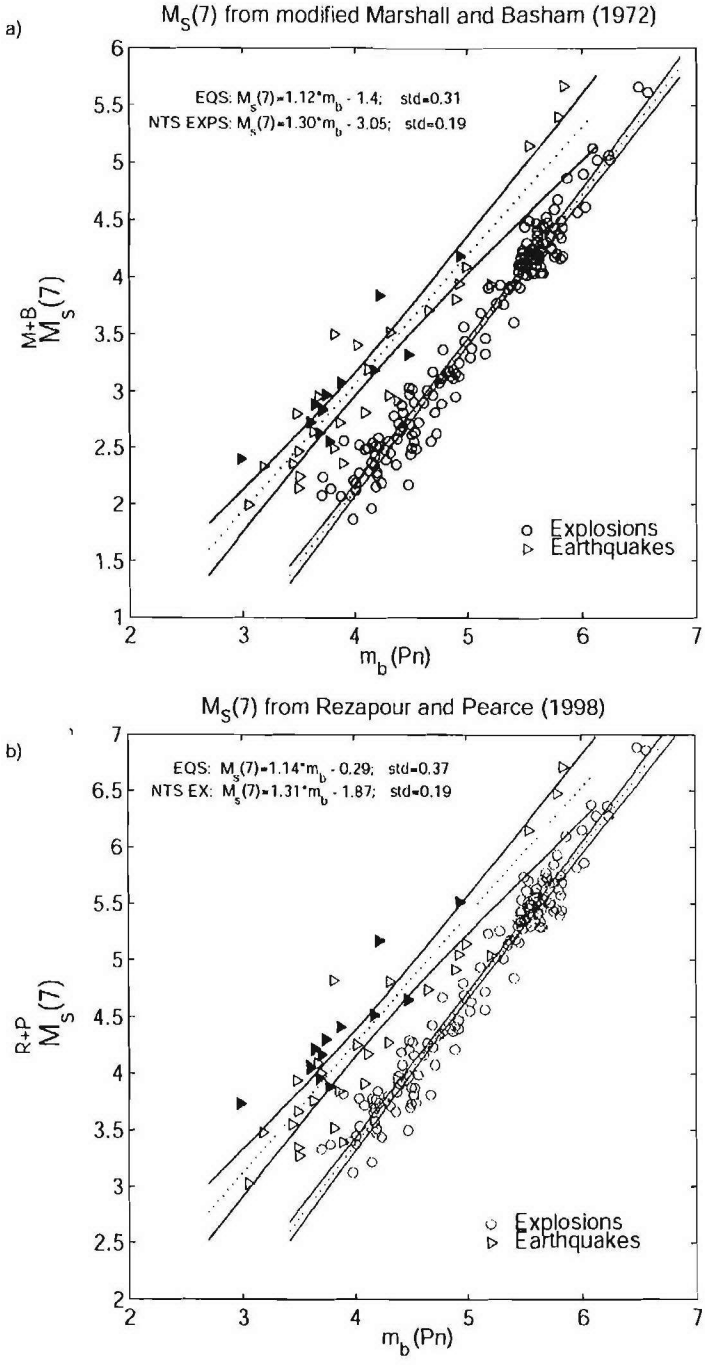


**Figure 1.10. a) $M_s^{M+B}(7)$-$m_b$ and b) $M_s^{R+P}(7)$-$m_b$ results for the earthquakes and explosions shown in Figure 1.1. For each population, the best-fitting regression line is the dotted line running through the data points surrounded by the pointwise 95% confidence intervals plotted as two solid lines. The earthquakes plotted as solid symbols represent single-station (MNV/NV31) estimates of both $M_s(7)$ and $m_b$.**

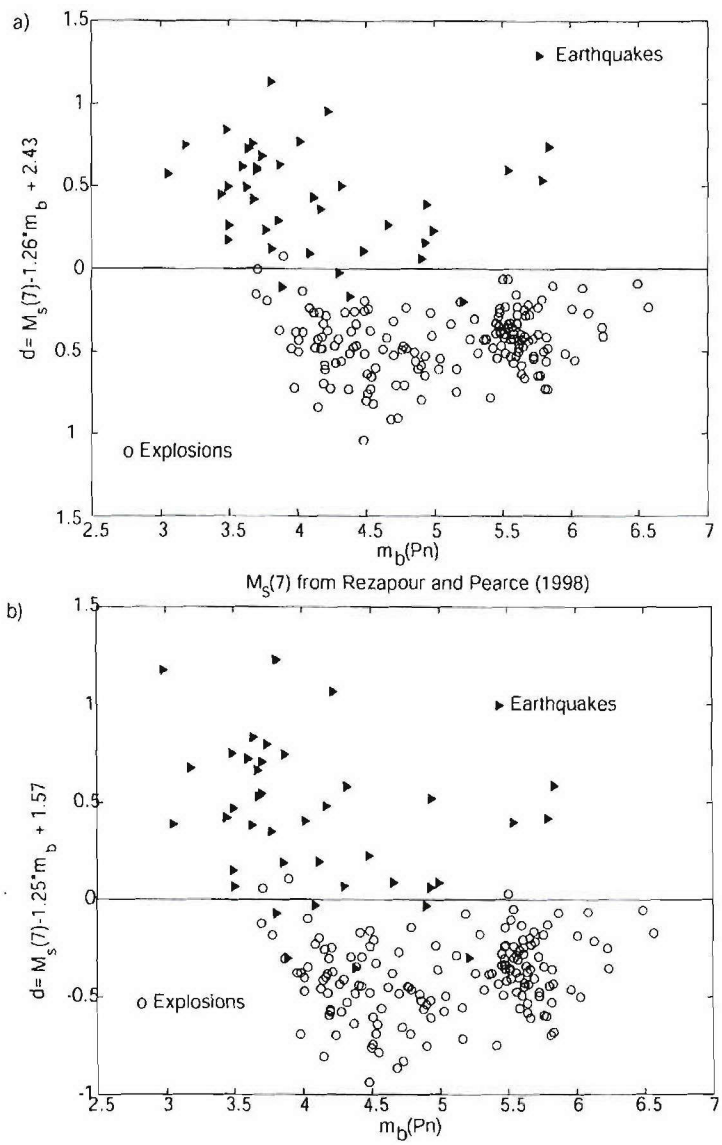


**Figure 1.11. Disrciminant functions for a) $M_s(7)^{M+B}$-$m_b$ and b) $M_s(7)^{R+P}$-$m_b$ for earthquakes and explosions considered in this study. The parameter *a* from Equation 1.4 represents the slope (1.26 and 1.25) of the $m_b$ versus $M_s$ populations and the decision line is determined from the means for both populations. Based upon our evaluation of the $M_s(7)^{M+B}$-$m_b$ relationship for this region, we calculated the probability of misclassifying an earthquake as an explosion as 10% and the probability of classifying an explosion as an earthquake as 1.2%. The results are slightly worse for $M_s(7)^{R+P}$-$m_b$, where 15% of the earthquakes are misclassified as explosions and 2% of the explosions labeled as earthquakes.**

**Table 1.5. Estimated intercepts and slopes for the $M_s^{M+B}(7)$ and $M_s^{R+P}(7)$ estimates. Standard errors are in parentheses.**

| Data | $\alpha_1$ | $\alpha_2$ | $\beta$ | $\sigma_1$ | $\sigma_2$ |
|---|---|---|---|---|---|
| $M_s^{M+B}(7)$ | -1.99(0.10) | -2.87(0.12) | 1.26(0.02) | 0.334 | 0.192 |
| $M_s^{R+P}(7)$ | -0.78(0.11) | -1.57(0.13) | 1.25(0.03) | 0.391 | 0.195 |

**Table 1.6. Jackknifed corrected decisions and errors for earthquakes (Q) and explosions (X).**

| | Q | X | Q | X |
|---|---|---|---|---|
| $M_s^{M+B}(7)$ | 36 | 156 | 4 | 2 |
| $M_s^{R+P}(7)$ | 34 | 155 | 6 | 3 |

explosions (10%) while only classifying two explosions (1.2%) as earthquakes. The misclassification rates are slightly higher for the $M_s^{R+P}(7)$ estimates as we identified 6 earthquakes(16%) as explosions and 3 explosions(2%) as earthquakes. A reviewer has suggested that the slopes may be unequal and indeed, the hypothesis of equal slopes can not be statistically rejected for this particular dataset. Following through on the discriminant analysis under the unequal slope assumption leads to results that are slightly worse than those shown in Table 1.5. We note that there were now five more incorrect decisions for explosions in the $M_s^{M+B}(7)$ case and eight more in the $M_s^{R+P}(7)$ case when the unequal slope case was considered. The inferior performance is taken as providing some evidence that generalizing to the unequal slope case may not be needed

It is also useful to look at theoretical operating characteristic curves for the two $M_s$ measures. Figure 1.12 shows the explosion detection probabilities expected for the two measures as a function of the explosion false alarm probabilities, assuming that the normal theory holds for the discriminant. Note that the $M_s^{M+B}(7)$ curve is better for both a false alarm probability of 0.01 (0.3 vs. 0.7 signal detection probability) and for a false alarm probability of 0.05 (0.8 vs. 0.95 signal detection probability). It is interesting in this case that the signal detection and false alarm probabilities change primarily as a function of the intercept difference $\delta = \alpha_1 - \alpha_2$ which is substantially larger (1.46 vs. 0.79) for the $M_s^{M+B}(7)$ and $M_s^{R+P}(7)$ populations, respectively. The suspected cause of the differences in the $M_s$-$m_b$ discriminant performance arises from the use of empirical path corrections for the Marshall and Basham (1972) estimates as compared to none for Rezapour and Pearce (1998). This study suggests that path correction make a substantial difference in the discrimination performance for this technique.

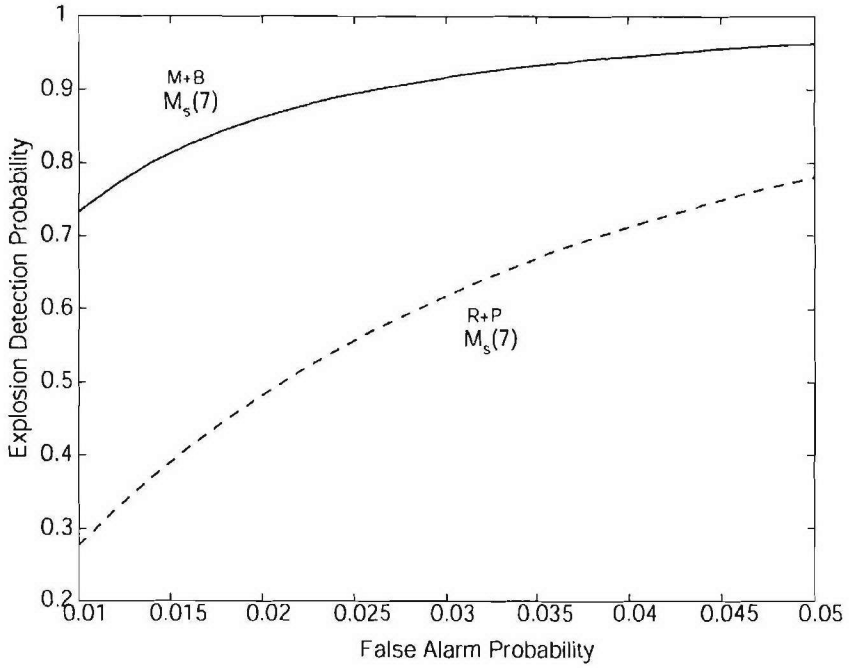


**Figure 1.12. Explosion detection as a function of false alarm probability for the linear discriminants using the modified Marshall and Basham (1972) and Rezapour and Pearce (1998) $M_s(7)$ estimates.**

## CONCLUSIONS

The $\overset{M+B}{M_s}(7)$-$m_b$ and $\overset{R+P}{M_s}(7)$-$m_b$ discriminants defined in this paper can now be used as tools to help screen explosions from earthquakes in the vicinity of the Nevada Test Site (NTS). The false classification rates for the method are small, and the method can be used in conjunction with other regional NTS discriminants, such as the phase and spectral ratios (Walter *et al.*, 1995) and body wave and moment magnitude ratios ($m_b$-$M_w$) (Patton, 2001).

Transportability of the $\overset{M+B}{M_s}(7)$-$m_b$ discriminant to regions other than NTS will be complicated due to bias in small magnitude $m_b$ measurements, deeper events, variable path lengths, and more complex propagation paths. Thus, our attempts to transport the discriminant will require both accurate $m_b$ estimates for regional events in different regions of the world using techniques such as coda $m_b$ (Mayeda, 1995) and $m_b(Lg)$ (Patton, 2001) as well as high quality dispersion curves in the period range of 5 to 20 seconds in order to estimate path corrections for $\overset{M+B}{M_s}(7)$. For the latter, the research efforts of Levshin *et al.* (2002), who have been developing group velocity maps for Rayleigh waves recorded in Asia with periods of 7 seconds and greater, will be extremely beneficial to our attempts at transporting this technique.

## ACKNOWLEDGMENTS

We are indebted to Howard Patton for his assistance in database acquisition and his comments concerning various aspects of the research. We also wish to thank Bill Walter for help in acquiring the MNV dataset. We express our gratitude to Marv Denny, Jeff Stevens, Steve Taylor, Nancy Cunningham, Delaine Reiter, Shelly Johnson, and James Lewkowicz for insightful discussions about the manuscript and research. Constructive comments from an anonymous reviewer were greatly appreciated. We thank the developers of the Generic Mapping Tools software (Wessel and Smith, 1998), Computer Programs in Seismology (Herrmann, 2002), and Matlab, which were all used to generate and present the results of our research. This research was sponsored by the Defense Threat Reduction Agency under Contract No. DTRA01-01-C-0080.

## REFERENCES

Basham, P.W. (1971). A new magnitude formula for short-period continental Rayleigh waves, *Geophys. J. R. Ast. Soc.*, **23**, 255.

Basham, P.W. and R. B. Horner (1973). Seismic magnitudes of underground nuclear explosions, *Bull. Seism. Soc. Am.*, **63**, 105-131.

Bath, M. (1952). Earthquake magnitude determination from the vertical component of surface waves, *Trans. Am. Geophys. Un*, **33**, 81.

Chael, E.P. (1997). An automated Rayleigh-wave detection algorithm, *Bull. Seism. Soc. Am.*, **87**, 157-163.

Day, S.M. and K.L. McLaughlin (1991). Seismic source representation for spall, *Bull. Seism. Soc. Am.*, **81**, 191-201.

Denny, M.D., S. R. Taylor, and E.S. Vergino (1987). Investigation of $m_b$ and $M_s$ formulas for the western United States and their impact on the $M_s/m_b$ discriminant, *Bull. Seism. Soc. Am.*, **77**, 987-995.

Denny, M.D., S. R. Taylor, and E.S. Vergino (1989). Erratum: Investigation of $m_b$ and $M_s$ formulas for the western United States and their impact on the $M_s/m_b$ discriminant, *Bull. Seism. Soc. Am.*, **79**, 230.

Denny, M. D. (1998) Mina Seismic Data: Historic background for CTBT Monitoring, *Lawrence Livermore Report UCRL-MI-130657.*

Dziewonski, A.M., J. Bloch, and M. Landisman (1969). A new technique for the analysis of transient seismic signals, *Bull. Seism. Soc. Am.*, **59**, 427-444.

Evernden, J. F. (1971). Variation of Rayleigh-wave amplitude with distance, *Bull. Seism. Soc. Am.*, **61**, 231.

Ewing, W.M., F. Press, and W.S. Jardetzky (1957). *Elastic waves in layered media,* McGraw-Hill, New York.

Gutenberg, B. (1945). Amplitudes of surface waves and the magnitudes of shallow earthquakes, *Bull. Seism. Soc. Am.*, **35**, 3.

Herak, M. and D. Herak (1993). Distance dependence of $M_s$ and calibrating function for 20 second Rayleigh waves, *Bull. Seism. Soc. Am.*, **83**, 1681.

Herrin, E.T. and T. Goforth (1977). Phase-match filtering: application to the study of Rayleigh waves, *Bull. Seism. Soc. Am.*, **67**, 1259-1275.

Herrmann, R. B. (2002). Computer Programs in Seismology Version 3.15, St. Louis University.

Keller, G.R., R.B. Smith, L.W. Braile, R. Heaney, and D.H. Shurbet (1976). Upper crustal structure of the eastern Basin and Range, northern Colorado plateau, and middle Rocky Mountains from Rayleigh-wave dispersion, *Bull. Seism. Soc. Am.*, **67**, 869-876.

Levshin, A., J. Stevens, M. Ritzwoller, and D. Adams (2002). Short-period (7-s to 15-s) group velocity measurements and maps in central Asia, *Proceedings of the 24th Seismic Research Review on Nuclear Explosion Monitoring: Innovation and Integration.*

Marshall, P.D. and P.W. Basham (1972). Discrimination between earthquakes and underground explosions employing an improved $M_s$ scale, *Geophys. J. R. Astr. Soc.*, **29**, 431-458.

Marshall, P.D., Springer, D.L, and Rodean, H.C. (1979). Magnitude corrections for attenuation in the upper mantle, *Geophys. J. R. Astr. Soc.*, **57**, 609-638.

Mayeda, K. M. (1993). $m_b$(*Lg*Coda): a stable single station estimator of magnitude, *Bull. Seism. Soc. Am.*, **83**, 851-861.

Patton, H. (1991). Seismic moment estimation and the scaling of the explosion source, *Geophysical Monograph 65: Explosion Source Phenomenology,* pp. 171-183, eds. Taylor, S.R., H.J. Patton, and P.G. Richards, *Am. Geophys. Un. Monogr.,* Washington, D.C.

Patton, H. (2001). Regional magnitude scaling, transportability, and $M_s$-$m_b$ discrimination at small magnitudes, in *Monitoring the Comprehensive Nuclear Test Ban Treaty: Source Processes and Explosion Yield Determination,* eds. Ekstrom, G., M. Denny, and J.R. Murphy, *Pure Appl. Geophys.*, **158**, 1951-2015.

Rezapour, M., and R.G. Pearce (1998). Bias in surface-wave magnitude $M_s$ due to inadequate distance correction, *Bull. Seism. Soc. Am.*, **88**, 43-61.

von Seggern, D. (1973). Joint magnitude determination and analysis of variance for explosion magnitude estimates, *Bull. Seism. Soc. Am.*, **63**, 827-845.

von Seggern, D. (1977). Amplitude distance relation for 20-Second Rayleigh waves, *Bull. Seism. Soc. Am.*, **67**, 405-411.

Selby, N. (2001). Association of Rayleigh waves using back azimuth measurements: application to test ban verification, *Bull. Seism. Soc. Am.*, **91**, 580-593.

Stevens, J.L., D.A. Adams, and E. Baker (2001). Surface wave detection and measurement using a one-degree global dispersion grid, *SAIC Final Report SAIC-01/1085.*

Stevens, J. L. and K.L. McLaughlin (2001). Optimization of surface wave identification and measurement, in *Monitoring the Comprehensive Nuclear Test Ban Treaty: Surface Waves*, eds. Levshin, A. and M.H. Ritzwoller, *Pure Appl. Geophys.*, **158**, 1547-1582.

Stevens, J. L. and J.R. Murphy (2001). Yield Estimation from Surface-wave Amplitudes, in *Monitoring the Comprehensive Nuclear Test Ban Treaty: Surface Waves: Source Processes and Explosion Yield Determination,* eds. Ekstrom, G., M. Denny, and J.R. Murphy, *Pure Appl. Geophys.*, **158**, 2227-2251.

Taylor, S.R. and G.E. Randall (1989). The effects of spall on regional seismograms, *Geophys. Res. Lett.*, **16**, 211-221.

Tibuleac, I.M., J.L. Bonner, E.T. Herrin, and D.G. Harkrider (2002). Calibration of the $M_s$-$m_b$ discriminant at NVAR, *Proceedings of the 24th Seismic Research Review on Nuclear Explosion Monitoring: Innovation and Integration.*

Vanek, J., A. Zatopek, V. Karnik, Y.V. Riznichenko, E.F. Saverensky, S.L. Solov'ev, and N.V. Shebalin (1962). Standardization of magnitude scales, *Bull. (Izvest.) Acad. Sci. U.S.S.R., Geophys. Ser.*, **2**, 108.

Vergino, E.S. and Mensing, R.W. (1989). Yield estimation using regional $m_b(Pn)$, *Lawrence Livermore National Laboratory Report UCID-101600.*

Walter, W. R., K.M. Mayeda, and H.J. Patton (1995). Phase and spectral ratio discrimination between NTS earthquakes and explosions. Part I. Empirical Observations. *Bull. Seism. Soc. Am.*, **85**, 1050-1067.

Wessel, P. and W.H.F. Smith (1998). New, improved version of the Generic Mapping Tools Released, *EOS. Trans. Am. Geophys. Un.*, **79**, *579.*

Woods, B. and D.G. Harkrider (1995). Determining surface-wave magnitudes from regional Nevada Test Site data, *Geophys. J. Int.*, **120**, 474.

Yacoub, N.K. (1983). Instantaneous amplitudes: a new method to measure seismic magnitude, *Bull. Seism. Soc. Am.*, **73**, 1345-1355.

Yang, X., R. North, and C. Romney (2000). CMR Nuclear Explosion Database, Center for Monitoring Research *Technical Report CMR-0016*, Alexandria, Va., 129 p.

Zhao, L.S. and D.G. Harkrider (1992). Wavefields from an off-center explosion in an imbedded solid sphere, *Bull. Seism. Soc. Am.*, **82**, 1927-1955.

# CHAPTER 2: $m_b$ CALIBRATION AT NVAR

*Ileana M. Tibuleac*

Weston Geophysical Corporation

## INTRODUCTION

The objective of this study is to calibrate the Denny, Taylor and Vergino (DTV) (Denny *et al.* 1987; 1989) body wave magnitude formula for the NVAR (Mina, Nevada) array.

Constants C for the formula:

$$\text{DTV } m_b = \log(A)+2.42*\log(\Delta)-3.95+C \qquad (2.1)$$

are calculated at the stations NV31, NV32, NV33 and NV08 using the value of the constant C calculated by DTV at MNV: C=-0.02.

The study consists of two tasks:

1. Calibration of NV31 and the collocated station MNV.
2. Calibration of NV08, NV32, NV33 and NV31.

## DATA

Two data sets are used in order to accomplish the objective tasks. For Task 1, we use 13 events, shown as squares in Figure 2.1. The earthquakes, located 250 to 1600 km from MNV, of USGS body wave magnitude ($m_b$) between 2.8 and 4.4, are recorded in the time frame when PIDC reported events from both NVAR and MNV, i.e. during the first 3 months of 1999.

The second data set, used for Task 2, consists of 52 events ($2.6 < m_b < 4.4$) located from 100 km to 1100 km epicentral distance to the east of the NVAR array. The location of the events is chosen such that they would be in the vicinity of the NTS and the ray paths would not travel across the complicated lithology of the Rocky Mountains.

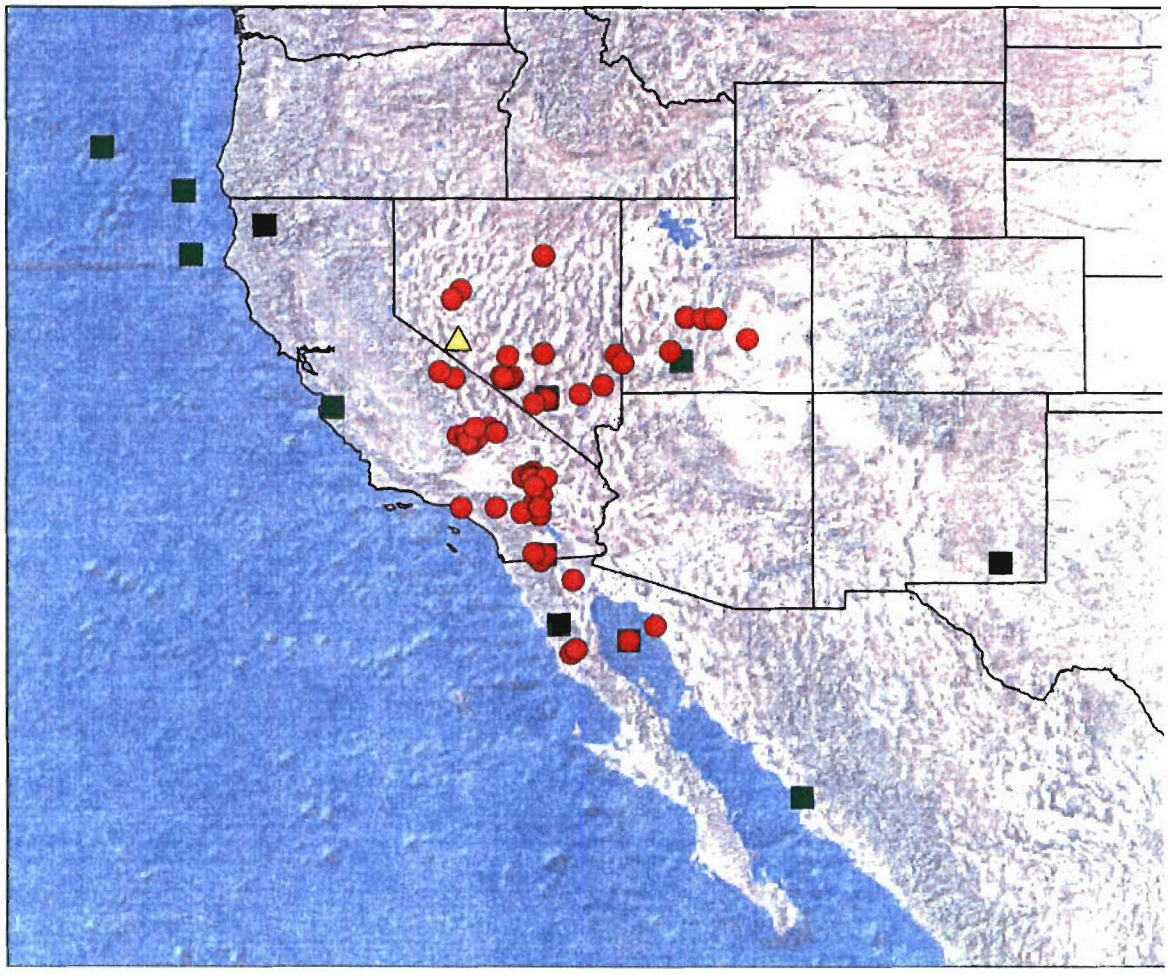

**Figure 2.1. Events used in this study. Green squares are events from the dataset used to calibrate NV31 and MNV, the red dots are events used to calibrate NV32, NV33 and NV08 relative to NV31 and the yellow triangle represents the NVAR seismic array.**

## METHDOLOGY

The maxim peak-to-peak velocity amplitude and the corresponding period for the first 4 seconds on each velocity trace are measured. When *Pn* is only a cycle or two, as in the case of events coming from locations close to NTS, the largest *Pn* amplitude is measured.

Amplitude in *nm* is measured for the CMG-3T instrument (at NV31 and MNV stations) or the respective instrument at stations NV08, NV32 and NV33. To follow the procedure used by DTV to calculate the MNV constant, data is corrected to the values of ground displacement that would be recorded by a WWSSP short period (SP) instrument. When the velocity is converted into ground displacement of a WWSP instrument it is assumed that the location of the

first arrival maxim amplitude does not change with the transformation from one instrument to another.

## RESULTS

### Task 1

Figure 2.2 shows DTV $m_b$ estimated at MNV and DTV $m_b$ calculated at NV31 with C=0. Velocity amplitude estimates at both stations are transformed into displacement at the WWSSP instrument. The constant was determined to be:

C @ NV31 = - 0.0025.

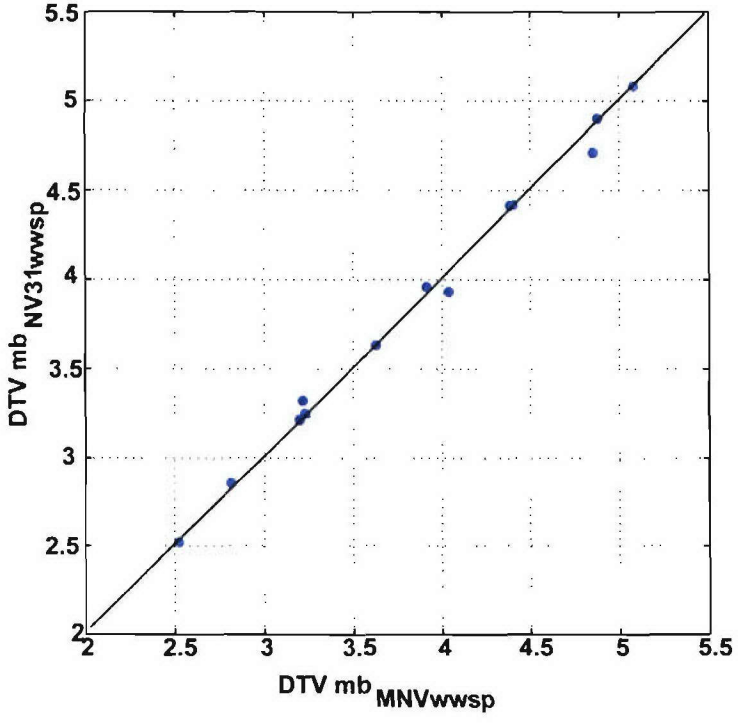


**Figure 2.2. Comparison of DTV $m_b$ values at MNV and NV31.**

When data at NV31 are not transformed into WWSSP values (none), but it was compared to WWSSP transformed values at MNV, C @ NV31(none)= -0.0635.

### Task 2.

NV31 DTV $m_b$ corrected with the constant estimated at Task 1 (C=-0.0025) is compared to DTV $m_b$ estimated for NV08, NV32 and NV33 without using any constants. We calculate constants for two cases: when all data is corrected to amplitude values recorded at a WWSSP SP instrument (Figure 2.3), and when none of the data (Figure 2.4), including data from MNV, is corrected (none). The median value of the DTV $m_b$ magnitude difference is considered the best

estimator of the difference between DTV $m_b$ constants at each station. Figure 2.3 presents a comparison between each pair of the stations NV08, NV31, NV32 and NV33 for the case when all amplitudes are expressed as the values of the ground motion recorded by a simulated WWSSP instrument. The vertical axis of each plot shows magnitudes at one station plus the median value of the magnitude differences between the two stations. In the ideal case, the magnitude values should follow the straight line shown in each of the plots of Figure 2.3.

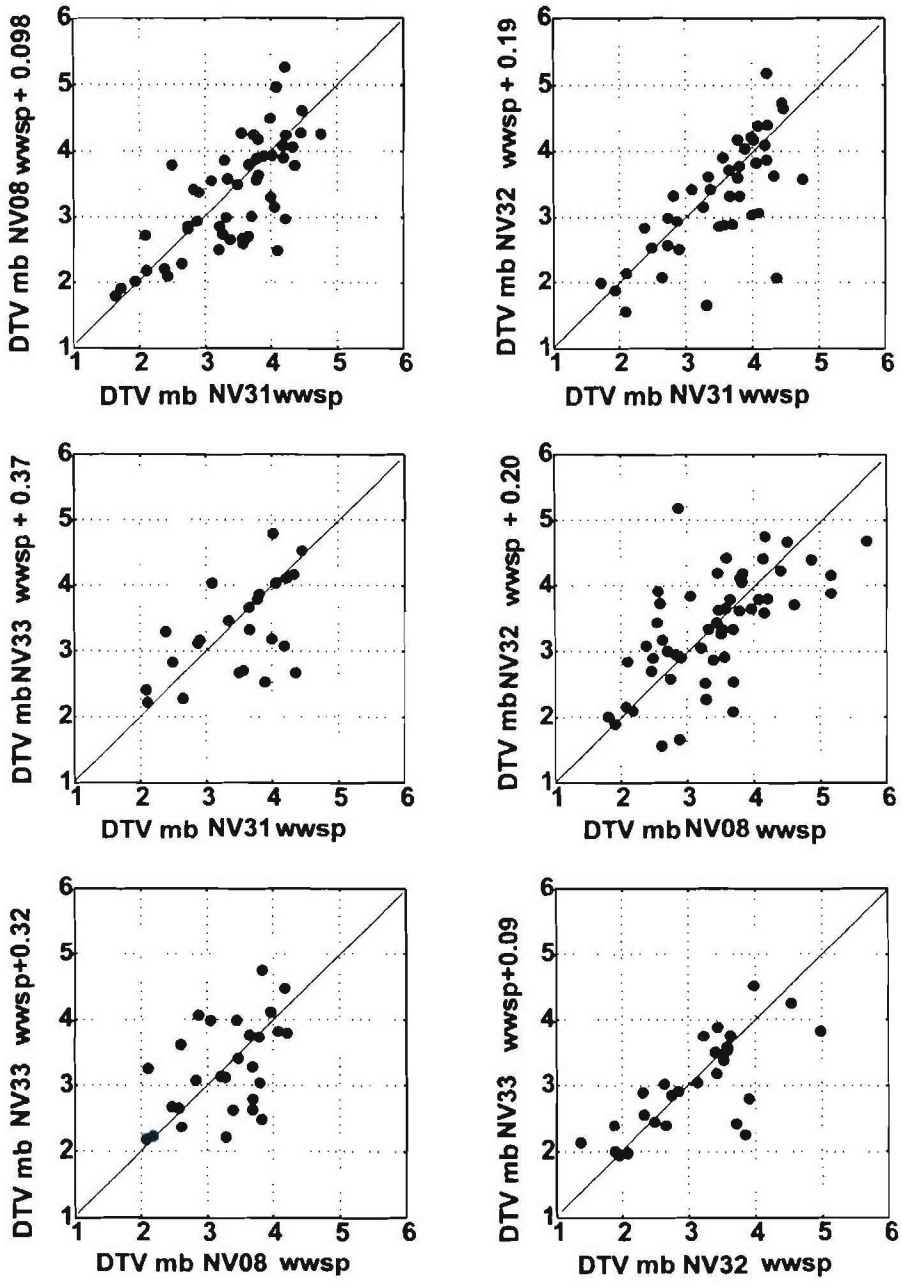


**Figure 2.3. Comparison between WWSSP corrected DTV $m_b$ at NV31, NV08, NV32 and NV33.**

The station magnitude constants are determined as follows: the median of the difference between the reference station (on the horizontal axis in Figure 2.3) and the station to calibrate (on the vertical axis in Figure 3) is calculated and subtracted from the constant of the reference station, *when the reference station is NV31*. For each array element, the constant C of the DTV formula (Equation 4.1) is presented in Table 2.1.

**Table 2.1. Constants of the DTV mb formula at each station. C-WWSP are obtained when all amplitudes are transformed into fictitious WWSP recorded displacement, C-NONE are obtained when all the amplitudes, including MNV data, are transformed into displacement in *nm* at the respective instrument.**

| Station | MNV | NV31 | NV08 | NV32 | NV33 |
|---|---|---|---|---|---|
| C-WWSP | -0.02 | -0.0025 | -0.10 | -0.19 | -0.37 |
| C-NONE | | -0.0025 | -0.14 | -0.22 | -0.27 |
| Nr. phases | 13 | 13 | 52 | 44 | 25 |
| C-WWSP mb > 4.0 | | -0.0025 | -0.03 | -0.29 | -0.27 |
| Nr. Phases **mb > 4.0** | | | 17 | 16 | 8 |

The inter-station data spread is observed to be slightly less in the case when we use only displacement in *nm*, not corrected to the WWSSP instrument (see Figure 2.4). The reason is probably related to the fact that differences between stations of the order of 0.1 sec in the estimated period (the period is typically 0.2 – 0.4 sec for the majority of the events) become important (ratio of correction factors up to 3) when correcting to the WWSSP instrument. Using only magnitudes greater than 4 does not seem to reduce significantly the data spread between stations and the reduced number of events affects the constants up to 0.1 m.u. (Table 4.1). There is no obvious pattern in the magnitude scatter function of backazimuth.

## CONCLUSIONS

The analysis described in this chapter allows estimation of DTV magnitudes for regional events recorded at the elements (NV31, NV08, NV32, and NV33) of the NVAR array. The magnitude estimates at these stations are calibrated to magnitude values estimated for MNV, a station collocated with NV31, which was calibrated against Nevada Test Site nuclear explosions by Denny *et al.*, (1988). The DTV magnitude formula with the constant C estimated for NV31 is used in Chapter 1 to measure the $m_b$ for recent earthquakes on or near the Nevada Test Site.

## REFERENCES


Denny, M.D., S. R. Taylor, and E.S. Vergino (1987). Investigation of $m_b$ and $M_s$ formulas for the western United States and their impact on the $M_s/m_b$ discriminant, *Bull. Seism. Soc. Am.*, 77, 987-995.

Denny, M.D., S. R. Taylor, and E.S. Vergino (1989). Erratum: Investigation of $m_b$ and $M_s$ formulas for the western United States and their impact on the $M_s/m_b$ discriminant, *Bull. Seism. Soc. Am.*, **79**, 230.

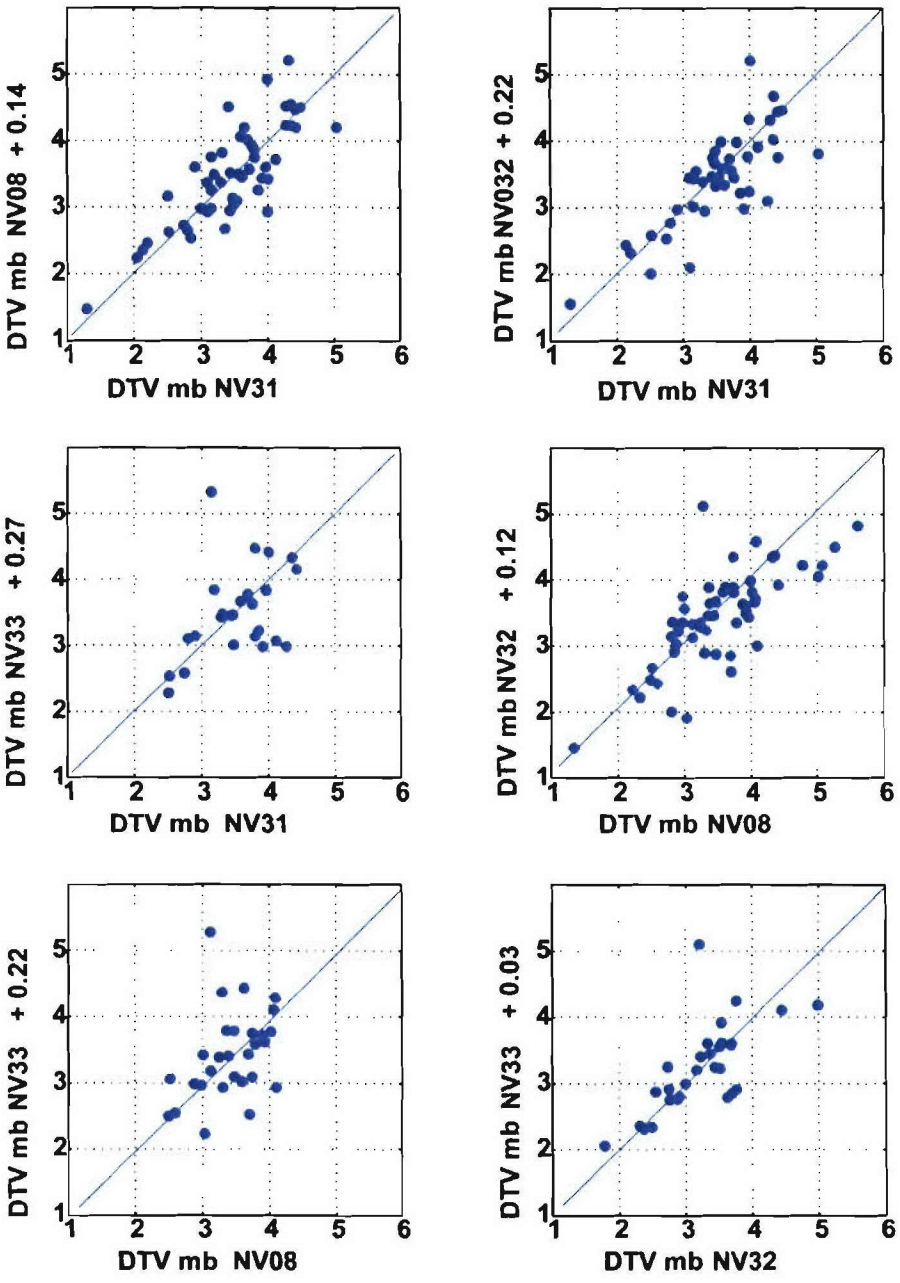


**Figure 2.4. Same as in Figure 2.3; however with no WWSSP corrections applied.**

# CHAPTER 3: WAVELET PRE-PROCESSING FOR STABLE MAGNITUDES ESTIMATION AND SPECTRAL $m_b$ MAGNITUDES

*Ileana M. Tibuleac*

Weston Geophysical Corporation

## INTRODUCTION

The preferred method for evaluating magnitudes should produce consistent and precise results at all stations. Coda techniques using *Lg* arrivals have shown promise for producing body wave magnitudes ($m_b$) with very small scatter between stations (Mayeda *et al.*, 2003); however, $m_b$ from body wave arrivals is less robust and often has more inter-station scatter than coda techniques. It is best to use raw data for magnitude estimation; however, filtering is required for small events recorded on broadband stations. Current filtering procedures do not use wavelet transforms. The potential advantage of wavelet pre-filtering is conservation of signal shape during filtering or denoising and the possibility of applying very narrow filters with little signal distortion and ringing. The main objective of this pilot study is to evaluate wavelet pre-processing of the waveforms as a method for measuring consistent inter-station body wave amplitudes for magnitude estimation. This signal processing technique leads to decreased $m_b$ scatter for small events.

## DATA

Wavelet pre-filtering and denoising techniques are applied to 32 events (Figure 3.1) recorded at the Mina, Nevada seismic array (NVAR) between January 1999 and Dec 2002, with body wave magnitudes ($m_b$) between 2.6 and 4.4, as reported by the USGS (NVAR database). The events are in a distance range from 250 to 1100 km from the Mina, Nevada, (NVAR) array.

A database of 28 events ($3.5 < m_b < 6.4$), reported by USGS within 1000 km of the Lop Nor test site (41.5 N, 88.5 E) is analyzed at the Kazahstan Seismic Network (KNET) stations (KNET database). Locations of the events and of the network are presented in Figure 3.2. The KNET seismic network is a ten station digitally telemetred broadband array located along the boundary of northern Tien Shan mountains and the Kazakh platform (hhtp://eqinfo.ucsd.edu).

## METHODOLOGY

Two methods were considered involving wavelet pre-processing of the signals. The two methods were first tested on events recorded at NVAR.

### Wavelet Denoising

The first method was denoising the signal using wavelet transforms, as follows:

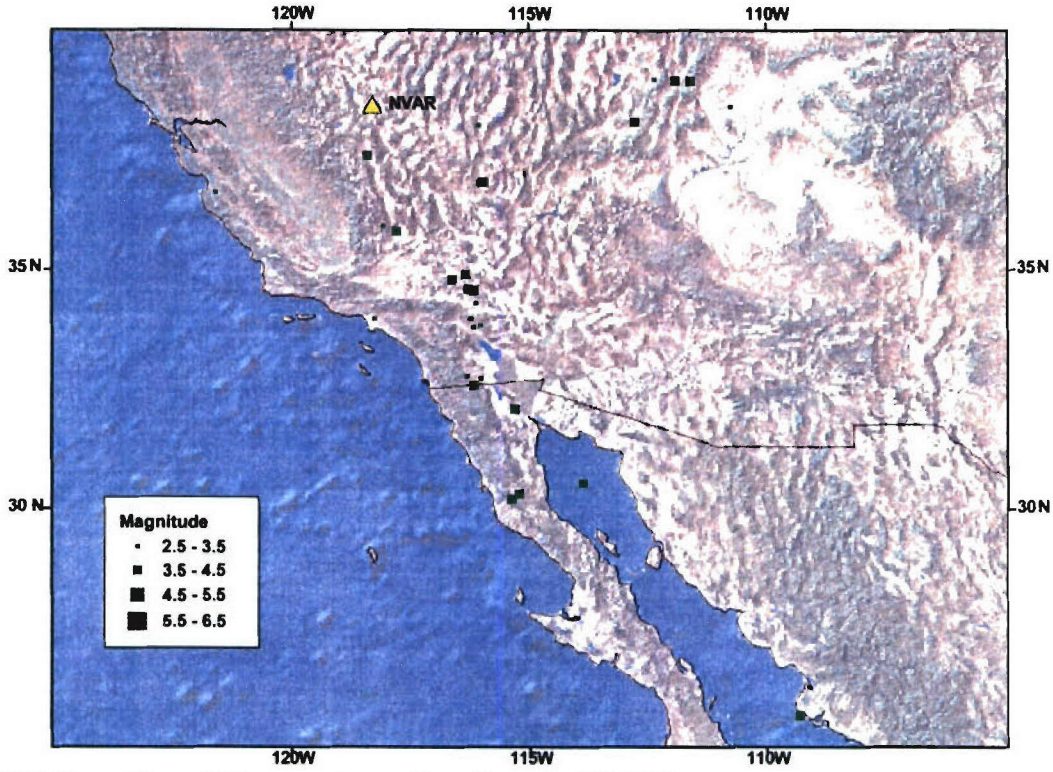


**Figure 3.1. Location of the events analyzed at the NVAR array.**

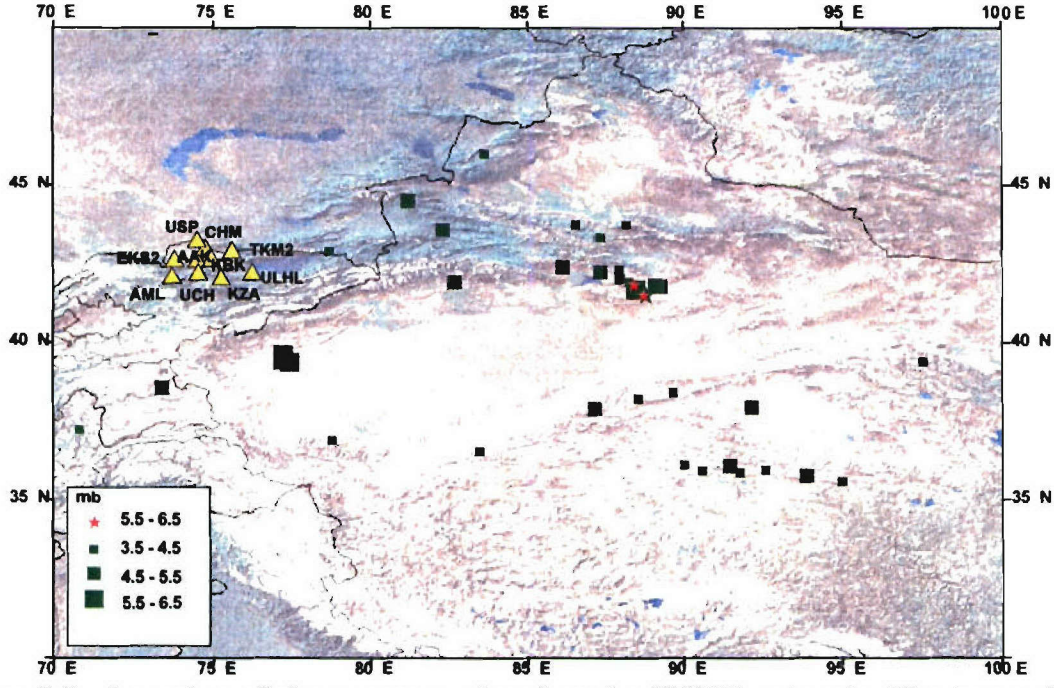


**Figure 3.2. Location of the events analyzed at the KNET network. The two red stars are nuclear explosions at the Lop Nor Test Site. Green squares represent earthquakes and yellow triangles represent the ten KNET stations used in this study.**

1. The waveform is decomposed with a 'bior3.7' wavelet at level 6. The *detail* at level 6 is centered on a 0.6 sec period for a sample rate of 40 samples/s (at the NVAR array). A Stationary Wavelet Transform is preferred to the Discrete Wavelet Transform, in order to decrease the effects of variance to translations.
2. The denoising threshold is calculated for each *detail* considering only the signal between the *Pn* and *Pg* arrivals, zero padded up to the nearest power of 2 and 15 seconds of noise before the *Pn* arrival.
3. The waveform, containing 15 seconds of noise and 50 seconds of signal, is then denoised using the threshold vector. Two methods are used for denoising: 'RIGSURE' and 'MINIMAXI' (Misiti *et al.*, 2000).
4. The signal is reconstructed after the *approximation* at level 6 is eliminated, which is equivalent with removing frequencies lower than 0.3 Hz from the waveform spectrum.

**Wavelet Spectral Magnitude Estimation**

The second magnitude estimation method is inspired by the 'instantaneous magnitudes' calculated by N. K Yakoub (1983) and will be subsequently called 'spectral $m_b$' calculation. Yakoub's idea is to measure Rayleigh wave amplitude at a given period after multiple filter analysis, then to mediate amplitudes for several periods around 20 seconds. He mentioned the possibility of applying his method to compressional waves. Instead of extending his idea to *P*-waves using traditional Fourier methods, we have used wavelet "spectral" amplitudes. In our case, filtering takes place in time domain, eliminating the necessity to estimate Fourier transforms and their inverses. Wavelet processing is chosen as a pre-filtering method for this application since it offers the advantage of narrow band filtering without ringing and preserves the shape of the signal.

The steps to evaluate spectral $m_b$ magnitudes are as follows:

1. A Continuous Wavelet Transform (CWT) using a 'bior3.7' wavelet and scales corresponding to the periods: 0.9, 1.1, 1.2, 1.3, respectively 1.5 seconds is applied to 15 seconds of noise followed by 50 seconds of signal.
2. The maximum amplitude peak-to-peak at each period (CWT) is measured.
3. WWSSP (wwsp) corrected DTV $m_b$ magnitudes (Denny *et al.*, 1989) are calculated for each scale and the resulting DTV $m_b$ magnitude is expressed as the mean of the values at all scales considered, for the events recorded at NVAR.

WWSSP (wwsp) corrected DTV $m_b$ are calculated for each of the stations NV08, NV31 and NV32 with the formula:

$$\text{DTV } m_b = \log(A)+2.42*\log(\Delta)-3.95+C \quad (5.1)$$

where C @ NV31 = - 0.0025 and, in the initial calculations, C is zero for the NV08 and NV32.

Body wave magnitudes are calculated at KNET using the Veith – Clawson (VC) formula (Veith and Clawson, 1972)

$$VC\ m_b = \log(A_{P\text{-}P}/T)+R \qquad (5.2)$$

where $A_{P\text{-}P}$ is the peak-to-peak short period vertical *P* wave amplitude in nm, T is the corresponding period in seconds and R are tabulated corrections factors depending on distance and depth. The KNET amplitudes are not WWSSP-SP corrected.

Based on the results from testing the two methods on events recorded at NVAR, as presented below, only the second method (CWT) is chosen for further analysis at the KNET network. CWT is compared to a pre-filtering method using a Butterworth forward and reverse 3-pole filter (BUTTERWORTH).

## RESULTS

### The NVAR Database

An example of typical pre-filtering for an event recorded at NVAR is presented in Figure 3.3. *Pn* (blue line) is enhanced on all three components by both BUTTERWORTH (Figure 3.3, left plot) and CWT (Figure 3.3, right plot) pre-filtering methods. The arrivals observed after CWT pre-filtering at scale 40 (centered on 0.9 seconds period) are clear and easy to pick. Both denoising methods (Figure 3.3, bottom lower plots) enhanced the NV32 *Pn* arrivals. *Pn* is filtered out at NV31. RIGSURE (left bottom plot) enhanced the signal on NV08 as well, while the MINMAXI denoising method filtered out the *Pn* pulse at this array element.

The summary of the results is presented in Figure 3.4. On the top left of Figure 3.4, blue stars represent the results obtained with forward and reverse Butterworth 3 poles pre-filtering between 0.6 and 4.5 Hz (BUTTERWORTH) when DTV $m_b$ at NV31 and DTV $m_b$ at NV08 are compared. Green triangles are used for comparison between NV31 and NV32 DTV $m_b$ magnitude estimates. Magnitudes at NV08 and NV32 are corrected for each plot using the constants represented on the figure. The middle plots present DTV $m_b$ estimates using wavelet denoising methods: 'MINIMAX' (MINIMAX) at the left, respectively 'RIGSURE' (RIGSURE) at the right. The bottom plot represents 'spectral $m_b$' estimation using CWT. While the standard deviation of magnitude difference between stations ($\sigma$) after BUTTERW0RTH pre-filtering is close to 0.4 magnitude units (m. u) for both pairs of stations, (see Table 1), $\sigma$ a factor of 2 smaller (less than 0.2 m. u.) for spectral magnitude calculations (CWT) as presented in the bottom plots of Figure 3.4 and Table 5.1. The upper right plot presents the NV31 DTV $m_b$ magnitude as a function of the USGS $m_b$ estimates. Red stars are NV31 DTV $m_b$ estimated after Butterworth filtering, the green crosses and 'x' represent NV31 magnitudes estimated after the 'MINIMAX', respectively 'RIGSURE' denoising and the blue triangles represent NV31 magnitudes estimated after applying the CWT pre-filtering methods.

**Table 3.1. The standard deviations of differences of DTV $m_b$ magnitudes between pairs of stations for each method at NVAR.**

| BUTTERWORTH | | MINIMAX | | RIGSURE | | CWT | |
|---|---|---|---|---|---|---|---|
| NV31-NV08 | NV31-NV32 | NV31-NV08 | NV31-NV32 | NV31-NV08 | NV31-NV32 | NV31-NV08 | NV31-NV32 |
| 0.39 | 0.37 | 0.74 | 0.61 | 0.76 | 0.64 | 0.16 | 0.16 |

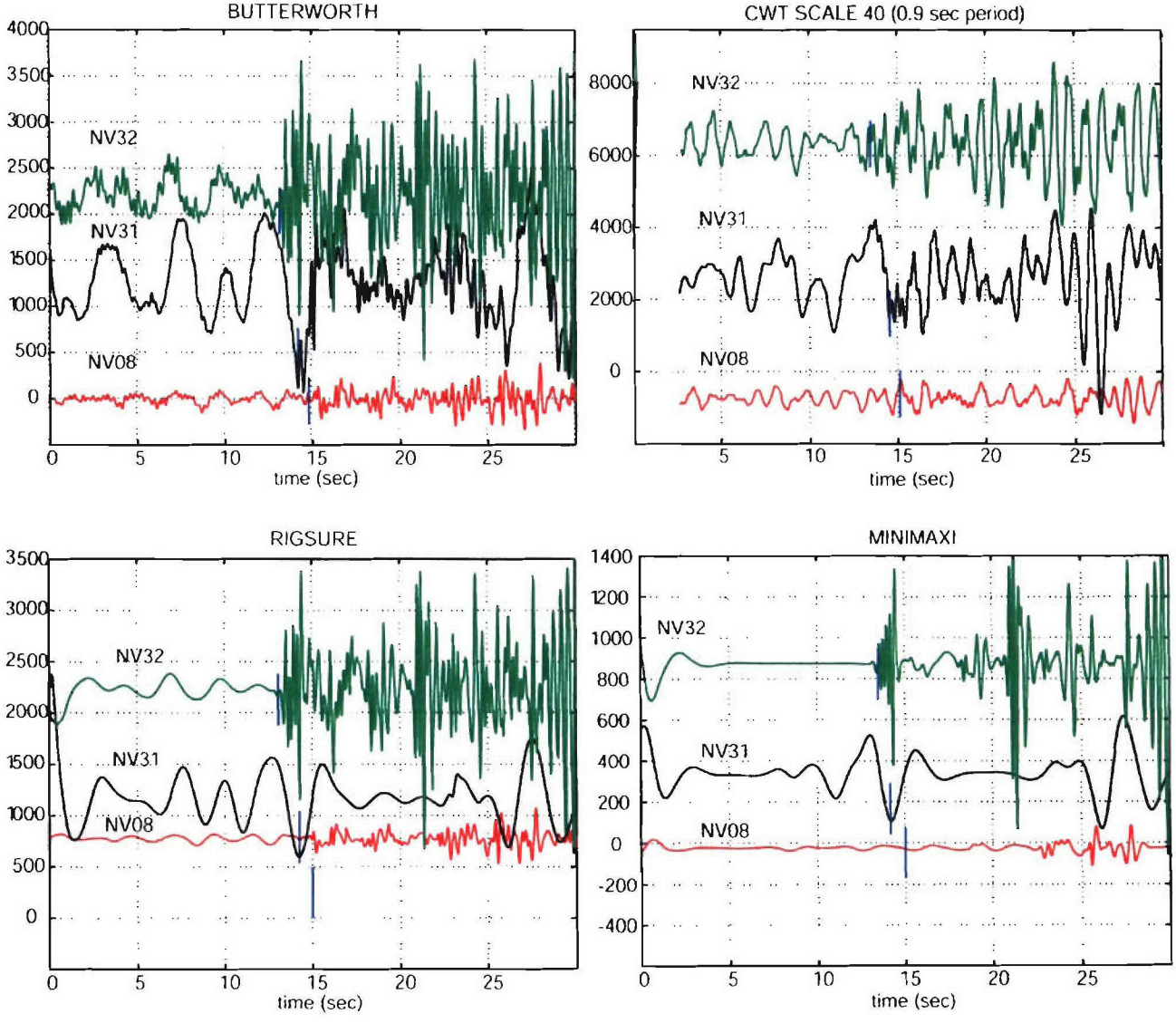


**Figure 3.3. Example of pre-filtering results for the 1999/03/13 13:31:22, $m_b$ =3.6 California event (32.7 N, 116W, 0 km depth) recorded at the NVAR array.**

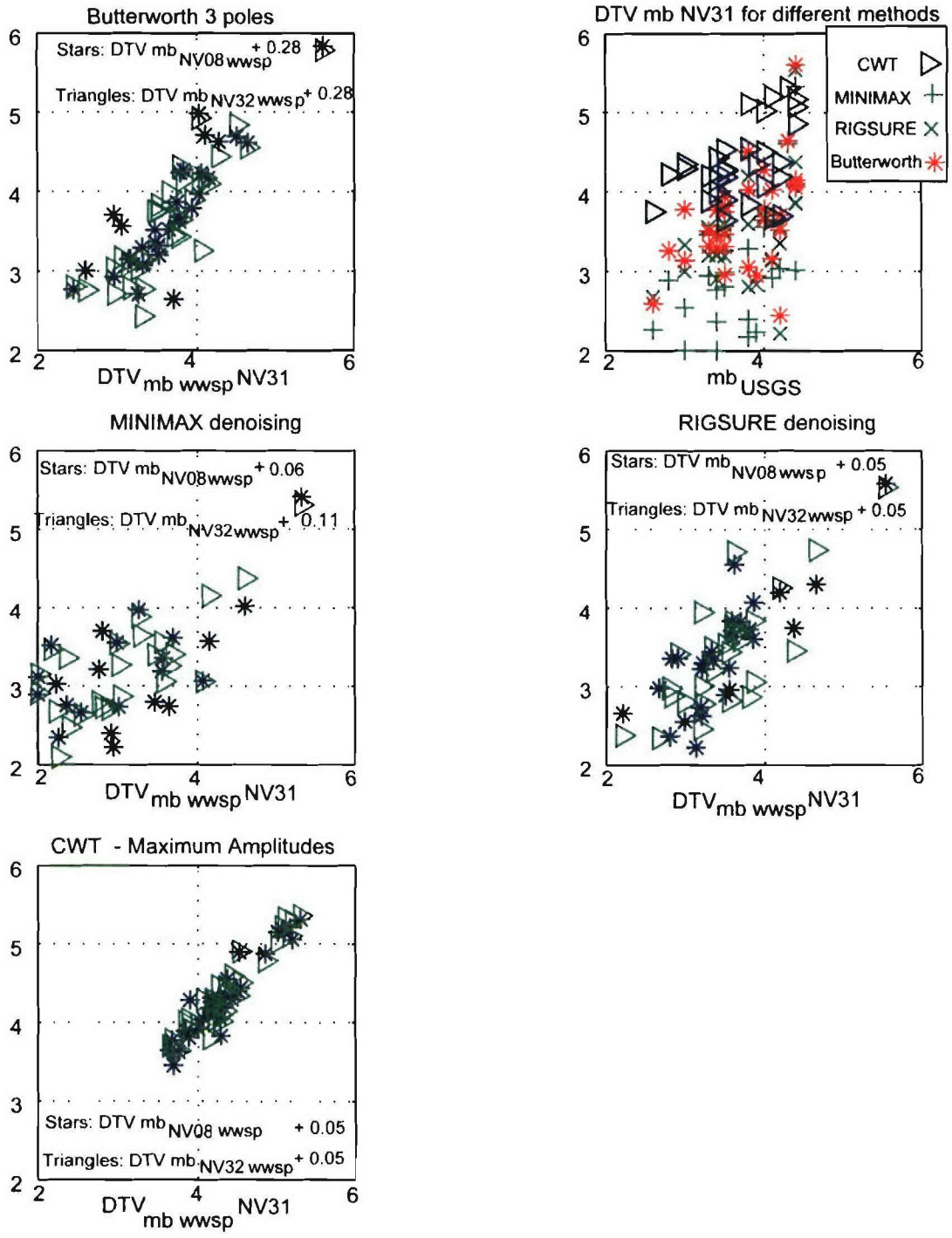


**Figure 3.4. DTV $m_b$ magnitude dependence for each pair of stations (NV31 and NV08 and NV31 and NV32) and for each pre-filtering method is presented in the left upper plot and the three plots below. The right upper plot presents DTV $m_b$ calculated at NV31 for each pre-filtering method as a function of the USGS $m_b$ values**

### The KNET Database

Considering the results for the NVAR database, only the BUTTERWORTH and CWT methods are tested on the KNET database. An example of typical pre-filtering for a nuclear explosion from Lop Nor recorded at KNET is presented in Figure 3.5. The $m_b$ = 6.5 nuclear explosion is detonated at 04:59:57, on 21'st May 1992 at the location of coordinates: 41.513 N and 88.774 E. The BUTTERWORTH method (upper plot), unlike CWT (lower plot), produced more complicated waveforms.

The summary of the results is presented in Figure 3.6. The top left of Figure 3.6 shows the results obtained with forward and reverse Butterworth 3 poles pre-filtering between 0.6 and 10 Hz (BUTTERWORTH) when VC $m_b$ at AAK and VC $m_b$ at all the other stations are compared. The CWT method results are represented in the upper right plot. The magnitudes represented on the vertical axes in the upper plots of Figure 3.5 are calculated for each station as the sum: VC $m_b$ +C1, where C1 is the median value of the difference between the VC $m_b$ at AAK and the VC $m_b$ at the respective station. C1 values used at each station for the BUTTERWORTH and CWT methods are presented in Table 3.2.

**Table 3.2. Constants used to calculate station magnitude in the upper plots of Figure 3.6**

| Method | AML | CHM | EKS2 | KBK | KZA | TKM2 | UCH | ULHL | USP |
|---|---|---|---|---|---|---|---|---|---|
| BUTTERW | 0.08 | 0.09 | 0.09 | -0.39 | -0.2 | -0.30 | -0.07 | 0.17 | 0.05 |
| CWT | 0.05 | 0.04 | -0.02 | -0.44 | -0.17 | -0.36 | -0.13 | -0.08 | 0.07 |

For five of the nine KNET stations compared to AAK the standard deviation of magnitude difference between stations ($\sigma$) after BUTTERW0RTH pre-filtering is larger than $\sigma$ for spectral magnitude calculations (CWT) as presented in the bottom right plot of Figure 3.5. At the stations KBK, TKM2, UCH and ULHL the CWT method had a data spread equivalent to the BUTTERWORTH method.

## DISCUSSION

### The NVAR Database

The magnitude consistency between stations is substantially increased when using the CWT pre-filtering methods and a spectral $m_b$ technique in the case of the NVAR local and regional database. The CWT decomposition, while preserving the sample rate and the shape of the signal is enhancing the *P* arrivals, such that the same arrival is measured at all stations. The best magnitude consistency between stations is obtained for the CWT pre-filtering method. When using this method, the constant for NV31 should be C=-0.7025. Since the magnitude spread is observed to be larger after the WWSP conversion, it is expected that the spread would be even lower for data not converted to WWSP. There is one aspect of the 'spectral mb' method that should be considered pending an opportunity of future studies: the dependence of the spectral DTV $m_b$ of low USGS $m_b$ seems to be not linear anymore (Figures 4 and 6), spectral magnitudes seem to have larger values. This effect could possibly be due to CWT signal enhancement or to imprecise USGS estimates for events smaller than 4 m. u.

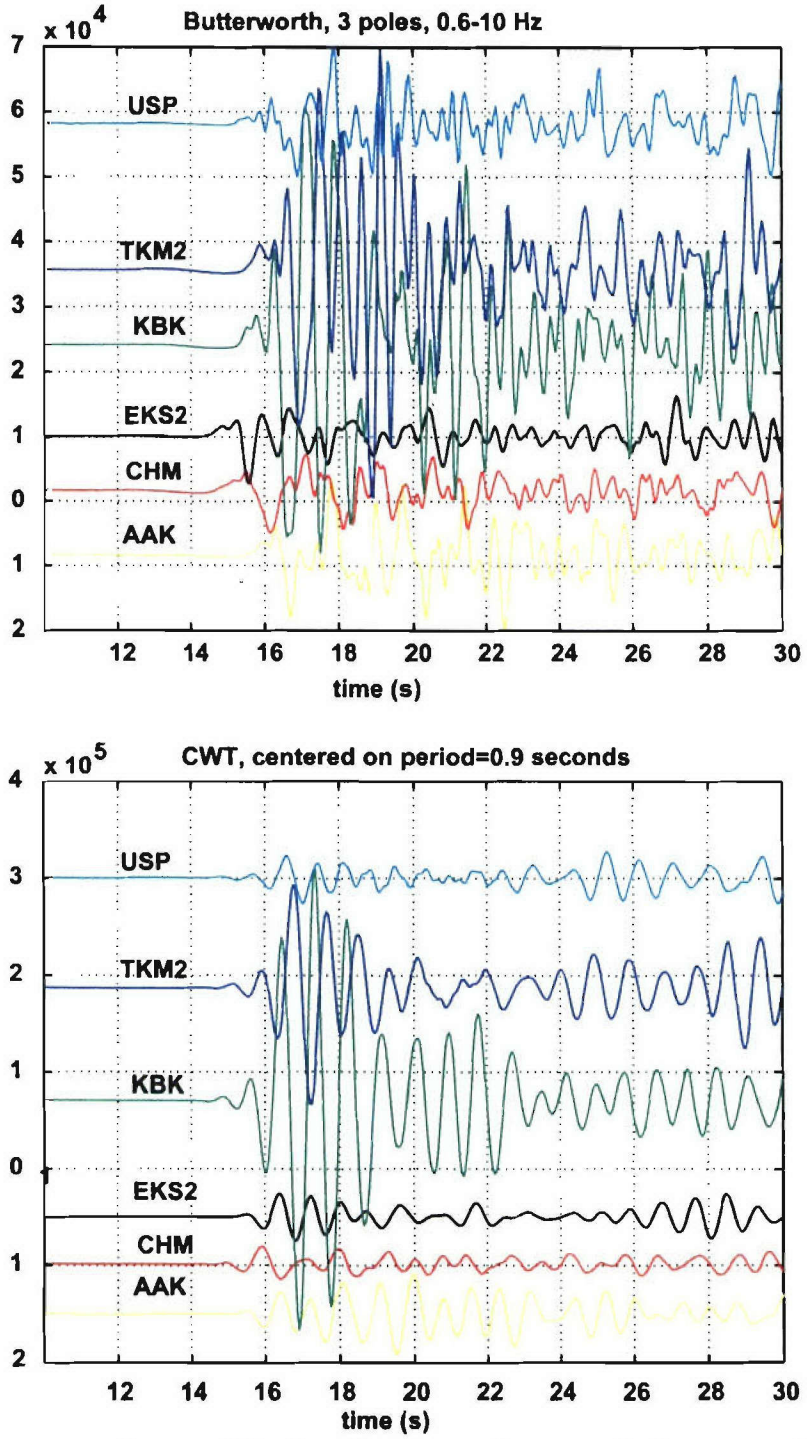


**Figure 3.5. An example pre-filtering for a nuclear explosion recorded at KNET.A Butterworth 3 pole forward and reverse filter is applied on the waveforms in the upper plot. The waveforms are manually aligned on the P phase (around 16 seconds). The maximum amplitude peak to peak in the first 4 seconds of signal is measured at each station.**

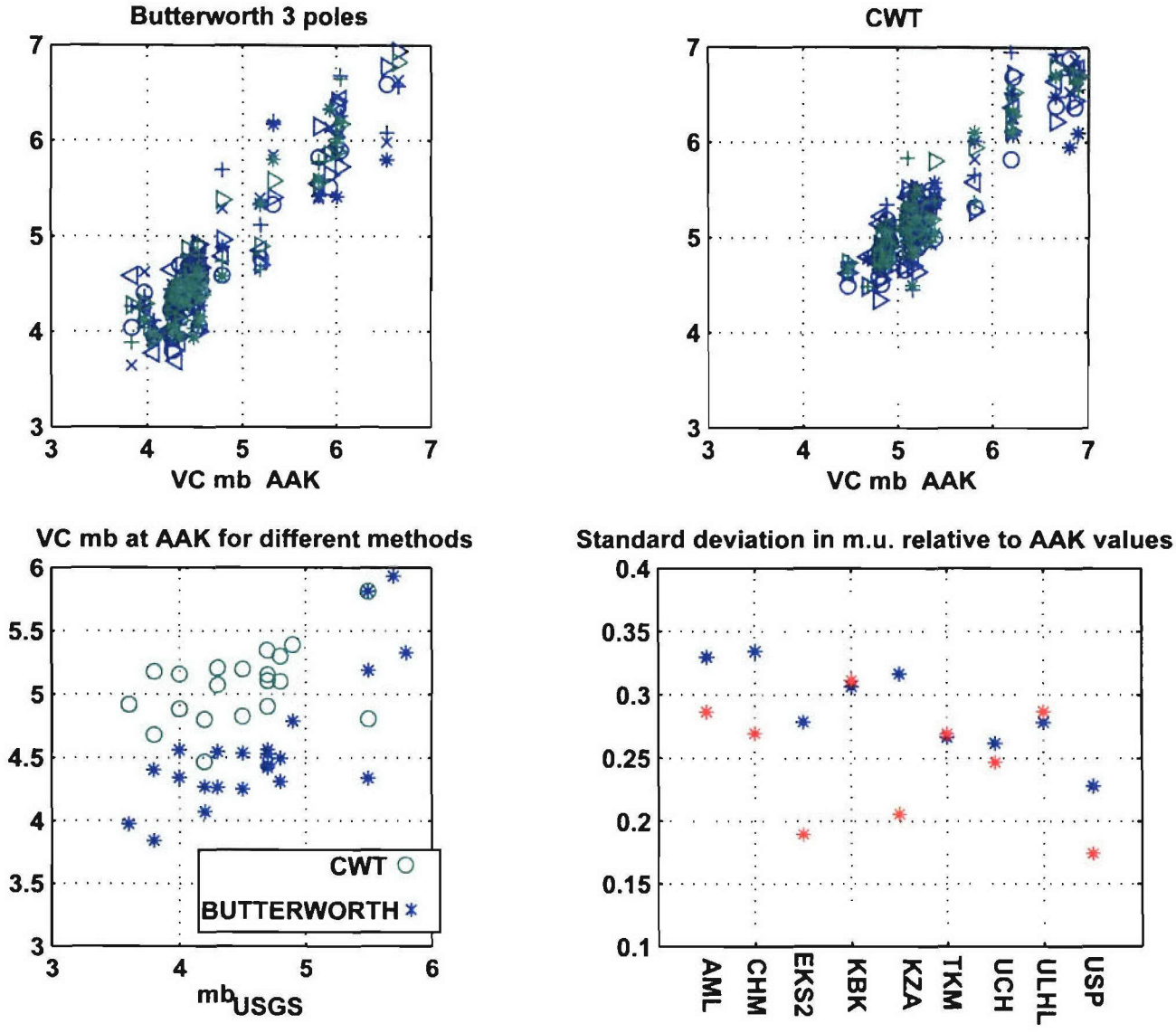


**Figure 3.6. The KNET database results are presented for the BUTTERWORTH (left upper plot) and CWT (right upper plot) methods. In the upper plots, values of the VC body wave magnitude calculated at AML (blue stars), CHM (blue crosses), EKS2 (blue 'x's), KBK (blue right triangles), KZA (blue left triangles), TKM2 (blue circles), UCH (green stars), ULHL (green crosses) and USP (green triangles) are represented as a function of VC body wave magnitude values calculated at AAK. The lower left plot presents VC $m_b$ at AAK as a function of $m_b$ from USGS, as calculated using each method. The lower right plot represents the standard deviation of differences between VC $m_b$ calculated at AAK and each one of the other stations for the CWT (red stars) and BUTTERWORTH (blue stars) methods.**

While preliminary manual denoising produced very encouraging results at NVAR, contrary to the expectations, automatic denoising produced the largest magnitude spread between stations (standard deviations larger than 0.6 m.u, as presented in Table 1). Denoising is a

powerful technique, it unveils and enhances individual arrivals (see Figure 3.3, bottom right plot, waveform at NV32), therefore measurements at different stations are consistent. However, the denoising thresholds, and therefore the amplitudes measured, depend on the length of the time series (time delay between *Pn* and *Pg*, different for each event) and the specific signal-to-noise ratio. When chosen manually, the threshold measurements depend on the analyst's skills and are not easy to reproduce. The SWT transform used for denoising is more stable to translations than CWT. However, for short time series, the SWT denoised signal amplitude still varies significantly for different (small) numbers of samples. Denoising is not recommended as pre-filtering method for amplitude measurements.

**The KNET Database**

Unlike NVAR, the KNET network has an aperture of about 300 km and a wide variety of geological structure beneath stations. Elevation varies from 600 m (on the Kazakh Platform) to 3800 m (in the Northern Tien Shan Mountains). Several major tectonic features are spanned by the network, including a series of thrust faults and ridges.

It is observed that the CWT method did not diminish the data spread at KNET for four stations: KBK, TKM2, UCH and ULHL (Figure 3.6, bottom right plot). Significantly larger amplitudes are consistently observed at the KBK and TKM2 stations (Figure 3.5). This amplitude difference is smaller for 1.3 and 1.5 seconds center periods than for pre-filtering around 1 second center period. According to this observation, a possible explanation of the large amplitudes could be that geological structure near the surface enhances the amplitude at KBK and TKM2. Since both stations are located on mountain slopes, a variation with back azimuth of the amplitude enhancement is also possible, therefore producing magnitude differences between stations. Further investigation could provide an answer to these problems. Large amplitudes are observed also at UCH and ULHL stations, for some of the events. However, while ULHL picks up considerable microseism noise from the Lake Issyk-kul, UCH is a very quiet station. Tibuleac *et. al*, (2003) demonstrated that focusing and defocusing of seismic waveforms in the mantle can produce variations of up to 30% in the seismic amplitudes. It is possible for variations in magnitude between stations to be influenced the presence of specific heterogeneities in the mantle in this region.

It is also observed that consideration of only events with body wave magnitude less than 5.5 diminished the standard deviation of magnitude difference between stations ($\sigma$) with 0.1 m.u., at the AML and CHM stations, for both methods. However, the improvement is not significant for all the other stations.

## CONCLUSIONS

Wavelet pre-processing is compared to conventional pre - filtering for estimation of DTV $m_b$ magnitudes for a selected group of events recorded at the NVAR array and at the KNET network.

The most consistent measurements at all NVAR stations are obtained for the CWT method. Larger values of the spectral $m_b$ magnitudes are observed when compared to small (< 4.0 ) USGS magnitudes. This effect needs to be further quantified.

Denoising procedures for magnitude estimation are not recommended as consistent and easy to reproduce methods.

The CWT method produced the most consistent measurements compared to the BUTTERWORTH method at five of nine stations of the KNET network. Of the stations where improvements are not observed, one, ULHL, is characterized by high microseismic noise. Effects of shallow geological structure combined with focusing/defocusing due to heterogeneity in the upper mantle might affect the amplitudes at the other three stations.

## REFERENCES


Mayeda, K., Hofstetter, A., O'Boyle, J.L., Walter, W.R., 2003, Stable and transportable regional magnitudes based on coda-derived moment-rate spectra, *Bull. Seismol. Soc. Am.*, **93**, 224-239, 2003.

Misiti, M., Misiti, Y., Oppenheim, G. and Poggi, J-M., Wavelet Toolbox User's Guide, (2000), The Mathworks, Inc.

Tibuleac, I. M., Nolet G., C. Michaelson and I. Koulakov, (2003), *P*-wave amplitudes in 3D Earth, *Geophys. J. Int.*, 155, 1-10.

Yakoub, N. K., (1983), "Instantaneous amplitudes": A new method to measure seismic magnitude, *BSSA*, **73,** pp. 1345-1355.

# CHAPTER 4: DEVELOPMENT OF A TIME-DOMAIN, VARIABLE PERIOD SURFACE WAVE MAGNITUDE MEASUREMENT PROCEDURE FOR APPLICATION AT REGIONAL AND TELESEISMIC DISTANCES

*Jessie L. Bonner,[1] David Russell,[2] David G. Harkrider,[1] Delaine T. Reiter,[1] and Robert Herrmann,[3]*

Weston Geophysical Corporation,[1] Air Force Technical Applications Center,[2] St. Louis University[3]

## ABSTRACT

The Russell (2005) surface-wave magnitude formula and the $M_s$(VMAX) measurement technique, discussed in this paper, provide a new method for estimating variable-period surface-wave magnitudes at regional and teleseismic distances. The $M_s$(VMAX) measurement method consists of applying Butterworth band-pass filters to data at center periods between 8 and 25 seconds. The filters are designed to help remove the effects of non-dispersed Airy phases at regional and teleseismic distances. We search for the maximum amplitude in all of the variable-period bands and then use the Russell formula to calculate a surface-wave magnitude.

In this companion paper, we demonstrate the capabilities of the method using applications to three different datasets. The first application utilizes a dataset that consists of large earthquakes in the Mediterranean region. The results indicate that the $M_s$(VMAX) technique provides regional and teleseismic surface-wave magnitude estimates that are in general agreement except for a small distance dependence of -0.002 magnitude units per degree. We also find that the $M_s$(VMAX) estimates are less than 0.1 magnitude unit different than those from other formulas applied at teleseismic distances such as Rezapour and Pearce (1998) and Vaněk *et al.* (1962).

In the second and third applications of the method, we demonstrate that measurements of $M_s$(VMAX) versus $m_b$ provide adequate separation of the explosion and earthquake populations at the Nevada and Lop Nor Test Sites. At the Nevada Test Site, our technique resulted in the misclassification of two earthquakes in the explosion population. We also determined that the new technique reduces the scatter in the magnitude estimates by 25% when compared to our previous studies using a calibrated regional magnitude formula. For the Lop Nor test site, we had no misclassified explosions or earthquakes; however, the data were less comprehensive.

A preliminary analysis of Eurasian earthquake and explosion data suggest that similar slopes are obtained for observed $M_s$(VMAX) versus $m_b$ data with $m_b < 5$. Thus the data are not converging at lower magnitudes. These results suggest that the discrimination of explosions from earthquakes can be achieved at lower magnitudes using the Russell (2005) formula and the $M_s$(VMAX) measurement technique.

## INTRODUCTION

The discrimination of small-to-intermediate magnitude ($3 < m_b < 5$) explosions and earthquakes remains a difficult problem for the nuclear monitoring community. For larger events, the relative difference between the body-wave ($m_b$) and surface-wave ($M_s$) magnitude for a seismic event is one of the best discriminant techniques available at teleseismic distances. The discriminant works because, at a given $m_b$, earthquakes usually generate substantially more surface-wave energy than explosions and thus are characterized by a larger surface-wave magnitude. Difference in focal mechanisms and the near-source material velocity also helps improve the discriminant performance (Stevens and Day, 1985). At regional distances, the measurement of surface-wave amplitudes is complicated due to non-dispersed Airy phases. Hence, a remaining problem for the nuclear monitoring community is to create a seamless relationship between estimating $M_s$ at regional and teleseismic distances for events of a wider range of magnitudes.

Many of the surface wave magnitude scales have been based on empirical formulas of the form:

$$M_s = \log A + B(\Delta) + C, \qquad (4.1)$$

where A is the instrument-corrected ground motion measured in the time domain, usually in nanometers; $B(\Delta)$ is an attenuation term; and C is either a station correction, a term to scale for consistency between magnitude scales, or a path correction. These latter two terms are often determined empirically by averaging across many events at various distances.

The notion of using surface waves to obtain an estimate of source size was first introduced by Gutenberg (1945) using the equation:

$$M_s = \log A + 1.656 \log \Delta - 1.182 + S_c, \qquad (4.2)$$

where A is the amplitude (in nanometers) of the horizontal ground motion at a period of 20 seconds, and Sc is a station correction term. Vaněk *et al.* (1962) improved on this scale by developing a formula that could be used at periods in the vicinity of 20 seconds over any epicentral distance. Thus for any distance $\Delta$ and period T approximately 20 seconds, they proposed the formula:

$$M_s = \log (A/T) + 1.66 \log (\Delta) + 0.3. \qquad (4.3)$$

At distances greater than 25°, the $M_s$ estimates from Gutenberg (1945) and Vaněk *et al.* (1962-also known as the Prague formula) agree within 0.2 magnitude units (m.u.) (Marshall and Basham, 1972). However, considerable problems arose, along with confusion in the literature, when the two scales were applied to both regional and teleseismic events. This led Marshall and Basham (1972) to reformulate the Vaněk *et al.* (1962) formula for use at regional and teleseismic distances; however, a path correction based on dispersion curves for shorter periods (< 20

seconds) was needed to account for Airy phase effects at these distances. Other improvements to empirical formulas have been developed by von Seggern (1977) and Herak and Herak (1993).

Recently, the trend has been to constrain surface-wave magnitude formulas to the theoretical aspects of surface-wave propagation, including dispersion, attenuation, and geometrical spreading. In the frequency domain, Kanamori and Stewart (1976) described the corrected amplitude ($A_c$) for a surface wave at distance $\Delta$ as:

$$A_C = A\sqrt{r_e \sin(\Delta)}e^{\frac{\pi\kappa\Delta}{UQT}}, \quad (4.4)$$

where A is the frequency domain amplitude, $r_e$ is the radius of the earth, $\kappa$ is the degrees to kilometers distance conversion term (111.2 km/deg), U is the group velocity at period T, and Q is the period-dependent quality factor. Okal (1989) used dispersion and attenuation relations to transform Eq. 4.4 into the time domain in order to compare a theoretical distance correction term to empirical terms in the Prague formula. While the theoretical and empirical terms agreed favorably at distances between 20° and 100°, there were discrepancies at regional distances.

Rezapour and Pearce (1998) sought to reconcile these discrepancies by developing a new formula for $M_s$ defined as:

$$M_s = \log\frac{A}{T} + \frac{1}{3}\log(\Delta) + \frac{1}{2}\log(\sin(\Delta)) + 0.0046\Delta + 2.370. \quad (4.5)$$

The Rezapour and Pearce (1998) equation was developed using theoretical aspects of dispersion, including Airy phase propagation, as evidenced by the 1/3 coefficient on the dispersion term, and geometrical spreading. However, because they did not consider frequency-dependent aspects of dispersion, the coefficient is not sufficient to account for dispersion effects at shorter periods (Bonner *et al.*, 2003). The formula was adopted by the prototype International Data Center in 1998 for calculating surface-wave magnitudes at distances between 20 and 100 degrees; however, it is now used by the International Data Centre to determine an $M_s$ for all surface waves recorded at distances less than 100 degrees (Stevens and McLaughlin, 2001).

Russell (2005) developed a time-domain method for measuring surface waves with minimum digital processing, using zero-phase Butterworth filters. The method can effectively measure surface-wave magnitudes at both regional and teleseismic distances, at variable periods between 8 and 25 seconds. For applications over typical continental crusts, the magnitude equation is:

$$M_{s(b)} = \log(a_b) + \frac{1}{2}\log(\sin(\Delta)) + 0.0031\left(\frac{20}{T}\right)^{1.8}\Delta - 0.66\log\left(\frac{20}{T}\right) - \log(f_c) - 0.43, \quad (4.6)$$

where $a_b$ is the amplitude of the Butterworth-filtered surface waves (zero-to-peak in nanometers) and $f_c \leq \frac{0.6}{T\sqrt{\Delta}}$ is the filter frequency of a third-order Butterworth band-pass filter with corner frequencies $1/T$-$f_c$, $1/T$+$f_c$. At the reference period $T$=20 seconds, the equation is equivalent to Von Seggern's formula (1977) scaled to Vaněk *et al.* (1962) at 50 degrees. For periods $8 \leq T \leq 25$, the equation is corrected to $T$=20 seconds, accounting for source effects, attenuation, and dispersion.

The purpose of this paper is to present the results of applying the Russell (2005) formula at teleseismic and regional distances for variable-period data. First, we applied the formula to a large earthquake dataset to demonstrate the analysis method and to determine if the regional and teleseismic magnitudes are unbiased with respect to each other. We compare the resulting magnitudes from the Russell equation with estimates from the Vaněk *et al.* (1962) and Rezapour and Pearce (1998). Then, we used the formula to estimate surface-wave magnitudes for explosions and earthquakes in Eurasia and North America to examine if we can improve discrimination performance.

## METHODOLOGY

The surface-wave magnitude estimation procedure currently employed at most data centers involves measuring the amplitude of surface waves near 20-seconds period. In our past research projects (Bonner *et al.*, 2003), we tried to extend the magnitude estimation to shorter periods (e.g., 7 seconds). We determined that shorter-period surface waves could be used for magnitude estimation for events with smaller $m_b$ values. While the 7-second magnitude scale formed a robust discriminant at the Nevada Test Site (NTS), it failed to provide adequate explosion/earthquake separation at other test sites where the earthquakes were deeper than typical NTS events. This was a primary factor in the development of a measurement technique for variable periods (between 8 and 25 seconds) and magnitude estimation using the Russell (2005) formula. We refer to this technique as VMAX for Variable-period, MAXimum amplitude estimates. In the following paragraphs, we describe how we positively identify Rayleigh wave motion and apply this new magnitude estimation technique.

### Surface Wave Identification

The largest amplitudes of near-regional surface waves for shallow events in North America and Eurasia typically occur at periods less than 20 seconds, and these amplitudes can often be 6 to 10 dB larger than the amplitudes measured at 20 seconds period. Therefore, $M_s$ scales that consider variable-period surface waves will be applicable to lower $m_b$ values. It is important to note that caution must be used to ensure that the measured signals are, in fact, Rayleigh waves and not microseisms, higher-mode energy, or Love wave contamination.

After correcting for the instrument response, we employ a surface-wave processing routine that is designed to positively identify small amplitude, fundamental-mode, Rayleigh-wave motion. The method is applied to all events with $m_b < 4.0$, since the signal-to-noise ratio (SNR) for larger events is great enough that amplitude measurements can be made by band-pass filtering the velocity records and measuring the amplitudes in a group velocity window

indicative of surface waves (2-4 km/sec). We note that this technique can be fully automated in an operational setting so that events of all magnitudes will utilize the same processing technique.

For events with $m_b < 4.0$, we first use the multiple-filter analysis technique (Dziewonski *et al.*, 1969) to generate a group velocity dispersion curve for each event-to-station path. We then overlay the theoretical fundamental- and first-higher mode dispersion curves predicted for the path from the Stevens *et al.* (2001) global shear-wave model. We require overlap (similar to Stevens and McLaughlin, 2001) in the observed dispersion, plus error in the 8 to 25 second period band, with the predicted fundamental-mode dispersion from the Stevens *et al.* (2001) model.

If the event passes the dispersion test, we then determine if the signal has retrograde elliptical particle motion and a back azimuth that is within ± 30 degrees of the true back azimuth. We have followed the methods of Chael (1997) and Selby (2001) to determine the back azimuth that corresponds to the largest positive value, indicative of retrograde elliptical motion, in a covariance matrix formed by the Hilbert-transformed vertical component and the two horizontal components. If a given event passes the dispersion, back azimuth, and particle motion tests, we feel that we have positively identified fundamental-mode Rayleigh waves for the event of interest.

**Butterworth Filtering**

Once we have positively identified the fundamental-mode Rayleigh waves, we apply a series of zero-phase 3rd-order Butterworth filters to the data with the corner frequencies $1/T\text{-}f_c$, $1/T\text{+}f_c$, where $f_c \leq \frac{0.6}{T\sqrt{\Delta}}$. The center periods are placed at 1-second intervals between 8 and 25 seconds. We note that increasing this interval to 3 seconds or lowering it to 0.1 seconds will typically result in less than a 0.05 m.u. change in the resulting magnitude. We construct the envelope function of the filtered signal and measure the maximum zero-to-peak amplitude in a group velocity window between 2.0 and 4.0 km/sec. An analyst then visually confirms that the correct waveform feature is being measured—a benefit of using a time-domain measurement.

In Figure 4.1 we show examples of filter panels from four stations that recorded an $m_b$=5.5 Dodecanese Islands event in August 2004. These four examples highlight characteristics of Rayleigh waves at regional and teleseismic distances that must be considered when developing a variable-period formula at both distances. The Russell (2005) formula has been developed to account for these differences in the excitation, attenuation, and propagation of variable-period surface waves.

For example, station LAST is located only 263 km from the event's epicenter, and its largest surface-wave amplitude occurs at a period of 8 seconds. It is notable that the relative amplitudes for the 20-second surface waves, where typical surface-wave measurements are estimated, are much smaller than the 8-second period waves. If the event had been significantly smaller than $m_b$=5.5, then the 20-second surface waves could have disappeared below the noise

level prior to the 8-second data, and a standard $M_s$ measurement would have been impossible to estimate.

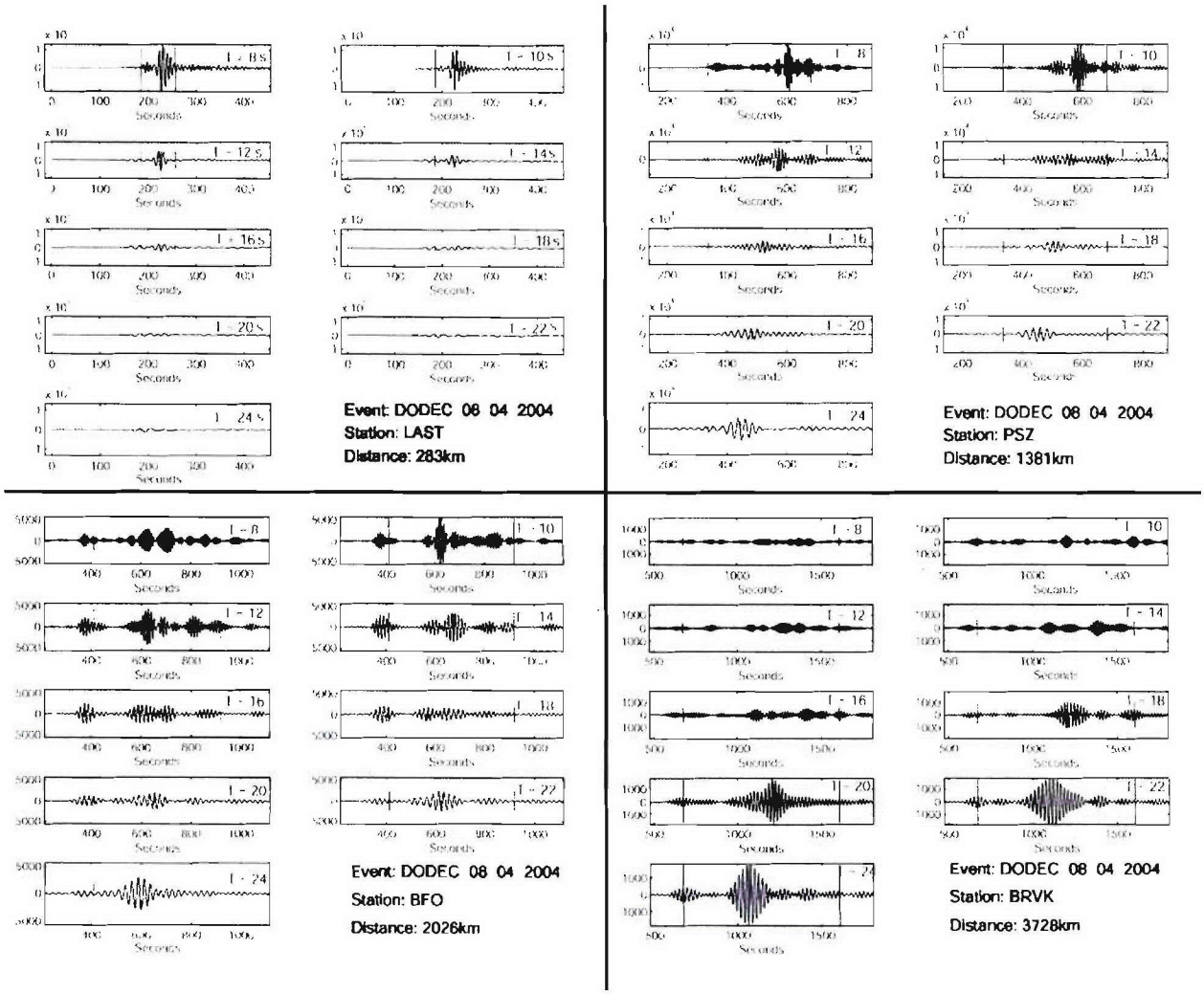


**Figure 4.1. Examples of Butterworth-filtered seismograms for a Dodecanese Islands event recorded at LAST, PSV, BFO, and BRVK. In each subplot, the y-axis is presented with the same amplitude scale. The x-axis is time in seconds from the event origin. Each filter panel has two vertical lines that represent group velocity windows of 2.0 and 4.0 km/sec. The location of the maximum amplitude at each center period is also marked by a thin vertical line.**

However, we point out that even though the maximum amplitude for station LAST is visually observed at a period of 8 seconds in the first subplot of Figure 4.1, an 8-second period may not be considered when we average stations for a final magnitude (as discussed in the following section of this paper). This is because the bandwidth chosen for filtering varies according to the formula $f_c \leq \frac{0.6}{T\sqrt{\Delta}}$, in order to remove the effects of Airy phases. To correct

the variable bandwidth to equivalent spectral amplitudes and thus get the true period of the maximum amplitude, the log amplitude data must be corrected using a $\log(f_c)$ factor. Note that the same amplitude-correction effect is taken into account in Equation 4.6 for magnitude estimation. We find that amplitude correction at station LAST results in a maximum amplitude at a period of 9 seconds, which is the period used to form a network average magnitude.

For station PSZ at 1381 km, the largest amplitude visually occurs at 8-seconds period, and the amplitude difference between the filter bands decreases as the period increases. The decrease in the difference between the shorter and longer-period surface waves results in a period of maximum Airy-corrected amplitude at 25 seconds. After the surface waves have traveled 2026 km to BFO, the filtered amplitudes at periods of 10 seconds are the largest for this event. After correction for the Airy phase filtering term, the period of maximum amplitude becomes 25 seconds. However, when the surface waves arrive at typical teleseismic distances (e.g., station BRVK at 3728 km), the largest amplitude surface waves (both visually and corrected) have a period of 23 seconds.

**Estimating the Magnitude**

We record the maximum amplitude in each of the 18 filter bands and then use Equation 4.6 to calculate a variable-period surface-wave magnitude. As noted in Figure 4.2, 18 different magnitudes are estimated for each station recording the event. For operational purposes, the technique will be simplified to search for the maximum corrected amplitude over all filter bands, thus reducing the number of magnitudes to be calculated from 18 to 1. However, for research purposes, it helps to understand the method to calculate magnitudes for each filter band.

We tried several different techniques to determine the final magnitude from the analysis of surface-wave data presented in Figure 4.2. For instance, for the $M_s$(VMAX) technique, we search the variable-period filtered data to determine the period of the maximum Airy-corrected amplitude. Then we use the uncorrected amplitude at that period for the final magnitude estimation. We use the uncorrected amplitude because of the $\log(f_c)$ term in Equation 4.6. The black large solid circles in Figure 4.2 show the period of the maximum Airy-corrected amplitudes and the magnitudes for the filtered data shown in Figure 4.1. In addition to the $M_s$(VMAX) technique, we have also studied a maximum magnitude technique in which we determine the maximum magnitude over all the estimates in Figure 4.2. Using this method we determined that there was 0.02 magnitude unit increase in the average values.

In another comparison, we calculated a mean magnitude using the magnitude estimates from the 8 to 25 second period band; however, this technique did not work when holes in the earthquake spectra were encountered or when the higher frequency data were attenuated at teleseismic distances. As shown in Figure 4.2, the shorter-period data for station BRVK have been attenuated. Our results will be improperly biased if we average the estimates over the 18 periods. In contrast, by using the period of maximum Airy-corrected amplitude in the $M_s$(VMAX) formula, we are able to diminish any influence that spectral holes or attenuation effects may cause in the magnitude estimation.

As noted in the introduction, another goal of this paper is to demonstrate that the $M_s$(VMAX) formula is valid for both the regional and teleseismic surface-wave estimates. A

regression of the estimates with epicentral distance shows that there is a 0.001 magnitude unit decrease per degree for these four stations that recorded this Dodecanese event on both regional (LAST and PSV) and teleseismic stations (BFO and BRVK).

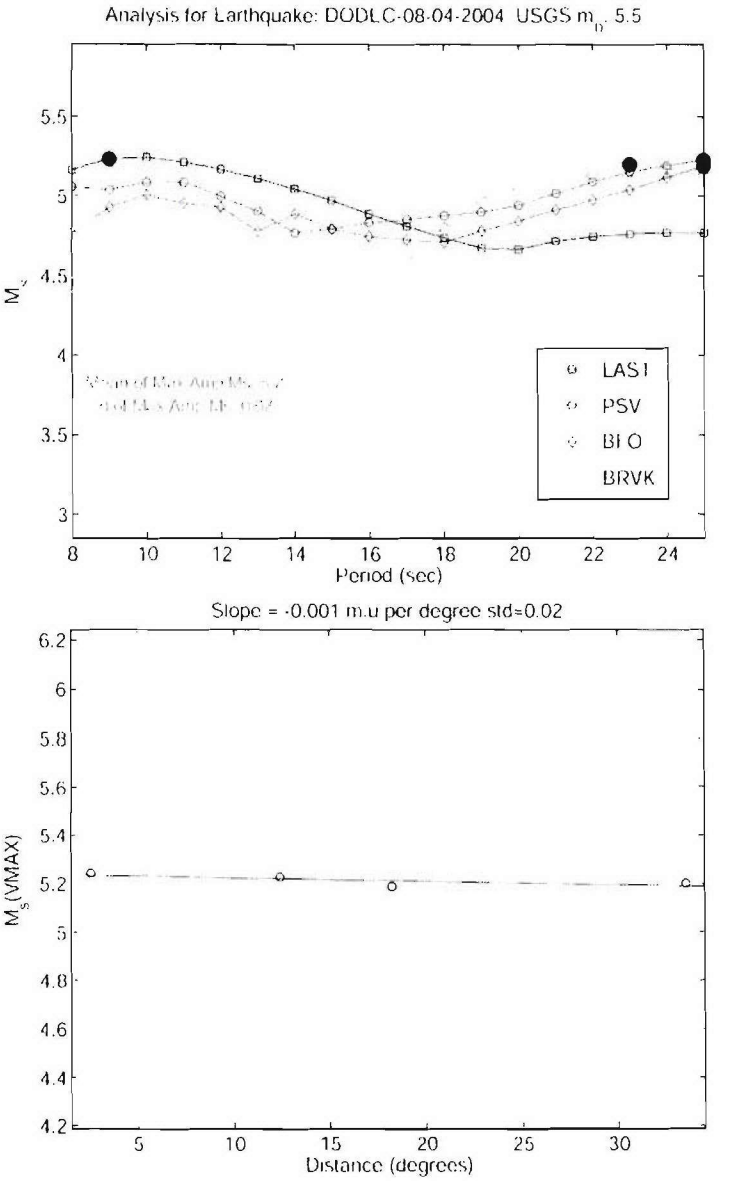


**Figure 4.2. (Top). Example of the magnitude estimation technique $M_s$(VMAX) for the Butterworth band pass filtered data shown in Figure 4.1. The symbols show the magnitudes estimated using Equation 4.6 at each center period. The larger filled circles show the period of maximum amplitude for the filtered seismic data corrected by a log($f_c$) term, and the average and standard deviation of these four estimates are provided. (Bottom). Linear regression of the magnitudes versus distance for the four estimates in the top subplot.**

**Excitation Correction.**

The source spectra for Rayleigh-waves generated from shallow explosions will typically be enriched in short-period surface wave energy. Thus the term 0.66 log ($\frac{20}{T}$) in Equation 4.6 is a source excitation correction. The correction was determined by considering synthetics generated from nuclear explosions at 1 km depth in various crustal velocity structures (as discussed in Bonner *et al.*, 2004). We apply the correction to all events even though it was developed using a shallow explosion assumption. This is essentially the same procedure as Stevens and McLaughlin (2001), except that they used spectral instead of time domain measurements, and derived the source and receiver functions from earth models.

To illustrate the effect of the corrections on our data, we present the $M_s$(VMAX) analysis of three near-regional recordings of Nevada Test Site explosions (Figure 4.3). The upper plot shows the magnitudes calculated using the same techniques presented in Figure 4.2 (e.g., using Equation 4.6). We have applied the excitation correction to these data and determined the magnitude to be 4.13. However, in the lower plot, we did not apply the excitation correction and the enriched short-period energy for the nuclear explosion is evident. We have estimated a magnitude of 4.38 for these uncorrected data which represents a 0.25 magnitude unit increase over the corrected results. Using the uncorrected estimate would result in decreased effectiveness of the $M_s$—$m_b$ discriminant.

The goal of the excitation correction is to flatten the explosion $M_s$ curves across the various periods. We are approaching that goal in Figure 4.3 for near-regional recordings of NTS explosions. To improve upon corrections in other regions, we could use empirically-determined source corrections measured from previous explosions. For this initial test of the method, we have chosen to remain with one standard global correction as opposed to station-specific corrections. That could be considered in the future to further reduce variances in the estimates.

## APPLICATION

We applied the Russell (2005) formula and our $M_s$(VMAX) technique to three different surface-wave datasets. For the first application of the formula, we estimated surface-wave magnitudes for several large earthquakes in the Mediterranean region of Europe. For the second and third applications, we estimated $M_s$(VMAX) for earthquakes and explosions in North America and Eurasia, respectively. And finally, we examined all of the data in Eurasia to determine the performance of the $M_s$—$m_b$ discriminant when our magnitude estimation techniques are used.

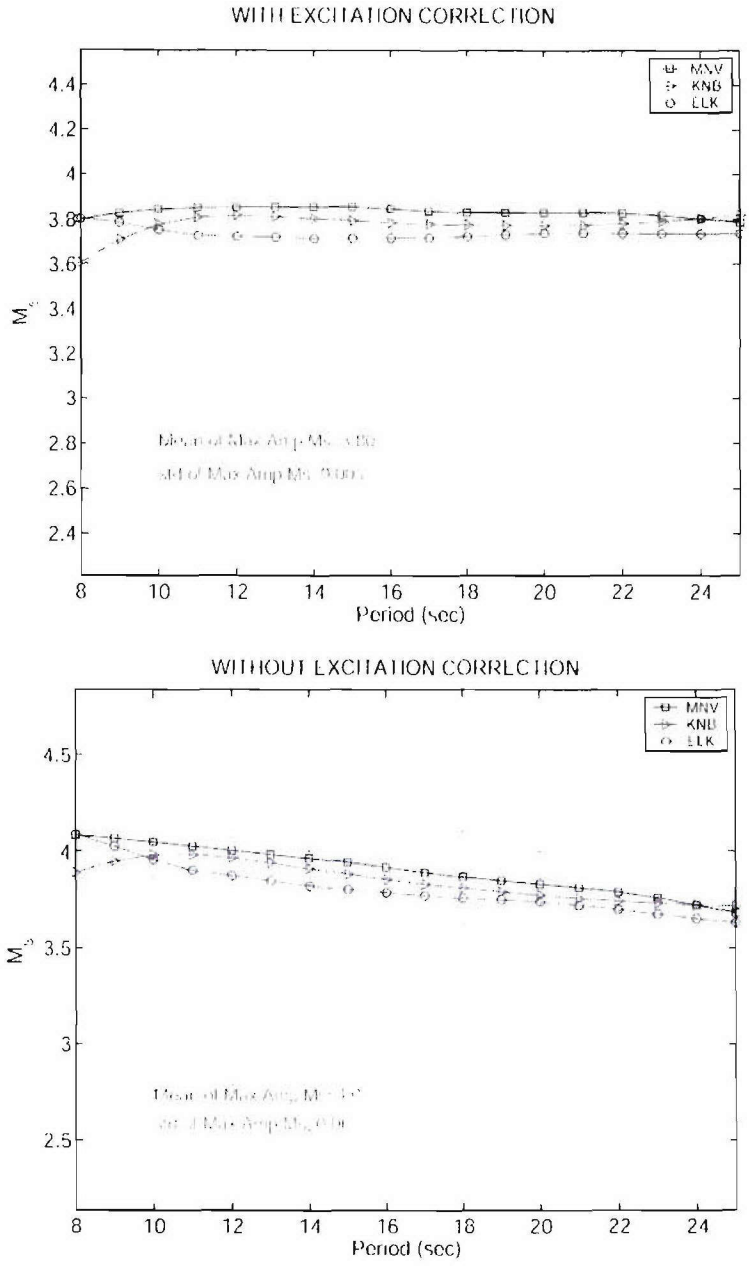


**Figure 4.3. (Top) Example of the magnitude estimation technique $M_S$(VMAX) for the Nevada Test Site explosion Paliza. The excitation correction 0.66 log (20/T) was applied to these magnitude estimates. (Bottom) Estimated $M_S$(VMAX) without applying an excitation correction.**

## Mediterranean Region

We applied the Russell (2005) formula and $M_S$(VMAX) measurement technique to earthquakes in the Mediterranean region to determine if a) we obtain consistent magnitudes at regional and teleseismic distances and b) our $M_S$ estimates match those obtained using the Vaněk *et al.* (1962) and Rezapour and Pearce (1998) formulas.

Data. We developed a database of broadband vertical component recordings of 34 earthquakes that occurred in the Mediterranean region of Europe (Figure 4.4 and Table 4.1). For this pilot study, we focused on larger events ($mb$ > 5.4) with depths of 50 km or less. These restrictions ensured adequate signal-to-noise ratios for the surface waves recorded at regional and teleseismic distances. The data were acquired from the Incorporated Research Institutions for Seismology (IRIS) and consisted of global and regional networks in the study region. The data were all transformed from counts to displacement in nanometers using the Seismic Analysis Code command "transfer" and the SEED response files. The data were decimated from their original sampling rates (> 20 samples/second) to approximately 1 sample/sec for the surface-wave analysis. Down sampling increases the analysis speed and eliminates digital filter problems associated with narrow-band filtering, as discussed in Appendix B of Russell (2005).

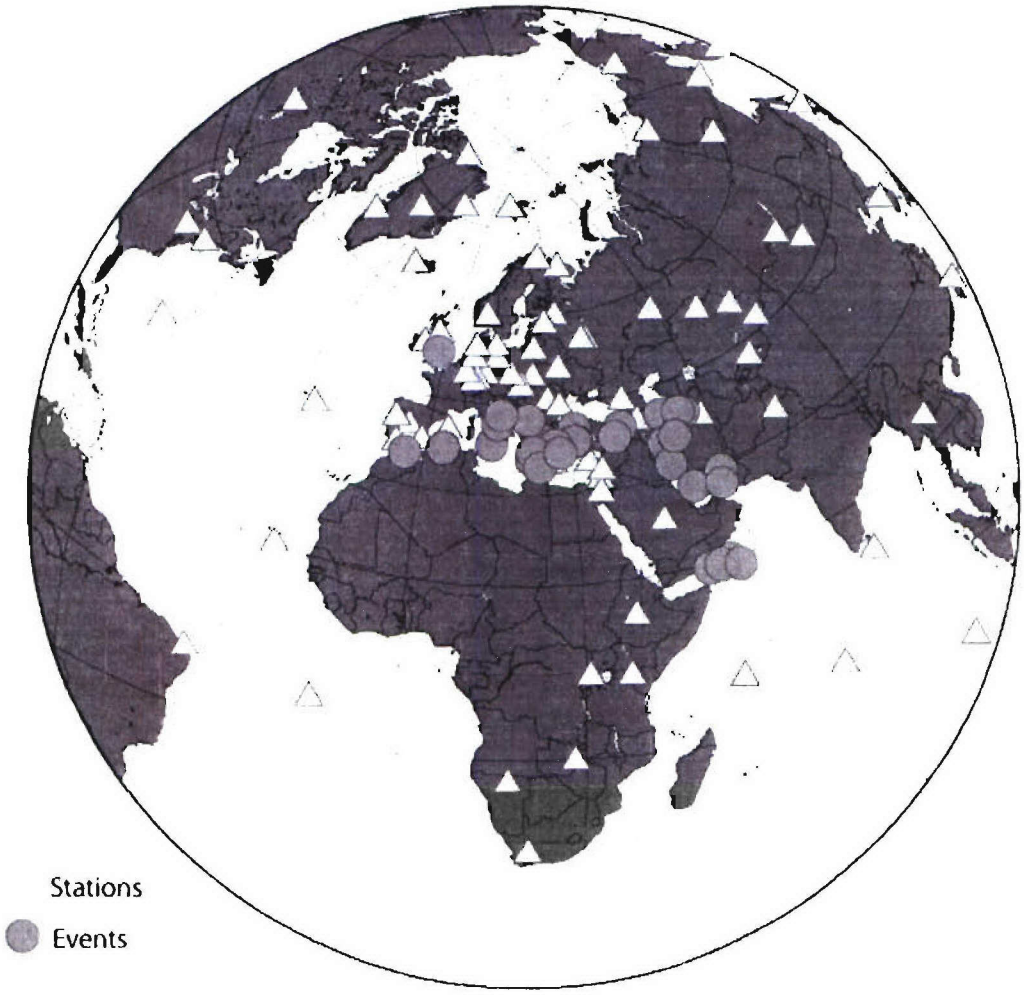


**Figure 4.4. Test dataset of events in the Mediterranean region and stations used to test the Russell (2005) formula and $M_s$(VMAX) measurement technique.**

**Table 4.1. Origin information and $M_s$(VMAX) test results for events in the Mediterranean region.**

| Year | Month | Day | Hour | Minute | Second | Lat | Long | Depth | $m_b$ | $M_s$ (VMAX) | STD | # |
|---|---|---|---|---|---|---|---|---|---|---|---|---|
| 2004 | 08 | 04 | 1 | 7 | 10 | 36.92 | 27.76 | 10 | 5.5 | 5.21 | 0.02 | 44 |
| 2004 | 08 | 11 | 15 | 48 | 21 | 38.38 | 39.25 | 10 | 5.5 | 5.54 | 0.17 | 41 |
| 2004 | 05 | 28 | 0 | 38 | 44 | 36.25 | 51.62 | 17 | 6.3 | 6.34 | 0.20 | 58 |
| 2004 | 05 | 28 | 12 | 38 | 46 | 36.27 | 51.57 | 26 | 6.2 | 6.30 | 0.19 | 46 |
| 2004 | 03 | 01 | 0 | 36 | 02 | 37.22 | 22.26 | 31 | 5.5 | 4.45 | 0.19 | 36 |
| 2004 | 03 | 17 | 5 | 21 | 01 | 34.59 | 23.48 | 25 | 6.1 | 5.71 | 0.2 | 42 |
| 2004 | 03 | 25 | 19 | 30 | 50 | 39.93 | 40.86 | 10 | 5.5 | 5.30 | 0.19 | 45 |
| 2004 | 01 | 14 | 16 | 58 | 51 | 27.7 | 52.31 | 33 | 5.4 | 4.34 | 0.21 | 34 |
| 2004 | 01 | 28 | 9 | 6 | 06 | 26.89 | 57.59 | 10 | 5.4 | 4.57 | 0.23 | 38 |
| 2004 | 02 | 13 | 0 | 41 | 40 | 13.69 | 57.25 | 10 | 5.5 | 4.86 | 0.24 | 35 |
| 2004 | 02 | 24 | 2 | 27 | 46 | 35.14 | -4 | 0 | 6.4 | 6.3 | 0.22 | 42 |
| 2003 | 12 | 26 | 3 | 6 | 17 | 28.86 | 58.32 | 33 | 5.4 | 5.31 | 0.17 | 39 |
| 2003 | 05 | 24 | 1 | 46 | 06 | 14.43 | 53.81 | 10 | 5.8 | 5.49 | 0.23 | 47 |
| 2003 | 04 | 10 | 0 | 40 | 15 | 38.21 | 26.87 | 10 | 5.6 | 5.41 | 0.18 | 33 |
| 2003 | 05 | 27 | 17 | 11 | 29 | 36.94 | 3.58 | 8 | 5.7 | 5.21 | 0.25 | 49 |
| 2003 | 03 | 29 | 17 | 42 | 18 | 43.26 | 15.49 | 33 | 5.5 | 5.14 | 0.24 | 34 |
| 2002 | 10 | 31 | 10 | 32 | 59 | 41.73 | 14.89 | 10 | 5.6 | 5.45 | 0.18 | 29 |
| 2002 | 09 | 06 | 1 | 21 | 28 | 38.37 | 13.72 | 10 | 6.1 | 5.63 | 0.2 | 26 |
| 2002 | 09 | 25 | 22 | 28 | 16 | 32.09 | 49.23 | 33 | 5.5 | 5.00 | 0.22 | 28 |
| 2002 | 08 | 13 | 8 | 37 | 23 | 14.75 | 55.85 | 10 | 5.8 | 5.49 | 0.26 | 49 |
| 2002 | 09 | 01 | 17 | 14 | 59 | 14.25 | 51.81 | 10 | 5.6 | 5.80 | 0.25 | 28 |
| 2002 | 04 | 24 | 10 | 51 | 51 | 42.43 | 21.51 | 10 | 5.5 | 5.42 | 0.19 | 23 |
| 2002 | 06 | 22 | 2 | 58 | 21 | 35.63 | 49.05 | 10 | 6.5 | 6.33 | 0.18 | 59 |
| 2002 | 04 | 17 | 8 | 47 | 22 | 27.61 | 56.76 | 33 | 5.4 | 4.62 | 0.20 | 39 |
| 2002 | 02 | 03 | 7 | 11 | 28 | 38.57 | 31.27 | 5 | 6.5 | 6.38 | 0.22 | 65 |
| 2002 | 02 | 03 | 9 | 26 | 43 | 38.63 | 30.9 | 10 | 5.8 | 5.48 | 0.22 | 68 |
| 2001 | 07 | 26 | 0 | 21 | 38 | 39.06 | 24.34 | 10 | 6.3 | 6.66 | 0.18 | 12 |
| 2001 | 06 | 10 | 1 | 52 | 08 | 39.84 | 53.89 | 34 | 5.6 | 5.00 | 0.25 | 21 |
| 2000 | 11 | 25 | 18 | 9 | 11 | 40.25 | 49.95 | 50 | 6.3 | 6.55 | 0.16 | 48 |
| 2000 | 12 | 06 | 17 | 11 | 06 | 39.57 | 54.8 | 30 | 7 | 7.3 | 0.28 | 69 |
| 2000 | 12 | 15 | 16 | 44 | 45 | 38.61 | 31.06 | 10 | 5.8 | 5.62 | 0.13 | 15 |
| 2000 | 05 | 24 | 5 | 40 | 38 | 36.04 | 22.01 | 33 | 5.7 | 5.57 | 0.16 | 51 |
| 1999 | 11 | 12 | 16 | 57 | 20 | 40.76 | 31.16 | 10 | 7.2 | 7.35 | 0.25 | 55 |

Results. Table 4.1 provides the $M_s$(VMAX) values obtained for the earthquakes in the Mediterranean region. Our first objective in this exercise was to determine if there is a distance dependence in the formula and measurement technique. As mentioned in the introduction of this paper, previous research has been unsuccessful at finding a single, variable-period formula valid at both regional and teleseismic distances.

We performed a distance analysis on all 34 events of our test database similar to the one performed in the lower plot of Figure 4.2. In order to compare events of different magnitudes, we removed the mean magnitude from each event's analysis. Figure 4.5 shows the results,

which include 1,348 $M_S$(VMAX) magnitude estimates from the events listed in Table 4.1. Our objective was to test the formula for a predominance of continental paths, thus data are at distances less than 70 degrees. A linear regression of the mean-removed magnitude estimates with increasing distance shows a small (0.002 magnitude unit per degree) decrease in magnitudes. The standard deviation for the regression analysis is 0.21 magnitude unit (m.u.). This suggests that if an event had an $M_S$(VMAX) magnitude estimate of 6.0 measured at a distance of 5 degrees, the magnitude estimated at a distance of 60 degree would be ~5.89. This difference is well within the scatter typically observed for surface-wave magnitude estimates resulting from focal mechanisms and path effects.

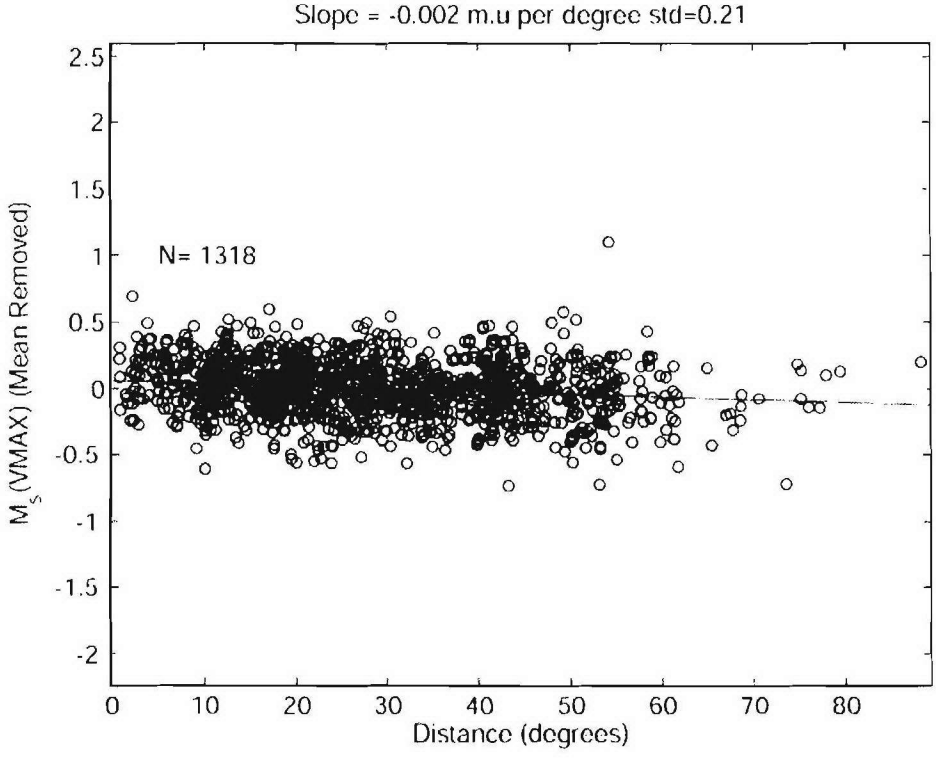


**Figure 4.5. Regression of mean-removed $M_S$(VMAX) magnitude estimates for the 34 events in Table 4.1 with distance. There is a very small decrease in magnitudes units (0.002 m.u. per degree) with increasing distance.**

Because $M_S$(VMAX) is a variable-period technique, we also examined the periods at which the estimates were formed (Figure 4.6). There is a general increase in the number of measurements in each bin from shorter to longer periods. This increase is reassuring, since it is consistent with past studies which found that the best period range to measure $M_s$ is between 17 and 23 seconds.

We observe an edge effect associated with ending the surface-wave magnitude analysis at 25 seconds. There are two explanations for this behavior. Because of the spectral shape of earthquakes, they will tend to select longer periods, especially when the events are deeper than the upper crust. In addition, because of the nature of surface wave propagation, we would expect to see a general trend of longer period measurements with increasing distances. This trend is

related to the rapid attenuation of shorter-period amplitudes compared to the longer periods at longer epicentral distances. In Figure 4.6, we plotted the distances and periods at which the magnitudes were estimated. The plot shows that for the magnitudes estimated at periods of 10 seconds or less, the corresponding epicentral distances were less than 30 degrees. From 10 to 18 seconds, we note a general increase in the cut-out distance from 30 to 60 degrees. For periods greater than 18 seconds, we note that the cut-out distance continues to increase but is less constrained by the available data. The results in Figure 4.6 suggest that the formula is behaving as we intended. It also hints that the analysis could be improved by increasing the long-period limit to periods greater than 25 seconds.

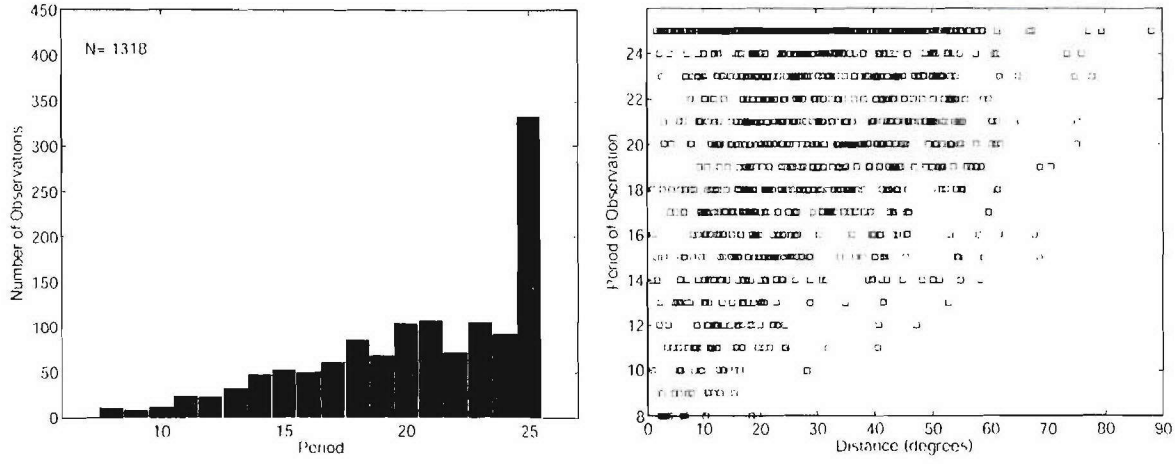


**Figure 4.6. (Left). Bins showing the periods used to estimate the $M_s$(VMAX) magnitudes at 1348 different station-source pairs. (Right). Comparison of the periods of the $M_s$(VMAX) estimates compared to the epicentral distance.**

As a final step in the analysis of the events in Table 4.1, we compared our $M_s$(VMAX) estimates to magnitude estimates published by the United States Geological Survey (USGS) and the International Data Center (IDC) in Vienna, and to the $M_w$ estimates obtained from Harvard's Centroid Moment Tensor (CMT) analysis. The results are shown in Figure 4.7. We note that the USGS uses the Vaněk *et al.* (1962) formula, while the IDC uses the Rezapour and Pearce (1998) formula. We performed a fixed slope (slope=1) regression of the $M_s$(VMAX) estimates against the results from the other organizations to determine the offset between the estimates. The results indicate that the $M_s$(VMAX) is -0.03 and 0.05 magnitude units different than the Vaněk *et al.* (1962) and Rezapour and Pearce (1998) formulas, respectively. Differences of this size for all three comparisons are well within the scatter of the observations. Also, the bottom subplot of Figure 4.7 shows that the $M_s$(VMAX) and $M_w$ estimates are approximately equal for $6.0 < M_w < 7.2$.

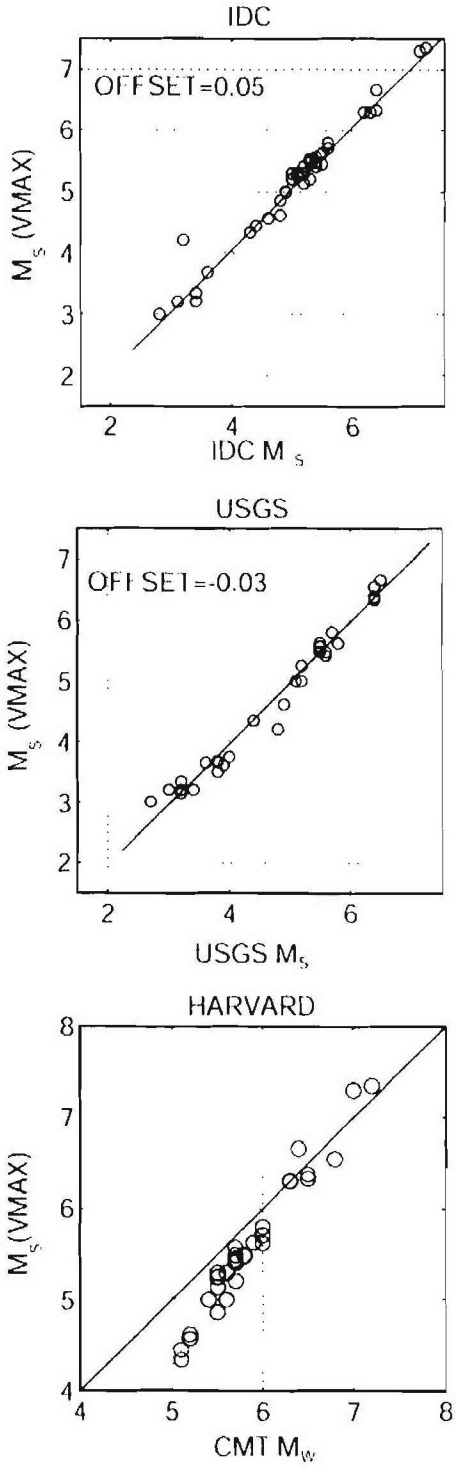


**Figure 4.7. (Top). Fixed slope (slope=1) regression of $M_s$(VMAX) network-average magnitudes versus the IDC $M_s$ for the Mediterranean events. (Middle). Fixed slope (slope=1) regression of $M_s$(VMAX) network-average magnitudes versus the USGS $M_s$. (Bottom). Comparison of the $M_s$(VMAX) network-average magnitudes versus the Harvard CMT $M_w$s.**

**Nevada Test Site Earthquake and Explosion Discrimination.**

We next examined the performance of the Russell (2005) formula and $M_s$(VMAX) measurement technique on earthquake and explosion discrimination at the Nevada Test site in the western United States.

Data. We developed a test dataset consisting of explosions and earthquakes in the western United States. The explosion data are vertical-component, digital broadband seismograms from NTS explosions recorded on two or more stations of the Lawrence Livermore Regional Seismic network (henceforth referred to as LNN). The LNN network consists of seismic stations at Landers, California (LAC); Mina, Nevada (MNV); Elko, Nevada (ELK); and Kanab, Utah (KNB), and has been in operation since the 1960's (Figure 4.8). All data were converted from counts to displacement in nanometers using the Seismic Analysis Code (SAC) "transfer" command and pole-zero files.

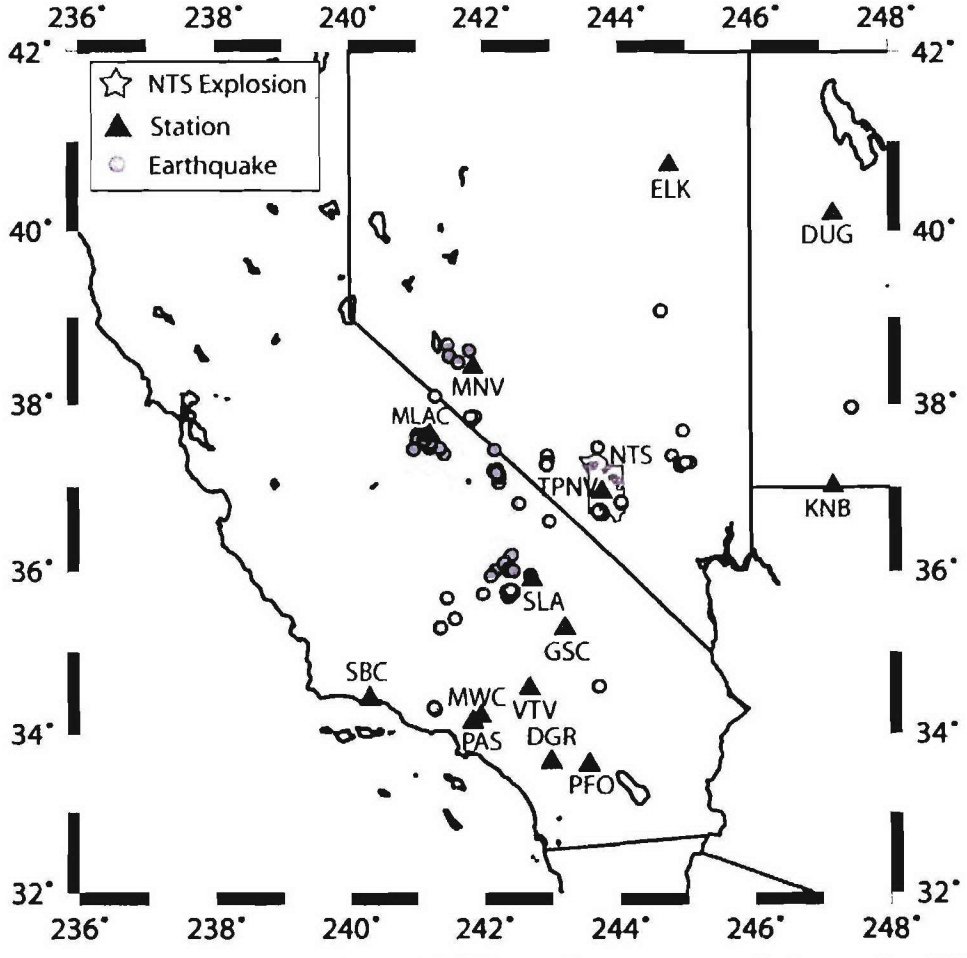


**Figure 4.8. Test dataset consisting of NTS explosions recorded on the LNN dataset together with western United States earthquakes recorded on at least one LNN station and other regional networks.**

We estimated $M_s$ (VMAX) for NTS explosions that occurred between December 1968 and September 1992. Our primary focus was on the 198 NTS explosions that were detonated

after August 1979, when digital data became available from the LNN stations. Of these 198 events, 133 had useable data, of which sixty-five (65) either had no available LNN data, were plagued by untimely data dropouts and glitches, or were too small for measurable surface-wave energy. We also analyzed 21 explosions detonated prior to July 1979 that were digitized from analog records, in order to compare our new results with previous $M_s$ studies completed by Yacoub (1983), Marshall *et al.* (1979), Stevens and Murphy (2001), and Woods and Harkrider (1995). In addition to the explosion dataset, we also estimated the $M_s$ and $m_b$ magnitudes for 69 earthquakes whose locations are shown as gray circles in Figure 4.8. These events were recorded on various networks in the region; however, we ensured that at least one LNN station recorded the event. This requirement allowed us to measure an unbiased $m_b$ using the Denny *et al.* (1987; 1989) *Pn* magnitude scale. Many of the $m_b(Pn)$*'s* used in this study were taken from Vergino and Mensing (1989) or Patton (2001).

**Results.** Table 4.2 provides the $M_s$(VMAX) estimates and standard deviations for the explosions on the Nevada Test Site. We compared the $M_s$(VMAX) measurements for the 154 explosions to the single 7-second period measurements from our previous research. Figure 4.9 shows that the $M_s$(VMAX) explosion magnitudes are approximately 0.25 m.u. larger than the regionally-calibrated Marshall and Basham $M_s$(7) estimates from Bonner *et al.* (2003). The slope of the best fit line between the two datasets is approximately equal to 1. The $M_s$(VMAX) methodology resulted in a 25% reduction of the variance for the explosions over the previous single-period techniques.

**Table 4.2. $M_s$(VMAX) test results for explosion on the Nevada Test Site**

| Date | Name | $m_b$ | $M_s$ (VMAX) | std | # |
|---|---|---|---|---|---|
| 1968354 | Benham | 6.49 | 5.88 | 0.21 | 3 |
| 1969302 | Calabash | 5.5 | 4.46 | 0.05 | 2 |
| 1970085 | Handley | 6.57 | 5.78 | 0.04 | 4 |
| 1970146 | Flask | 5.47 | 4.17 | 0.09 | 4 |
| 1970351 | Carpetbag | 5.79 | 4.69 | 0.14 | 4 |
| 1972265 | Osocurro | 5.6 | 4.47 | 0.06 | 3 |
| 1972270 | Delphinium | 4.54 | 2.69 | 0.08 | 3 |
| 1973116 | Starwort | 5.49 | 4.05 | 0.04 | 4 |
| 1973157 | Alemendro | 6.23 | 5.33 | 0.19 | 3 |
| 1974191 | Escabosa | 5.54 | 4.59 | 0.04 | 2 |
| 1975059 | Topgallant | 5.7 | 4.44 | 0.05 | 4 |
| 1975154 | Stilton | 6.03 | 4.77 | 0.06 | 4 |
| 1975154 | Mizzen | 5.66 | 4.52 | 0.03 | 4 |
| 1975170 | Mast | 6.24 | 5.18 | 0.12 | 4 |
| 1975324 | Inlet | 6.01 | 5.03 | 0.13 | 4 |
| 1975354 | Chiberta | 5.76 | 4.62 | 0.05 | 4 |
| 1976035 | Keelson | 5.61 | 4.41 | 0.04 | 4 |
| 1976035 | Esrom | 5.69 | 4.59 | 0.06 | 3 |
| 1976045 | Cheshire | 6.13 | 5.18 | 0.07 | 4 |
| 1976069 | Estuary | 6.09 | 5.25 | 0.13 | 4 |
| 1976077 | Strait | 5.87 | 4.81 | 0.09 | 3 |
| 1979215 | Burzet | 4.78 | 3.14 | 0.08 | 3 |
| 1979220 | Offshore | 4.85 | 3.38 | 0.04 | 3 |

| 1979241 | Nessel | 4.93 | 3.41 | 0.14 | 4 |
|---|---|---|---|---|---|
| 1979249 | Hearts | 5.83 | 4.67 | 0.02 | 4 |
| 1979269 | Sheepshead | 5.73 | 4.60 | 0.05 | 4 |
| 1980059 | Tarko | 4.43 | 3.12 | 0.16 | 3 |
| 1980094 | Liptauer | 4.9 | 3.15 | 0.28 | 4 |
| 1980107 | Pyramid | 5.45 | 4.28 | 0.20 | 4 |
| 1980117 | Colwick | 5.66 | 4.60 | 0.05 | 4 |
| 1980123 | Canfield | 4.38 | 2.84 | 0.03 | 3 |
| 1980164 | Kash | 5.61 | 4.67 | 0.04 | 3 |
| 1980176 | Huron King | 4.2 | 2.45 | 0.10 | 3 |
| 1980207 | Tafi | 5.8 | 4.70 | 0.05 | 4 |
| 1980213 | Verdello | 4.12 | 2.67 | 0.14 | 2 |
| 1980269 | Bonarda | 4.5 | 2.44 | 0.16 | 4 |
| 1980298 | Dutchess | 4.43 | 3.00 | 0.12 | 4 |
| 1980305 | Miners Iron | 4.65 | 3.34 | 0.12 | 4 |
| 1980319 | Dauphin | 4.39 | 3.01 | 0.07 | 4 |
| 1980352 | Serpa | 5.26 | 4.05 | 0.06 | 4 |
| 1981015 | Baseball | 5.56 | 4.41 | 0.02 | 4 |
| 1981149 | Aligote | 4.19 | 2.75 | 0.06 | 3 |
| 1981157 | Harzer | 5.62 | 4.42 | 0.09 | 4 |
| 1981191 | Niza | 4.18 | 2.58 | 0.06 | 4 |
| 1981239 | Islay | 3.96 | 2.40 | 0.03 | 2 |
| 1981247 | Trebbiano | 3.98 | 2.12 | 0.11 | 4 |
| 1981274 | Paliza | 5.12 | 3.80 | 0.01 | 3 |
| 1981315 | Tilci | 4.9 | 3.41 | 0.12 | 4 |
| 1981316 | Rousanne | 5.38 | 4.17 | 0.05 | 4 |
| 1981337 | Akavi | 4.7 | 3.23 | 0.18 | 4 |
| 1981350 | Caboc | 4.53 | 2.80 | 0.10 | 4 |
| 1982028 | Jornada | 5.76 | 4.65 | 0.04 | 4 |
| 1982043 | Molbo | 5.48 | 4.42 | 0.15 | 4 |
| 1982043 | Hosta | 5.76 | 4.45 | 0.06 | 4 |
| 1982107 | Tenaja | 4.49 | 2.95 | 0.09 | 4 |
| 1982115 | Gibne | 5.47 | 4.42 | 0.04 | 4 |
| 1982126 | Kryddost | 4.19 | 2.48 | 0.06 | 2 |
| 1982127 | Bouschet | 5.66 | 4.28 | 0.05 | 4 |
| 1982167 | Kesti | 4.01 | 2.33 | 0.03 | 3 |
| 1982175 | Nebbiolo | 5.73 | 4.57 | 0.09 | 4 |
| 1982210 | Monterey | 4.68 | 2.86 | 0.23 | 4 |
| 1982217 | Atrisco | 5.82 | 4.71 | 0.07 | 4 |
| 1982266 | Frisco | 4.9 | 3.49 | 0.13 | 3 |
| 1982266 | Huron Landing | 4.88 | 3.35 | 0.11 | 3 |
| 1982316 | Seyval | 4.18 | 2.35 | 0.01 | 2 |
| 1982344 | Manteca | 4.72 | 3.10 | 0.10 | 4 |
| 1983085 | Cabra | 5.36 | 4.12 | 0.04 | 3 |
| 1983104 | Turquoise | 5.64 | 4.18 | 0.05 | 4 |
| 1983112 | Armada | 4.15 | 2.33 | 0.25 | 3 |
| 1983125 | Crowdie | 4.37 | 2.65 | 0.09 | 3 |
| 1983146 | Fahada | 4.52 | 3.21 | 0.07 | 4 |
| 1983160 | Danablu | 4.73 | 2.80 | 0.02 | 2 |

| | | | | | |
|---|---|---|---|---|---|
| 1983215 | Laban | 4.48 | 2.59 | 0.14 | 2 |
| 1983223 | Sabado | 4.17 | 2.46 | 0.18 | 3 |
| 1983239 | Jarlsberg | 3.87 | 2.27 | 0.20 | 2 |
| 1983244 | Chancellor | 5.52 | 4.22 | 0.11 | 3 |
| 1983264 | MidniteZ | 4.04 | 2.66 | 0.21 | 4 |
| 1983265 | Techado | 4.2 | 2.48 | 0.08 | 4 |
| 1983350 | Romano | 4.97 | 3.77 | 0.07 | 3 |
| 1984031 | Gorbea | 4.51 | 2.79 | 0.11 | 4 |
| 1984061 | Tortugas | 5.82 | 4.51 | 0.03 | 3 |
| 1984091 | Agrini | 4.35 | 2.60 | 0.15 | 2 |
| 1984122 | Mundo | 5.47 | 4.38 | 0.04 | 2 |
| 1984152 | Caprock | 5.61 | 4.51 | 0.09 | 3 |
| 1984207 | Kappeli | 5.62 | 4.40 | 0.10 | 3 |
| 1984215 | Correo | 4.57 | 2.91 | 0.06 | 4 |
| 1984243 | Dolcetto | 4.49 | 3.15 | 0.11 | 3 |
| 1984257 | Breton | 4.98 | 3.64 | 0.05 | 4 |
| 1984276 | Vermejo | 4.28 | 2.62 | 0.03 | 2 |
| 1984344 | Egmont | 5.51 | 4.32 | 0.12 | 4 |
| 1984350 | Tierra | 5.64 | 4.36 | 0.12 | 4 |
| 1985074 | Vaughn | 4.42 | 3.09 | 0.07 | 3 |
| 1985096 | Misty Rain | 4.7 | 3.44 | 0.08 | 4 |
| 1985122 | Towanda | 5.63 | 4.48 | 0.07 | 4 |
| 1985163 | Salut | 5.62 | 4.49 | 0.03 | 4 |
| 1985206 | Serena | 5.48 | 4.48 | 0.18 | 3 |
| 1985270 | Ponil | 4.49 | 3.15 | 0.10 | 4 |
| 1985282 | Diamond Beech | 4.01 | 2.42 | 0.09 | 4 |
| 1985289 | Roquefort | 4.62 | 3.07 | 0.06 | 4 |
| 1985339 | Kinibito | 5.6 | 4.26 | 0.06 | 3 |
| 1985362 | Goldstone | 5.45 | 4.28 | 0.01 | 4 |
| 1986081 | Glencoe | 5.41 | 3.74 | 0.09 | 3 |
| 1986100 | Mighty Oak | 4.93 | 3.52 | 0.05 | 2 |
| 1986112 | Jefferson | 5.48 | 4.42 | 0.14 | 3 |
| 1986141 | Panamint | 3.78 | 2.33 | 0.04 | 3 |
| 1986156 | Tajo | 5.29 | 4.18 | 0.00 | 1 |
| 1986176 | Darwin | 5.58 | 4.41 | 0.05 | 3 |
| 1986198 | Cybar | 5.57 | 4.51 | 0.02 | 3 |
| 1986205 | Cornucopia | 4.3 | 2.61 | 0.08 | 3 |
| 1986247 | Galveston | 3.71 | 2.50 | 0.08 | 2 |
| 1986273 | Labquark | 5.54 | 4.50 | 0.04 | 2 |
| 1986289 | Belmont | 5.56 | 4.52 | 0.05 | 3 |
| 1986318 | Gascon | 5.58 | 4.43 | 0.00 | 1 |
| 1986347 | Bodie | 5.52 | 4.55 | 0.00 | 1 |
| 1987042 | Tornero | 4.24 | 2.40 | 0.07 | 3 |
| 1987077 | Middle Note | 4.22 | 2.67 | 0.01 | 2 |
| 1987108 | Delamar | 5.51 | 4.40 | 0.07 | 3 |
| 1987120 | Hardin | 5.54 | 4.53 | 0.07 | 3 |
| 1987169 | Brie | 4.15 | 2.38 | 0.04 | 3 |
| 1987225 | Tahoka | 5.72 | 4.58 | 0.00 | 1 |
| 1987267 | Lockney | 5.61 | 4.60 | 0.07 | 2 |

| | | | | | |
|---|---|---|---|---|---|
| 1988046 | Kernville | 5.48 | 4.30 | 0.11 | 3 |
| 1988134 | Schellbourne | 4.77 | 3.36 | 0.03 | 3 |
| 1988142 | Laredo | 4.27 | 2.75 | 0.10 | 4 |
| 1988154 | Comstock | 5.58 | 4.34 | 0.02 | 2 |
| 1988189 | Alamo | 5.78 | 4.64 | 0.19 | 3 |
| 1988230 | Kearsarge | 5.64 | 4.41 | 0.10 | 4 |
| 1988243 | Bullfrog | 5.04 | 3.57 | 0.06 | 4 |
| 1988287 | Dalhart | 5.67 | 4.59 | 0.05 | 4 |
| 1988345 | Misty Echo | 4.79 | 3.48 | 0.00 | 1 |
| 1989041 | Texarkana | 5.32 | 3.99 | 0.02 | 3 |
| 1989055 | Kawich-Red | 4.41 | 2.47 | 0.14 | 3 |
| 1989068 | Ingot | 4.86 | 3.52 | 0.07 | 3 |
| 1989135 | Palisade-1 | 4.55 | 2.71 | 0.07 | 3 |
| 1989146 | Tulia | 3.7 | 2.23 | 0.12 | 3 |
| 1989173 | Contact | 5.43 | 4.26 | 0.08 | 3 |
| 1989178 | Amarillo | 5.03 | 3.58 | 0.21 | 3 |
| 1989257 | Disko Elm | 4.04 | 2.40 | 0.17 | 4 |
| 1989304 | Hornitos | 5.83 | 4.40 | 0.09 | 4 |
| 1989342 | Barnwell | 5.56 | 4.19 | 0.16 | 4 |
| 1990069 | Metropolis | 5.16 | 3.66 | 0.03 | 4 |
| 1990164 | Bullion | 5.96 | 4.76 | 0.06 | 4 |
| 1990172 | Austin | 4.21 | 2.72 | 0.12 | 4 |
| 1990206 | Mineral Quarry | 4.53 | 3.23 | 0.18 | 4 |
| 1990318 | Houston | 5.46 | 4.13 | 0.05 | 4 |
| 1991067 | Coso-Bronze | 4.51 | 2.91 | 0.16 | 3 |
| 1991094 | Bexar | 5.65 | 4.36 | 0.04 | 3 |
| 1991257 | Hoya | 5.69 | 4.47 | 0.04 | 3 |
| 1991262 | Distant Zenith | 4.09 | 2.62 | 0.12 | 3 |
| 1991291 | Lubbock | 5.16 | 3.57 | 0.10 | 3 |
| 1991330 | Bristol | 4.79 | 3.35 | 0.17 | 3 |
| 1992086 | Junction | 5.81 | 4.16 | 0.31 | 3 |
| 1992175 | Galena-Yellow | 4.13 | 2.52 | 0.06 | 3 |
| 1992262 | Hunters Trophy | 4.16 | 2.59 | 0.12 | 3 |

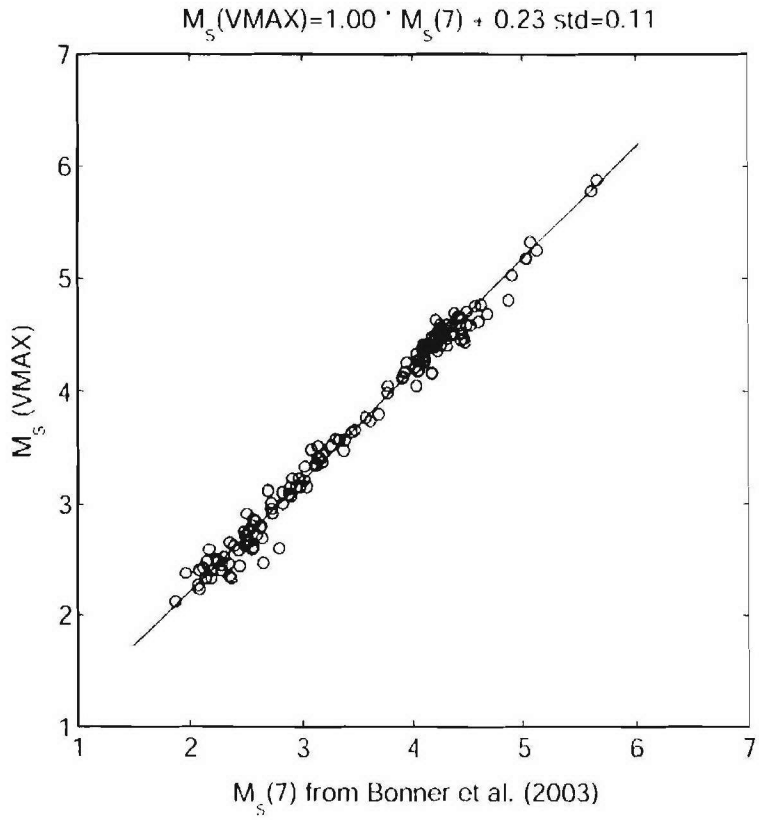


**Figure 4.9. $M_s$(VMAX) magnitude estimates compared to 7-second estimates based on a regionally-calibrated Marshall and Basham formula. The $M_s$(VMAX) estimates result in a 25% reduction in variance as compared to the 7-second estimates and are 0.25 m.u. larger.**

An important goal of our research is the ability to estimate near-regional $M_S$ values for NTS events that can be calibrated to conventional $M_S$ scales. Figure 4.10 shows the comparison of our $M_s$(VMAX) estimates, which are taken directly from the regional surface waves, to $M_S$ measurements obtained from a modeling technique derived by Woods and Harkrider (1995) and to estimates from far-regional/teleseismic data (Yacoub, 1983). Woods and Harkrider modeled the surface waves recorded at regional distances, and then propagated the regional synthetics to distances of 40 degrees. At 40 degrees, their synthetics displayed significant 20-second surface-wave energy, and the authors used a modified von Seggern (1977) formula to measure $M_S$ from the synthetics. We performed a fixed-slope (slope=1) linear regression to compare the $M_S$(VMAX) values with the Woods and Harkrider (1995) values and found a strong correlation. The offset shows that the $M_S$(VMAX) estimates are -0.11 m.u. lower than the Woods and Harkrider (1995) estimates.

We also compared the $M_S$(VMAX) estimates with teleseismic $M_S$ estimates from Yacoub (1983). The results, shown in Figure 4.10, indicate that the two magnitude scales have similar scaling relationships, based on the fixed-slope regression analysis. In this case, the $M_S$(VMAX) estimates are offset from Yacoub's (1983) estimates by approximately +0.03 m.u.

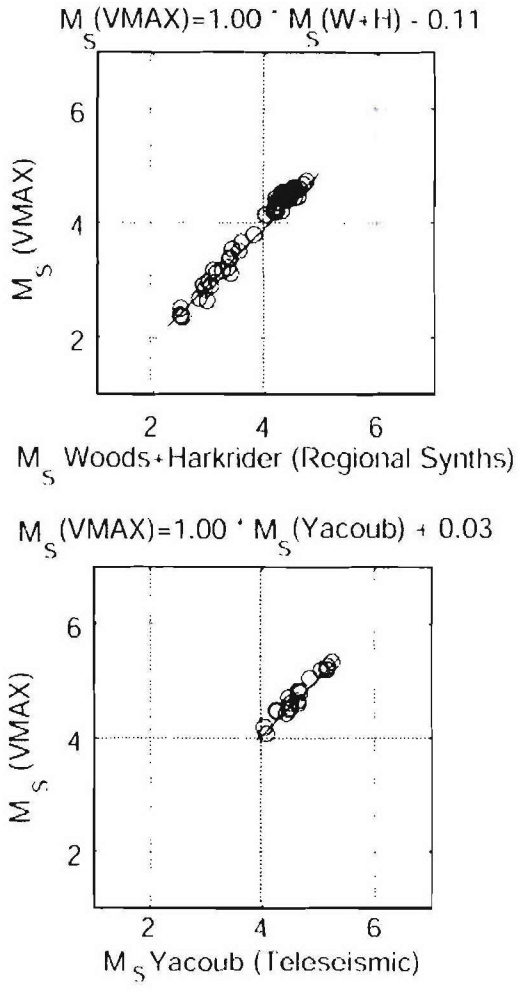


**Figure 4.10. Fixed slope=1 regressions of $M_s$ (VMAX) versus top) Woods and Harkrider (1995) and bottom) Yacoub (1983). The best-fitting regression line, with a fixed slope = 1.0, is given by the solid line running through the data points, and the offset is referenced in the equation above each plot.**

Figure 4.11 shows the regression of the $M_s$ (VMAX) versus the Denny *et al.* (1987; 1989) $m_b$ for both the earthquake (Table 4.3) and explosion (Table 4.2) populations in our test dataset. The best-fitting regression lines are plotted as solid lines, and the slope and intercepts for the lines are presented in the left subplot. The populations plotted in Figure 4.11 suggest that $M_s$ and $m_b$ will be fitted well by linear regressions, with approximately equal slopes assumed for the earthquake and explosion populations. While we did observe slightly different slopes in the regression analyses for the two populations, we believe that this is due to inadequate sampling of earthquakes at $m_b$ magnitudes greater than 5.2. Our dataset does not present any evidence that the two populations are converging at smaller magnitudes, although other $M_s$-$m_b$ studies (Stevens and McLaughlin, 2001) suggest that convergence does occur. The classification equation based on the parallel-slope assumption becomes:

$$d = M_s(\text{VMAX}) - 1.3m_b, \qquad (4.7)$$

where d is the decision value. We chose to use the explosion slope as we believe that it is better constrained with the available data and synthetic studies suggest (Bonner and Herrmann, 2004) that it does not change with increasing magnitude. If d < -2.30, the event will reside in the explosion population. We note that this does not require the event to be a nuclear explosion, as additional testing is needed to ensure the event is shallow enough to be a candidate explosion. If d > 2.30, the event falls into the earthquake classification. We misclassified 2 earthquakes in the explosion population. In our previous studies based on 7-second data (Bonner *et al.*, 2003), we misclassified 4 earthquakes as explosions.

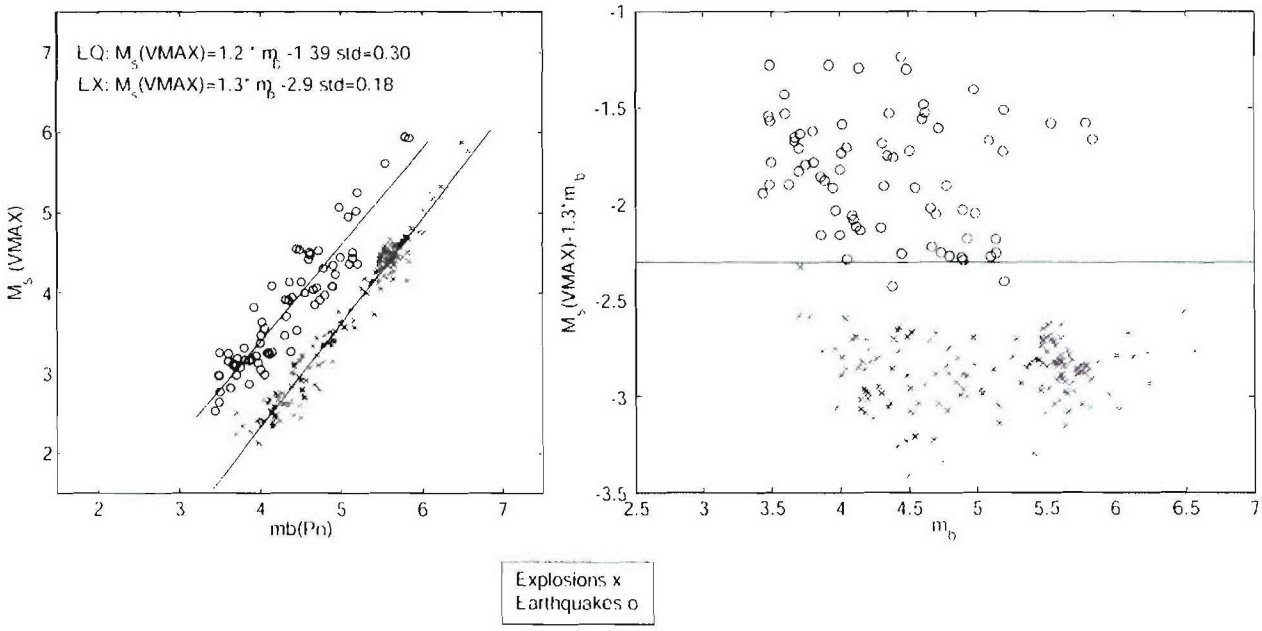


**Figure 4.11. Discrimination results for $M_s$ (VMAX) at the Nevada Test Site. a) $M_s$ (VMAX) vs. $m_b$ for western United States earthquakes and nuclear explosions. b) Linear discrimination of the two datasets showing the decision line for classifying an event as a possible nuclear explosion. If d=$M_s$ (VMAX) – 1.3$m_b$ is less than -2.45, the event may be an explosion, and additional analysis will be required to prove the event is not a deep and/or anomalous earthquake.**

**Table 4.3. Origin information and $M_s$(VMAX) test results for earthquakes in the Nevada Test Site Region**

| Year | Month | Day | Hour | Min | Sec | Lat | Long | Depth | $m_b$ | $M_s$ (VMAX) | STD | # |
|---|---|---|---|---|---|---|---|---|---|---|---|---|
| 1979 | 08 | 12 | 11 | 31 | 19 | 37.26 | -115.08 | 5.0 | 3.18 | 2.67 | 0.12 | 3 |
| 1979 | 12 | 25 | 00 | 0 | 00 | 37.27 | -117.06 | 5.0 | 3.67 | 3.12 | 0.07 | 4 |
| 1980 | 01 | 15 | 20 | 28 | 22 | 36.18 | -117.60 | 8.0 | 3.63 | 2.82 | 0.12 | 3 |
| 1980 | 02 | 25 | 23 | 43 | 32 | 36.20 | -117.58 | 5.0 | 3.86 | 2.86 | 0.18 | 4 |
| 1980 | 05 | 27 | 14 | 50 | 57 | 37.48 | -118.81 | 13.0 | 5.79 | 5.95 | 0.31 | 4 |
| 1981 | 12 | 01 | 16 | 18 | 50 | 38.62 | -118.19 | 11.0 | 4.02 | 3.64 | 0.14 | 2 |
| 1981 | 12 | 19 | 20 | 56 | 52 | 38.63 | -118.21 | 17.0 | 4.12 | 3.24 | 0.12 | 3 |
| 1982 | 01 | 24 | 15 | 44 | 07 | 37.45 | -117.83 | 5.0 | 4.09 | 3.26 | 0.09 | 4 |
| 1982 | 03 | 16 | 08 | 47 | 00 | 36.60 | -117.03 | 6.0 | 3.48 | 2.98 | 0.06 | 3 |
| 1982 | 05 | 12 | 19 | 29 | 24 | 37.27 | -115.08 | 10.0 | 3.49 | 2.97 | 0.08 | 4 |
| 1982 | 07 | 06 | 02 | 10 | 43 | 37.69 | -115.05 | 3.0 | 4.3 | 3.47 | 0.05 | 3 |
| 1982 | 09 | 24 | 07 | 40 | 24 | 37.85 | -118.12 | 5.0 | 4.99 | 4.44 | 0.16 | 4 |
| 1983 | 06 | 04 | 11 | 37 | 40 | 37.39 | -115.21 | 6.0 | 3.44 | 2.53 | 0.16 | 4 |
| 1984 | 08 | 02 | 11 | 1 | 34 | 37.30 | -114.94 | 5.0 | 3.49 | 2.64 | 0.13 | 4 |
| 1984 | 11 | 23 | 18 | 8 | 25 | 37.48 | -118.66 | 5.0 | 5.54 | 5.62 | 0.20 | 4 |
| 1985 | 12 | 10 | 06 | 10 | 25 | 37.30 | -115.01 | 5.0 | 3.7 | 3.10 | 0.07 | 2 |
| 1992 | 06 | 29 | 10 | 31 | 02 | 36.69 | -116.24 | 5.0 | 4.66 | 4.04 | 0.05 | 2 |
| 1992 | 06 | 29 | 15 | 52 | 39 | 36.71 | -116.29 | 7.9 | 3.89 | 3.18 | 0.31 | 2 |
| 1992 | 06 | 29 | 17 | 1 | 16 | 36.74 | -116.29 | 7.6 | 3.81 | 3.17 | 0.03 | 2 |
| 1992 | 06 | 30 | 16 | 6 | 24 | 36.72 | -116.26 | 5.0 | 3.5 | 2.77 | 0.47 | 2 |
| 1992 | 07 | 05 | 06 | 54 | 12 | 36.69 | -116.28 | 5.0 | 4.38 | 3.27 | 0.27 | 2 |
| 1993 | 05 | 17 | 23 | 20 | 49 | 37.17 | -117.78 | 6.0 | 5.84 | 5.93 | 0.35 | 3 |
| 1993 | 05 | 18 | 01 | 3 | 06 | 37.15 | -117.76 | 2.0 | 4.9 | 4.08 | 0.29 | 4 |
| 1993 | 05 | 18 | 23 | 48 | 53 | 37.06 | -117.78 | 3.0 | 4.93 | 4.23 | 0.22 | 4 |
| 1993 | 05 | 20 | 20 | 14 | 14 | 36.10 | -117.70 | 0.0 | 4.32 | 3.71 | 0.14 | 2 |
| 1995 | 06 | 26 | 08 | 40 | 27 | 34.31 | -118.73 | 7.0 | 4.72 | 4.53 | 0.24 | 9 |
| 1995 | 08 | 17 | 22 | 39 | 58 | 35.75 | -117.66 | 4.7 | 5.09 | 4.95 | 0.20 | 12 |
| 1995 | 08 | 30 | 15 | 54 | 22 | 35.73 | -117.59 | 3.4 | 3.67 | 3.10 | 0.23 | 9 |
| 1995 | 09 | 20 | 23 | 27 | 36 | 35.69 | -117.64 | 5.0 | 4.98 | 5.07 | 0.2 | 12 |
| 1995 | 09 | 22 | 14 | 47 | 22 | 38.70 | -118.54 | 17.9 | 4.80 | 3.97 | 0.13 | 6 |
| 1996 | 01 | 07 | 14 | 32 | 53 | 35.72 | -117.65 | 2.1 | 4.45 | 4.55 | 0.19 | 13 |
| 1996 | 01 | 08 | 08 | 57 | 10 | 35.76 | -117.57 | 0.7 | 3.75 | 3.08 | 0.17 | 9 |
| 1996 | 01 | 08 | 10 | 52 | 29 | 35.75 | -117.57 | 5.1 | 3.92 | 3.82 | 0.29 | 10 |
| 1996 | 04 | 02 | 01 | 50 | 09 | 37.60 | -118.91 | 7.1 | 4.05 | 3.56 | 0.14 | 8 |
| 1996 | 05 | 01 | 19 | 49 | 56 | 34.33 | -118.75 | 22.3 | 4.00 | 3.38 | 0.23 | 10 |
| 1996 | 06 | 02 | 07 | 0 | 06 | 39.09 | -115.37 | 63.4 | 3.49 | 3.26 | 0.16 | 7 |
| 1996 | 11 | 27 | 20 | 17 | 24 | 36.01 | -117.62 | 5.0 | 5.14 | 4.50 | 0.15 | 13 |
| 1997 | 04 | 14 | 11 | 20 | 54 | 38.09 | -118.72 | 0.0 | 4.00 | 3.04 | 0.18 | 7 |
| 1997 | 05 | 06 | 19 | 12 | 53 | 35.43 | -118.43 | 11.0 | 3.70 | 2.98 | 0.15 | 8 |
| 1997 | 07 | 03 | 17 | 49 | 36 | 35.77 | -117.61 | 0.3 | 3.97 | 3.13 | 0.17 | 11 |
| 1997 | 08 | 21 | 16 | 11 | 24 | 38.55 | -118.50 | 5.1 | 4.55 | 4.00 | 0.14 | 8 |
| 1997 | 08 | 21 | 16 | 36 | 47 | 38.56 | -118.51 | 9.4 | 4.67 | 3.85 | 0.14 | 8 |
| 1997 | 11 | 02 | 08 | 51 | 54 | 37.81 | -118.18 | 5.5 | 5.19 | 5.02 | 0.19 | 7 |
| 1997 | 11 | 02 | 15 | 3 | 04 | 37.85 | -118.19 | 5.0 | 4.51 | 4.14 | 0.2 | 7 |

| 1997 | 11 | 05 | 23 | 0 | 08 | 37.20 | -117.85 | 4.7 | 4.45 | 3.53 | 0.04 | 7 |
|---|---|---|---|---|---|---|---|---|---|---|---|---|
| 1997 | 11 | 15 | 06 | 0 | 20 | 37.18 | -117.81 | 5.0 | 4.61 | 4.51 | 0.10 | 8 |
| 1997 | 11 | 22 | 12 | 6 | 57 | 37.63 | -118.96 | 8.4 | 4.14 | 4.09 | 0.16 | 8 |
| 1997 | 11 | 22 | 17 | 20 | 37 | 37.64 | -118.99 | 7.0 | 4.49 | 4.54 | 0.18 | 7 |
| 1997 | 11 | 22 | 18 | 11 | 01 | 37.63 | -118.99 | 8.1 | 4.35 | 3.91 | 0.25 | 8 |
| 1997 | 11 | 30 | 21 | 17 | 07 | 37.57 | -118.99 | 7.1 | 4.62 | 4.48 | 0.22 | 7 |
| 1997 | 12 | 31 | 20 | 36 | 49 | 37.65 | -118.85 | 6.6 | 4.78 | 4.31 | 0.10 | 6 |
| 1998 | 03 | 06 | 07 | 36 | 34 | 36.01 | -117.63 | 2.1 | 4.15 | 3.26 | 0.10 | 6 |
| 1998 | 03 | 07 | 00 | 36 | 46 | 36.00 | -117.56 | 1.7 | 4.74 | 3.91 | 0.19 | 8 |
| 1998 | 04 | 24 | 16 | 17 | 27 | 38.49 | -118.38 | 9.8 | 4.01 | 3.48 | 0.13 | 7 |
| 1998 | 06 | 09 | 05 | 24 | 41 | 37.59 | -118.81 | 6.7 | 5.14 | 4.43 | 0.19 | 5 |
| 1998 | 06 | 18 | 11 | 0 | 41 | 37.96 | -112.55 | 2.1 | 3.80 | 3.32 | 0.14 | 6 |
| 1998 | 07 | 02 | 03 | 39 | 51 | 36.82 | -117.48 | 7.1 | 5.20 | 4.36 | 0.02 | 4 |
| 1998 | 07 | 15 | 04 | 53 | 21 | 37.55 | -118.81 | 16.9 | 4.90 | 4.34 | 0.17 | 8 |
| 1999 | 01 | 27 | 10 | 44 | 23 | 36.84 | -115.97 | 0.5 | 4.36 | 4.14 | 0.24 | 7 |
| 1999 | 05 | 15 | 13 | 22 | 12 | 37.49 | -118.81 | 5.8 | 5.20 | 5.25 | 0.21 | 8 |
| 1999 | 05 | 15 | 17 | 54 | 10 | 37.51 | -118.84 | 8.0 | 4.89 | 4.08 | 0.33 | 7 |
| 1999 | 05 | 17 | 06 | 37 | 20 | 37.54 | -118.80 | 3.6 | 3.86 | 3.16 | 0.18 | 8 |
| 1999 | 08 | 01 | 16 | 27 | 20 | 37.35 | -117.05 | 26.4 | 4.70 | 4.06 | 0.17 | 8 |
| 1999 | 08 | 02 | 05 | 40 | 27 | 37.39 | -117.06 | 1.8 | 3.60 | 3.25 | 0.14 | 6 |
| 1999 | 08 | 02 | 06 | 5 | 14 | 37.30 | -117.06 | 14.8 | 5.10 | 4.36 | 0.27 | 10 |
| 1999 | 11 | 08 | 01 | 53 | 13 | 37.40 | -118.60 | 5.0 | 3.60 | 3.15 | 0.16 | 7 |
| 2001 | 05 | 17 | 21 | 53 | 45 | 35.73 | -118.02 | 4.2 | 4.05 | 2.98 | 0.08 | 8 |
| 2001 | 07 | 17 | 12 | 59 | 59 | 35.95 | -117.90 | 0.4 | 4.60 | 4.42 | 0.17 | 9 |
| 2001 | 08 | 02 | 16 | 21 | 19 | 37.22 | -117.79 | 9.0 | 3.95 | 3.22 | 0.12 | 4 |
| 2002 | 06 | 14 | 12 | 40 | 44 | 36.72 | -116.30 | 11.9 | 4.31 | 3.92 | 0.17 | 5 |
| 2002 | 09 | 28 | 10 | 34 | 47 | 35.95 | -117.30 | 3.7 | 4.10 | 3.25 | 0.21 | 7 |
| 2003 | 01 | 25 | 09 | 16 | 10 | 35.32 | -118.65 | 5.6 | 4.39 | 3.95 | 0.30 | 6 |
| 2003 | 03 | 08 | 15 | 35 | 02 | 37.57 | -118.89 | 5.5 | 3.71 | 3.19 | 0.18 | 5 |

**Lop Nor Test Site Earthquake and Explosion Discrimination.**

In our third application of the Russell (2005) formula and $M_s$(VMAX) measurement technique, we examined earthquake and explosion discrimination at the Lop Nor nuclear test site in China.

**Data.** We developed a test dataset consisting of 9 nuclear explosions and 38 earthquakes that occurred within 5 degrees of the Lop Nor test site. The broadband vertical-component data were acquired from IRIS and consisted of global and regional networks in the study region (Figure 4.12). The data were all transformed from counts to displacement in nanometers using the SAC command "transfer" and SEED response files. The data were decimated from their original sampling rates (> 20 samples/second) to approximately 1 sample/sec for the surface-wave analysis. We note that we do not have access to a calibrated body-wave magnitude scale for the Lop Nor region; thus, we have used the USGS-estimated $m_b$ values in our discrimination analysis.

**Table 4.5 Origin information and $M_s$(VMAX) test results for earthquakes near Lop Nor**

| Year | Month | Day | Hour | Minute | Second | Lat | Lon | Depth | $m_b$ | $M_s$ (VMAX) | STD | Stations |
|---|---|---|---|---|---|---|---|---|---|---|---|---|
| 1995 | 08 | 02 | 11 | 59 | 43 | 41.63 | 88.45 | 10 | 4.1 | 3.32 | 0 | 1 |
| 1995 | 09 | 04 | 18 | 43 | 45 | 43.90 | 87.44 | 33 | 4.1 | 2.91 | 0.13 | 5 |
| 1995 | 12 | 12 | 17 | 31 | 16 | 42.12 | 86.91 | 33 | 4.3 | 3.32 | 0.2 | 6 |
| 1996 | 03 | 04 | 14 | 02 | 22 | 44.12 | 87.20 | 33 | 3.9 | 3.22 | 0.07 | 4 |
| 1996 | 03 | 20 | 02 | 11 | 21 | 42.18 | 87.63 | 24 | 4.8 | 3.76 | 0.2 | 9 |
| 1996 | 03 | 31 | 03 | 07 | 14 | 43.02 | 88.68 | 33 | 4.2 | 3.24 | 0.21 | 6 |
| 1996 | 05 | 12 | 01 | 00 | 38 | 43.67 | 86.96 | 33 | 3.7 | 2.95 | 0.22 | 2 |
| 1997 | 02 | 08 | 17 | 12 | 09 | 42.34 | 86.99 | 9 | 4.6 | 3.54 | 0.35 | 2 |
| 1997 | 05 | 27 | 01 | 56 | 24 | 42.62 | 86.16 | 21 | 4.9 | 3.64 | 0.14 | 7 |
| 1997 | 06 | 08 | 20 | 25 | 53 | 39.06 | 89.28 | 33 | 4.7 | 3.2 | 0.17 | 7 |
| 1998 | 01 | 20 | 19 | 35 | 04 | 42.01 | 84.75 | 33 | 3.5 | 2.75 | 0 | 1 |
| 1998 | 02 | 07 | 22 | 42 | 44 | 42.55 | 86.01 | 33 | 4.1 | 3.1 | 0.11 | 3 |
| 1998 | 04 | 13 | 23 | 14 | 32 | 41.99 | 85.80 | 33 | 4 | 2.92 | 0.28 | 2 |
| 1998 | 08 | 19 | 12 | 26 | 19 | 43.81 | 86.33 | 19 | 4.6 | 3.71 | 0.2 | 9 |
| 1998 | 10 | 20 | 18 | 39 | 23 | 42.56 | 87.15 | 33 | 4.7 | 3.2 | 0.12 | 7 |
| 1999 | 01 | 27 | 06 | 25 | 01 | 41.62 | 88.36 | 33 | 4.5 | 3.36 | 0.16 | 8 |
| 1999 | 01 | 30 | 03 | 51 | 05 | 41.67 | 88.46 | 23 | 5.9 | 5.25 | 0.14 | 6 |
| 1999 | 04 | 29 | 05 | 27 | 55 | 41.62 | 90.82 | 33 | 4.3 | 3.26 | 0.21 | 8 |
| 1999 | 05 | 01 | 13 | 48 | 52 | 42.04 | 87.96 | 21 | 4.2 | 2.96 | 0.21 | 5 |
| 1999 | 05 | 17 | 04 | 52 | 34 | 42.28 | 87.92 | 33 | 4.2 | 2.92 | 0.35 | 3 |
| 1999 | 10 | 18 | 02 | 42 | 20 | 41.77 | 89.25 | 33 | 5 | 4.25 | 0.15 | 8 |
| 2000 | 10 | 03 | 03 | 07 | 28 | 41.99 | 84.92 | 33 | 5.2 | 4.37 | 0.28 | 7 |
| 2001 | 03 | 13 | 03 | 18 | 38 | 42.39 | 86.12 | 24 | 4.7 | 3.67 | 0.11 | 9 |
| 2001 | 12 | 21 | 23 | 05 | 50 | 43.74 | 86.53 | 10 | 4.5 | 3.68 | 0.2 | 9 |
| 2002 | 01 | 13 | 05 | 27 | 16 | 43.36 | 89.04 | 33 | 4.3 | 3.22 | 0.18 | 9 |
| 2002 | 03 | 11 | 23 | 26 | 49 | 42.39 | 85.90 | 33 | 4.6 | 3.52 | 0.14 | 9 |
| 2002 | 10 | 02 | 09 | 50 | 52 | 43.57 | 89.08 | 29 | 4.6 | 3.32 | 0.06 | 3 |
| 2002 | 10 | 07 | 03 | 01 | 47 | 43.42 | 87.09 | 29 | 4.8 | 3.98 | 0.11 | 8 |
| 2003 | 01 | 22 | 13 | 33 | 02 | 42.21 | 87.33 | 24 | 4.7 | 3.33 | 0.23 | 9 |
| 2003 | 02 | 13 | 18 | 32 | 47 | 41.91 | 88.24 | 51 | 4.3 | 3.5 | 0.22 | 9 |
| 2003 | 02 | 23 | 22 | 34 | 20 | 43.75 | 87.71 | 33 | 4.2 | 3.13 | 0.22 | 9 |
| 2003 | 03 | 13 | 15 | 07 | 07 | 41.80 | 89.08 | 33 | 4.8 | 3.64 | 0.19 | 9 |
| 2003 | 07 | 03 | 05 | 53 | 52 | 43.85 | 86.26 | 37 | 4.8 | 4.09 | 0.21 | 7 |
| 2003 | 08 | 24 | 21 | 54 | 36 | 44.30 | 87.20 | 33 | 4.1 | 3.11 | 0.21 | 8 |
| 2003 | 12 | 19 | 15 | 01 | 22 | 41.95 | 88.85 | 33 | 4.7 | 3.82 | 0.18 | 3 |
| 2004 | 01 | 29 | 15 | 29 | 08 | 42.54 | 86.13 | 15 | 4.3 | 3.14 | 0.09 | 6 |
| 2004 | 03 | 20 | 22 | 55 | 03 | 43.87 | 86.50 | 10 | 4.1 | 3.25 | 0.14 | 3 |
| 2004 | 03 | 29 | 20 | 30 | 32 | 43.04 | 88.65 | 21 | 4.2 | 2.9 | 0.33 | 4 |

## DISCUSSION

There is a general disagreement among researchers in the nuclear monitoring community as to how well the $M_s$—$m_b$ discriminant performs at small-to-intermediate body-wave magnitudes. Some researchers believe that the available $M_s$—$m_b$ datasets suggest that the two

populations converge at smaller magnitudes (e.g., Stevens and McLaughlin, 2001). These researchers believe that the population convergence is caused by earthquake and explosion sources that become phenomenologically similar at smaller magnitudes. Lambert and Alexander (1971) determined that the earthquake and explosion populations at the Nevada Test Site are characterized by parallel $M_s$ vs. $m_b$ curves, with slopes of 1 and a difference of 0.82 magnitude units based on linear regression fits. Alexander (2002; personal communication, 2004) suggests that any convergence at the smaller magnitudes is related to depth and not the phenomenology behind explosion and earthquake sources.

To determine whether depth or source phenomenology is responsible for converging $M_s$—$m_b$ behavior at smaller magnitudes, we pooled all of the Eurasian earthquakes (Tables 1 and 5) $M_s$(VMAX) estimates. We also calculated $M_s$(VMAX) for 11 additional nuclear explosions in Eurasia (Table 4.6), and combined them with the Lop Nor explosions from Table 4.4. Figure 4.14 shows the $M_s$(VMAX) estimates from all these data plotted versus USGS $m_b$.

**Table 4.6. Origin information and $M_s$(VMAX) test results for additional Eurasian explosions.**

| Year | Month | Day | Hour | Minute | Sec | Lat | Long | Depth | $m_b$ | $M_s$ (VMAX) | STD | # | Test Site |
|---|---|---|---|---|---|---|---|---|---|---|---|---|---|
| 1989 | 10 | 19 | 9 | 49 | 59 | 49.927 | 78.972 | 0 | 6 | 4.38 | 0.07 | 3 | Shagan |
| 1989 | 10 | 4 | 11 | 30 | 0 | 49.751 | 78.005 | 0 | 4.7 | 3.23 | 0 | 1 | Shagan |
| 1989 | 9 | 2 | 4 | 16 | 59 | 50.019 | 78.998 | 0 | 5.1 | 3.29 | 0.24 | 2 | Shagan |
| 1989 | 7 | 8 | 3 | 47 | 0 | 49.869 | 78.775 | 0 | 5.6 | 3.78 | 0.15 | 3 | Shagan |
| 1989 | 2 | 12 | 4 | 15 | 9 | 49.911 | 78.704 | 0 | 5.9 | 4.24 | 0 | 1 | Shagan |
| 1989 | 1 | 22 | 3 | 57 | 9 | 49.934 | 78.815 | 0 | 6.1 | 4.28 | 0 | 1 | Shagan |
| 1988 | 12 | 17 | 4 | 18 | 9 | 49.879 | 78.924 | 0 | 5.9 | 4.15 | 0 | 1 | Shagan |
| 1988 | 11 | 23 | 3 | 57 | 9 | 49.765 | 78.029 | 0 | 5.4 | 3.56 | 0 | 1 | Shagan |
| 1990 | 10 | 24 | 14 | 57 | 58 | 73.331 | 54.757 | 0 | 5.7 | 4.08 | 0.17 | 7 | Novaya Zemlya |
| 1998 | 5 | 11 | 10 | 13 | 44 | 27.078 | 71.719 | 0 | 5.2 | 3.17 | 0.11 | 8 | India |
| 1998 | 5 | 28 | 10 | 16 | 17 | 28.83 | 64.95 | 0 | 4.9 | 3.27 | 0.18 | 8 | Pakistan |

Because of corner frequency effects for earthquakes and $m_b$ measurement procedures, there should be a change in slope for regressed $M_s$(VMAX) vs $m_b$ near $m_b$ = 5 (Nuttli, 1983). As shown in Figure 4.14, the slope for the best fit regressions above $m_b$ = 5 is 1.46 with a standard deviation of 0.21 magnitude units. The slope for the regressions below $m_b$ = 5 is 0.94, which is similar to the slope determined for the observed explosion data (1.04). With the current dataset, we can not rule out the possibility that a single line with slope equal to 1.54 can fit all of the earthquake data. In fact, the correlation coefficients for single-line or two-line fits are essentially the same ($R^2 > 0.85$). If the earthquake data were fit with a single line, we would see convergence of the populations near $m_b$ = 3.5, which agrees with Stevens and McLaughlin (2001).

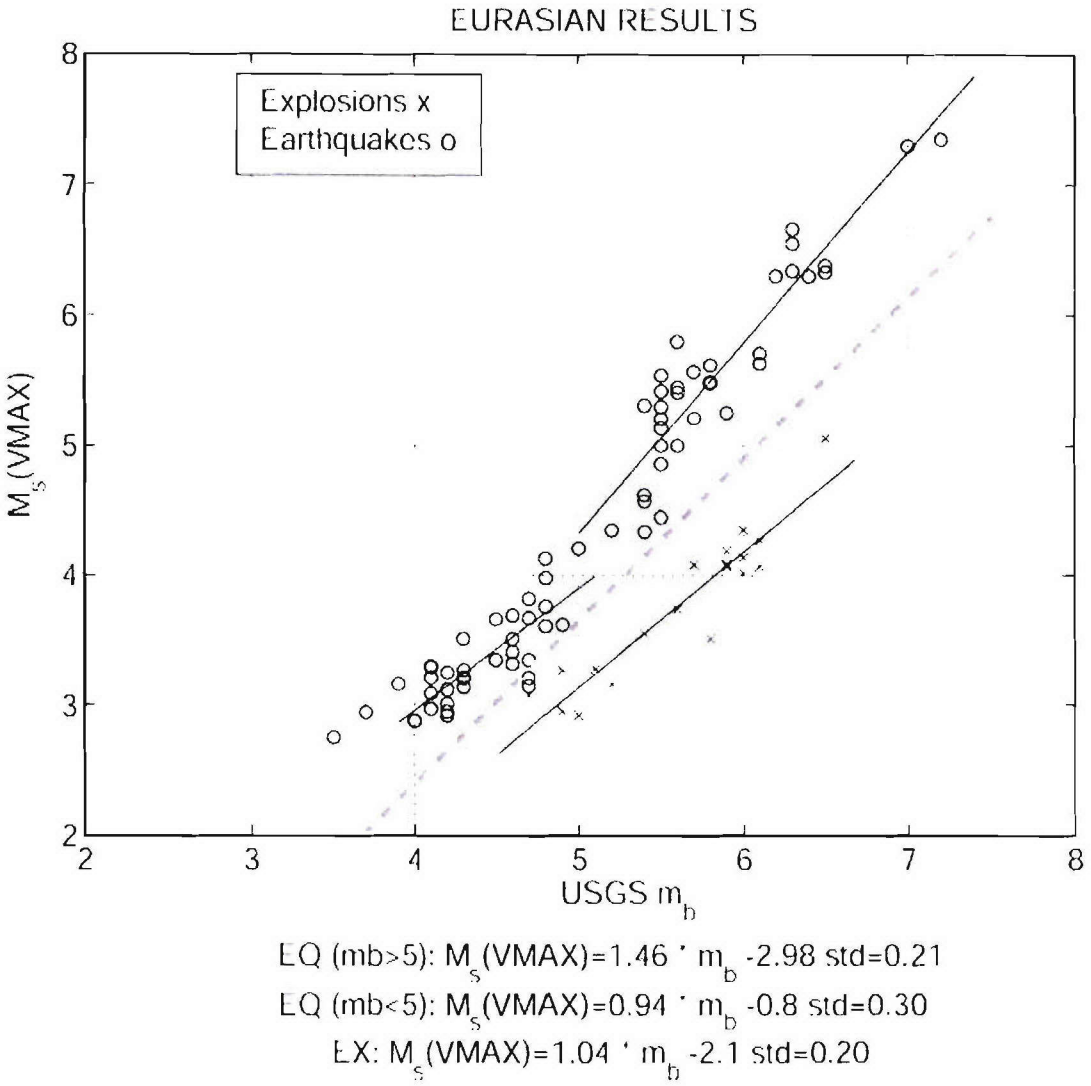


**Figure 4.14. $M_s$—$m_b$ relationships for all Eurasian earthquake and explosion data for which an $M_s$ (VMAX) was estimated during this study. The body wave magnitudes are all from the United States Geological Survey. We split the earthquake data at $m_b$ = 5 based on corner frequency effects for earthquakes and $m_b$. The earthquake and explosion populations both have slopes that are approximately 1 for $m_b$ < 5 and are separated by an average of 0.90 magnitude units. The dashed line is the Murphy *et al.* (1997) criterion for event screening.**

However, if we focus on the two-line case, the slopes for our earthquake and explosion populations at $m_b$ values < 5 are similar to the Lambert and Alexander (1971) results. Additionally, we observed 0.90 magnitude units separation between the two populations at $m_b$s below 5, while Lambert and Alexander (1971) noted a difference of 0.82 magnitude units, based on the fitted regression lines for their NTS earthquakes and explosions. Differences between the theoretical and observed slopes above $m_b$ > 5 may be related to the difficulties of measuring body-wave magnitudes for large events. While more data will be required to finalize the two-slope hypothesis, these preliminary results suggest that the discrimination of explosions from

earthquakes can be achieved at lower magnitudes using the Russell (2005) formula and the $M_s$(VMAX) measurement technique.

Murphy *et al.* (1997) determined an event screening relationship based on $M_s$—$m_b$ estimates. For USGS estimated $m_b$, the screening criterion is:

$$M_s = 1.25\, m_b - 2.60. \qquad (4.10)$$

We plotted the Murphy *et al.* (1997) criterion in Figure 4.14 as the dashed line and note that two of the earthquakes fall below this line. More importantly, none of our explosions plotted above this line.

## CONCLUSIONS

The Russell surface-wave magnitude formula and the $M_s$(VMAX) measurement technique provide a new method for estimating surface-wave magnitudes. There are several benefits to the new method. First, the technique allows for time domain measurements of surface wave amplitudes, giving an analyst the ability to visually confirm that the pick is correct and is an actual surface wave. Also, it allows for surface wave magnitudes to be measured at local and regional distances where traditional 20-second magnitudes cannot be used. And these magnitudes are not biased with respect to teleseismic estimates using the same $M_s$(VMAX) measurement technique. Additionally, the application of narrow-band Butterworth filtering techniques appropriately handles Airy phase phenomena that prior to this study, had to be accounted for using Marshall and Basham's (1972) empirical corrections. Finally, because the method is variable period and not restricted to near 20-seconds period, the analyst is allowed to measure $M_s$ where the signal is largest. The new method has been successfully tested on three research datasets, and the results suggest that the method can be used to screen out a large percentage of small earthquakes at $m_b < 5$. Thus, we are currently implementing the technique for operational testing.

## ACKNOWLEDGMENTS

The data used in this study comes from a variety of sources. We wish to thank the following organizations for access to their data: the Geological Survey of Canada; Institut de Physique du Globe de Paris; GFZ Potsdam, Germany; United States Geological Survey, National Science Foundation, University of California, San Francisco; California Institute of Technology; Lamont Doherty Earth Observatory, and Istituto Nazionale di Geofisica e Vulcanologia, Rome, Italy. We are also indebted to Howard Patton for his assistance in the LNN database acquisition and his comments concerning various aspects of the research. We also wish to thank Bill Walter and Marv Denny for help in acquiring the MNV dataset (Denny, 1998). We express our gratitude to Mark Leidig and Ileana Tibuleac, who helped with database preparation, and Jack Murphy, Heather Hooper and James Lewkowicz for insightful discussions about the paper and research. Karl Veith and an anonymous reviewer helped improve the paper during the review process. We thank the developers of the Generic Mapping Tools software (Wessel and Smith, 1998), Computer Programs in Seismology (Herrmann, 2004), and Matlab, all of which were used to generate and present the results of our research. We are also grateful to Harvard University for making their CMT estimates readily available. This research was sponsored by the U.S. Air

Force Research Laboratory and the Defense Threat Reduction Agency under Contract No. DTRA01-01-C-0080

## REFERENCES

Alexander, S.S. 2002, Seismic Monitoring for Underground Nuclear Explosions, in Science, Technology and National Security, Eds. Majumbar, S.K., Alexander, S.S., Rosenfeld, L.M., Rieders, M.F., Miller, E.W., and Panah, A.I., The Pennsylvania Academy of Sciences, Easton, PA 18042. 267pp.

Bonner, J.L., D.T. Reiter, and D. Harkrider, (2004). Development of a Time-Domain, Variable-Period Surface Wave Magnitude Measurement Procedure for Application at Regional Distances, *Proceedings of the 26th Annual Seismic Research Review Meeting, Orlando, Florida.*

Bonner, J., D. Harkrider, E.T. Herrin, R.H. Shumway, S.A. Russell and I.M. Tibuleac (2003). Evaluation of short-period, near-regional $M_S$ scales for the Nevada Test Site. *Bull. Seism. Soc. Am.*, **93**, 1773-1791.

Bonner, J. and R. B. Herrmann (2004). A Synthetic $M_s$—$m_b$ study. Weston Geophysical Scientific Report. 20p.

Boore, D.M. (1983). Stochastic simulation of high-frequency ground motions based on seismological models of the radiated spectra, *Bull. Seism. Soc. Am.*, 73(6), 1865-1894.

Brune, J.N. (1970). Tectonic stress and the spectra of seismic shear waves from earthquakes, *J. Geophys. Res.* **75**, 4997-5009.

Brune, J.N. (1971). Correction, *J. Geophys. Res.* **76**, 5002.

Chael, E.P. (1997). An automated Rayleigh-wave detection algorithm, *Bull. Seism. Soc. Am.*, **87**, 157-163.

Denny, M.D., S. R. Taylor, and E.S. Vergino (1987). Investigation of $m_b$ and $M_S$ formulas for the western United States and their impact on the $M_S/m_b$ discriminant, *Bull. Seism. Soc. Am.*, **77**, 987-995.

Denny, M.D., S. R. Taylor, and E.S. Vergino (1989). Erratum: Investigation of $m_b$ and $M_S$ formulas for the western United States and their impact on the $M_S/m_b$ discriminant, *Bull. Seism. Soc. Am.*, **79**, 230.

Denny, M. D. (1998), Mina Seismic Data: Historic background for CTBT Monitoring, *Lawrence Livermore Report UCRL-MI-130657.*

Dziewonski, A.M., J. Bloch, and M. Landisman (1969). A new technique for the analysis of transient seismic signals, *Bull. Seism. Soc. Am.*, **59**, 427-444.

Gutenberg, B. (1945). Amplitudes of surface waves and the magnitudes of shallow earthquakes, *Bull. Seism. Soc. Am.*, **35**, 3.

Herak, M. and D. Herak (1993). Distance dependence of $M_S$ and calibrating function for 20 second Rayleigh waves, *Bull. Seism. Soc. Am.*, **83**, 1681.

Herrmann, R. B. (2004). Computer Programs in Seismology Version 3.30, St. Louis University.

Kanamori, H., and G.S. Stewart (1976). Mode of strain release along the Gibbs Fracture Zone, Mid-Atlantic Ridge, *Phys. Earth Planet. Inter.*, 11, 312-332.

Lambert, D.G. and S.S. Alexander, (1971). Relationship of body and surface wave magnitudes for small earthquakes and explosions, SDL Report 245, Teledyne Geotech, Alexandria, VA.

Marshall, P.D. and P.W. Basham (1972). Discrimination between earthquakes and underground

explosions employing an improved $M_S$ scale, *Geophys. J. R. Astr. Soc.*, **29**, 431-458.

Marshall, P.D., Springer, D.L, and Rodean, H.C. (1979). Magnitude corrections for attenuation in the upper mantle, *Geophys. J. R. Astr. Soc.*, **57**, 609-638.

Mueller, R. A., and J. R. Murphy, (1971). Seismic characteristics of underground nuclear detonations: Part I, Seismic scaling law of underground detonations. *Bull. Seism. Soc. Am.*, **61**, 1675

Murphy, J. R., B. W. Barker, and M. E. Marshall, (1997). Event screening at the IDC using the Ms/mb discriminant. Maxwell Technologies Final Report. 23 p.

Nuttli, O.W. (1983). Average seismic source-parameter relations for mid-plate earthquakes. *Bull. Seism. Soc. Am.*, **73**, 519-535.

Okal, E.A., (1989). A theoretical discussion of time domain magnitudes: the Prague formula for $M_S$ and the mantle magnitude $M_m$, *J. Geophys. Res.* **94,** 4194-4204.

Patton, H. (2001). Regional magnitude scaling, transportability, and $M_S$-$m_b$ discrimination at small magnitudes, in *Monitoring the Comprehensive Nuclear Test Ban Treaty: Source Processes and Explosion Yield Determination*, eds. Ekstrom, G., M. Denny, and J.R. Murphy, *Pure Appl. Geophys.*, **158**, 1951-2015.

Rezapour, M., and R.G. Pearce (1998). Bias in surface-wave magnitude $M_S$ due to inadequate distance correction, *Bull. Seism. Soc. Am.*, **88**, 43-61.

Russell, D.R. (2005). Development of a time-domain, variable-period surface wave magnitude measurement procedure for application at regional and teleseismic distances. Part I—Theory. Submitted to *the Bull. Seism. Soc. Am.*

von Seggern, D. (1973). Joint magnitude determination and analysis of variance for explosion magnitude estimates, *Bull. Seism. Soc. Am.*, **63,** 827-845.

von Seggern, D. (1977). Amplitude distance relation for 20-Second Rayleigh waves, *Bull. Seism. Soc. Am.*, **67,** 405-411.

Selby, N. (2001). Association of Rayleigh waves using back azimuth measurements: application to test ban verification, *Bull. Seism. Soc. Am.*, **91**, 580-593.

Stevens, J. L. and S. M. Day (1985), The physical basis of the mb:Ms and variable frequency magnitude methods for earthquake/explosion discrimination, *J. Geophys. Res.*, 90, 3009-3020.

Stevens, J.L., D.A. Adams, and E. Baker (2001). Surface wave detection and measurement using a one-degree global dispersion grid, *SAIC Final Report SAIC-01/1085.*

Stevens, J. L. and K.L. McLaughlin (2001). Optimization of surface wave identification and measurement, in *Monitoring the Comprehensive Nuclear Test Ban Treaty: Surface Waves*, eds. Levshin, A. and M.H. Ritzwoller, *Pure Appl. Geophys.*, **158**, 1547-1582.

Stevens, J. L. and J.R. Murphy (2001). Yield Estimation from Surface-wave Amplitudes, in *Monitoring the Comprehensive Nuclear Test Ban Treaty: Surface Waves: Source Processes and Explosion Yield Determination*, eds. Ekstrom, G., M. Denny, and J.R. Murphy, *Pure Appl. Geophys.*, **158**, 2227-2251.

Vaněk, J., A. Zatopek, V. Karnik, Y.V. Riznichenko, E.F. Saverensky, S.L. Solov'ev, and N.V. Shebalin (1962). Standardization of magnitude scales, *Bull. (Izvest.) Acad. Sci. U.S.S.R., Geophys. Ser.*, **2**, 108.

Veith K.F., and G.E. Clawson (1972). Magnitude from short-period P-wave data. *Bull. Seism. Soc. Am.*, Vol. **62**, pp.435-452.

Vergino, E.S. and Mensing, R.W. (1989). Yield estimation using regional $m_b(Pn)$, *Lawrence Livermore National Laboratory Report UCID-101600.*

Wessel, P. and W.H.F. Smith (1998). New, improved version of the Generic Mapping Tools Released, *EOS. Trans. Am. Geophys. Un.*, **79**, *579.*

Woods, B. and D.G. Harkrider (1995). Determining surface-wave magnitudes from regional Nevada Test Site data, *Geophys. J. Int.*, **120**, 474-498.

Yacoub, N.K. (1983). Instantaneous amplitudes: a new method to measure seismic magnitude, *Bull. Seism. Soc. Am.*, **73**, 1345-1355.

Yang, X. (1997), Mining explosion and collapse source characterization and modeling with near-source seismic data, Ph.D. Thesis, Southern Methodist University, Dallas, Texas.

# CHAPTER 5. PRELIMINARY RESULTS OF APPLYING $M_s$(VMAX) TO LOVE WAVES FROM NTS EARTHQUAKES AND EXPLOSIONS

Jessie Bonner

*Weston Geophysical Corporation*

## OBJECTIVES

During a Seismic Review Panel held at Pinedale, Wyoming (July, 2005), several panel members suggested that the $M_s$:$m_b$ discriminant technique could be improved by including Love and Rayleigh waves in the analysis. This paper presents the preliminary results of applying the Russell (2005) surface wave magnitude formula and Bonner *et al.* (2005) measurement procedure, $M_s$(VMAX), to both Love and Rayleigh waves from explosions and earthquakes on or near the Nevada Test Site.

## INTRODUCTION

Russell (2005) developed a time-domain method for measuring Rayleigh waves with minimum digital processing, using zero-phase Butterworth filters. The method can effectively measure surface-wave magnitudes at both regional and teleseismic distances, at variable periods between 8 and 25 seconds. For applications over typical continental crusts, the magnitude equation is:

$$M_S = log(a_b) + \frac{1}{2} log(sin(\Delta)) + 0.0031\left(\frac{20}{T}\right)^{1.8}\Delta - 0.66\,log\left(\frac{20}{T}\right) - log(f_C) - 0.43 \quad (5.1)$$

where $a_b$ is the amplitude of the Butterworth-filtered surface waves (zero-to-peak in nanometers) and

$$f_C \le \frac{0.6}{T\sqrt{\Delta}} \quad (5.2)$$

is the filter frequency of a third-order Butterworth band-pass filter with corner frequencies $1/T$-$f_c$, $1/T$+$f_c$. At the reference period $T$=20 seconds, the equation is equivalent to Von Seggern's formula (1977) scaled to Vaněk *et al.* (1962) at 50 degrees. For periods $8 \le T \le 25$, the equation is corrected to $T$=20 seconds, accounting for source effects, attenuation, and dispersion.

*Is the Russell(2005) formula valid for Love waves?* The terms in Eq. 5.1 that might be different for Rayleigh and Love waves include the source excitation term (-0.66 log (20/T)), the empirical calibration constant (0.43), and *Gmin* (the 0.6 term) in Eq. 5.2. I will assume that the frequency-dependent attenuation for Love and Rayleigh-waves is equivalent for this initial

comparison. For the Love-wave dispersion at the periods of interest (8-25 seconds), I assume that the *Gmin* term of 0.6 is still applicable.

The source excitation term in Eq. 5.1 was determined by modeling Rayleigh waves generated by 1 km deep explosions in a variety of different velocity structures. Given that isotropic explosions do not generate Love waves, I can not use the same technique to determine the Love wave excitation correction. Thus, I used a 1 km deep double-couple earthquake and estimated the source excitation term for five different velocity structures as shown in Figure 5.1. The corrections are all relative to 20-seconds period. A better expression for the Love wave source excitation term might be -0.45 log (20/T). However, the difference between this new expression and the one used in the Russell (2005) equation is small (<0.1 m.u.), thus it does not make sense to change it for this preliminary study.

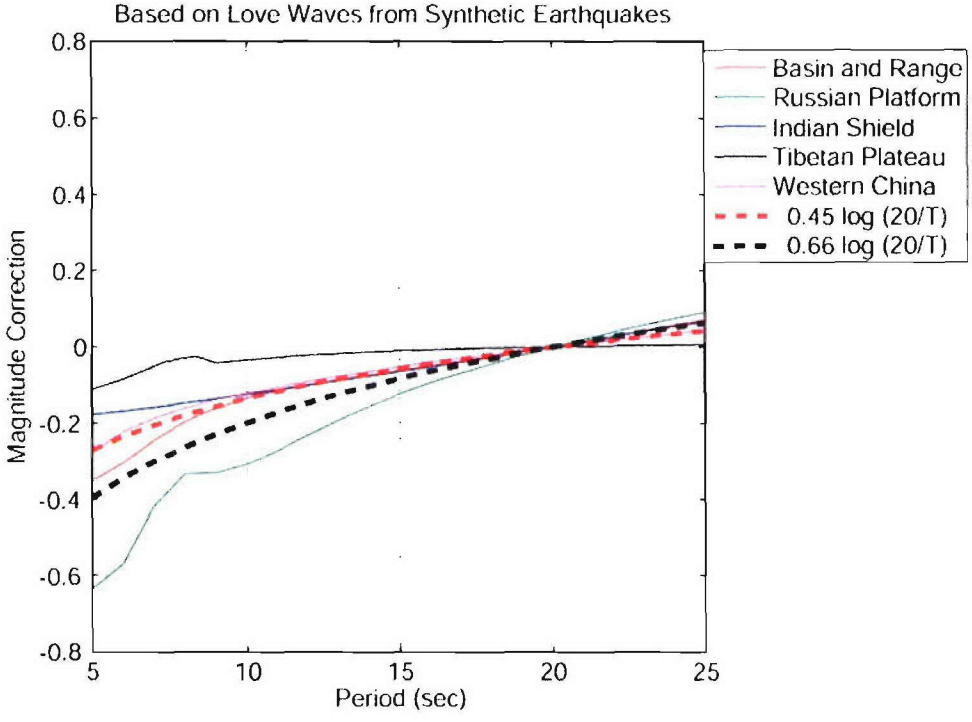


**Figure 5.1. A comparison of Love-wave excitation terms relative to 20-seconds period for a 1 km deep double couple earthquake in a variety of different structures. The red dashed line shows a representative source excitation expression for Love waves (-0.45 log (20/T)). The black dashed line shows the source excitation used in Eq. 5.1 based on a similar analysis for explosion-generated Rayleigh waves. Because the red and dashed lines show only a small separation, I chose to use the -0.66 log (20/T) correction for this preliminary study.**

## APPLICATION TO EARTHQUAKES

For this pilot study, I analyzed a set of 25 Western United States earthquakes from the database used in our previous chapters. These were earthquakes for which I had at least two Livermore Network stations with three component data. For each event, I used SAC to rotate the

horizontal components to the great circle path, thus isolating the transverse and radial components. I then filtered the transverse (Love; Figure 5.2) and vertical (Rayleigh; Figure 5.3) components using Eq. 5.2. The only difference between the processing shown in Figures 5.2 and 5.3 and what we did in Chapter 4 is that I changed the starting group velocity window (first blue line on each filter comb) from 4 to 4.5 km/sec to allow for the Love waves. The end of the group velocity window remains at 2.0 km/sec. The waveforms in the two Figures at corresponding periods show similarities except for the arrival time differences between the Love and Rayleigh waves.

I used Eq. 5.1 and the $M_s$(VMAX) technique to estimate a network $M_s$(VMAX) for Love (Figure 5.4) and Rayleigh (Figure 5.5) waves. Two things to note in Figures 5.4 and 5.5 include the increased $M_s$(VMAX) values for Love relative to Rayleigh and increased variance. Figure 5.6 shows that on average, the Love wave $M_s$(VMAX) estimates are 0.24 m.u. larger than estimates obtained from Rayleigh waves. Later in this report, I use this 0.24 m.u. value to calibrate $M_s$(VMAX) for the two phases. The variance for the magnitude analysis is on average 12% larger for Love waves.

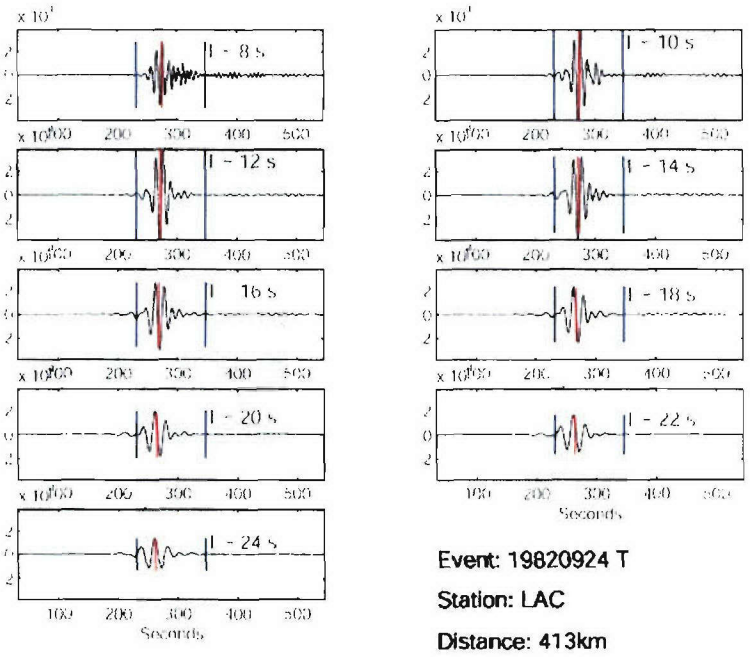


**Figure 5.2. Filter combs of Love waves at periods of 8,10,12,..,24 seconds for a western United States earthquake recorded at LAC. The first blue line is 4.5 km/sec while the second is 2.0 km/sec. The red line marks the largest amplitude. Amplitudes are in nm.**

## APPLICATION TO EXPLOSIONS

For this pilot study, I picked a set of 55 Nevada Test Site explosions from the database used in previous chapters. These were explosions that occurred between 1979 and 1983 for which I had at least two Livermore Network stations with three component data. The data had been previously rotated to isolate the transverse and radial components.

I filtered the transverse (Love; Figure 5.7) and vertical (Rayleigh; Figure 5.8) components using Eq. 5.2. I then used Eq. 5.1 and the $M_s$(VMAX) technique to estimate a network $M_s$(VMAX) for Love (Figure 5.9) and Rayleigh (Figure 5.10) waves. Two things to note in Figures 9 and 10 include the decreased $M_s$(VMAX) values for Love relative to Rayleigh and increased variance for Love waves. Figure 5.11 shows that on average, the Love wave $M_s$(VMAX) estimates are 0.40 m.u. smaller than estimates obtained from Rayleigh waves. This is obviously related to the fact that the Love waves are not generated by the explosion, but instead by secondary processes such as tectonic release which have moments smaller than the actual explosion. The variance for the magnitude analysis is on average 26% larger for Love waves.

Of the 55 explosions studied during this pilot study, only 39 had a $M_s$(VMAX) determined for the Love waves. For the other 16 events, the signal-to-noise ratio was too high to estimate a magnitude. This represents a problem as these results suggest it will be difficult to extend the Love-wave analysis to explosions with $m_b < 4.3$ (Figure 5.12).

Chapter 3 of Brad Wood's dissertation (1994; Advisor: David Harkrider) estimated isotropic and double couple moments for many of the Nevada Test Site explosions. He used estimates of these moments, obtained from long-period Rayleigh and Love waves, to estimate an F-factor (Toksöz *et al.* 1965) which is approximated for near-Poisson solids as:

$$F \sim \frac{3}{2}\frac{M_{DC}}{M_I} \quad , (5.3)$$

where $M_{DC}$ is the double couple moment and $M_I$ is the isotropic moment. I compared the ratio of the Love and Rayleigh $M_s$(VMAX) estimates to Woods' F-factors for 17 events that he and I both analyzed. The results are shown in Figure 5.13. While there is general agreement in the trend between the two datasets, there is a large amount of scatter in the data.

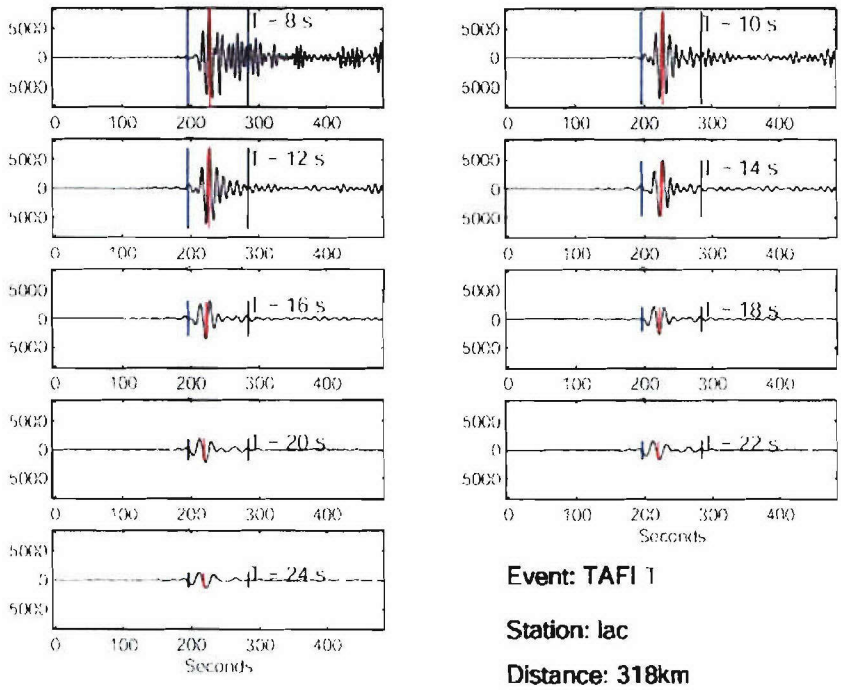


**Figure 5.7. Filter combs of Love waves at periods of 8,10,12,..,24 seconds for a Nevada Test Site explosion (TAFI) recorded at LAC. Amplitudes are in nm.**

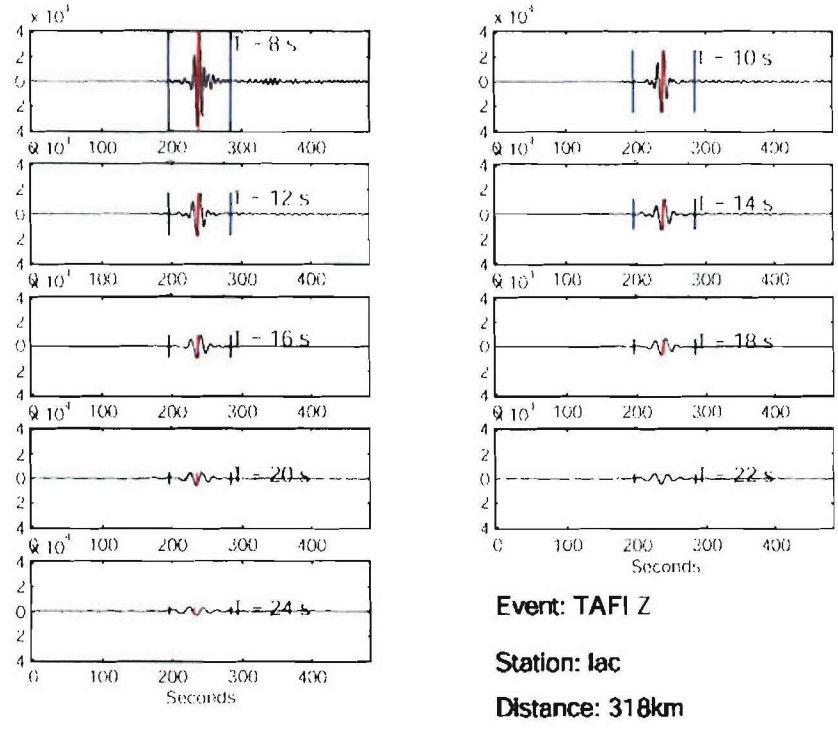


**Figure 5.8. Filter combs of Rayleigh waves at periods of 8,10,12,..,24 seconds for a Nevada Test Site explosion (TAFI) recorded at LAC. Amplitudes are in nm.**

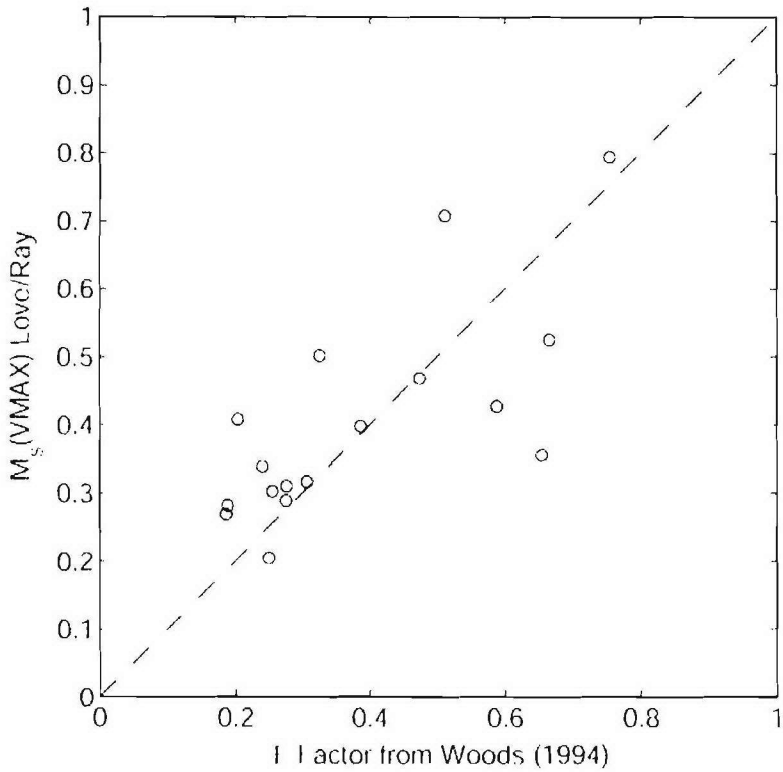


**Figure 5.13. A comparison of F factors from Woods (1994) with the ratio of the Love- and Rayleigh-wave estimated $M_s$(VMAX). The dashed line represents a 1:1 relationship.**

## DISCRIMINATION

I applied the 0.24 m.u. calibration constant to all of the Love-wave magnitude estimates, both earthquakes and explosions, and then plotted them as a function of $m_b(Pn)$ in Figure 5.14. For comparison, I plotted the Rayleigh-wave magnitudes also as a function of $m_b(Pn)$. The results show that the separation between the earthquake and explosion populations based on Love waves magnitudes is approximately 1.3 m.u. For the Rayleigh-wave estimates, the average separation is 0.8 m.u. The increase separation is a nice feature of this technique and may help further discriminate nuclear explosions from earthquakes; however, the combined Love/Rayleigh discriminant may not be available in the $3 < m_b < 4$ range.

Using the corrected Love wave magnitudes, I then combined the Rayleigh and Love wave values to form a single magnitude. I defined $M_s$(VMAX (L+R)) as:

$$M_s(\text{VMAX (L+R)}) = \sqrt{(Ms_{CorrectedLove})^2 + (Ms_{Ray})^2} \quad . \quad (5.4)$$

The combined magnitude is shown in Figure 5.15 and highlights how the inclusion of the Love waves helps increase the separation between the two populations. More work will be

needed before I can determine how general such an equation might be and its possible usefulness to improve single-station magnitude estimation.

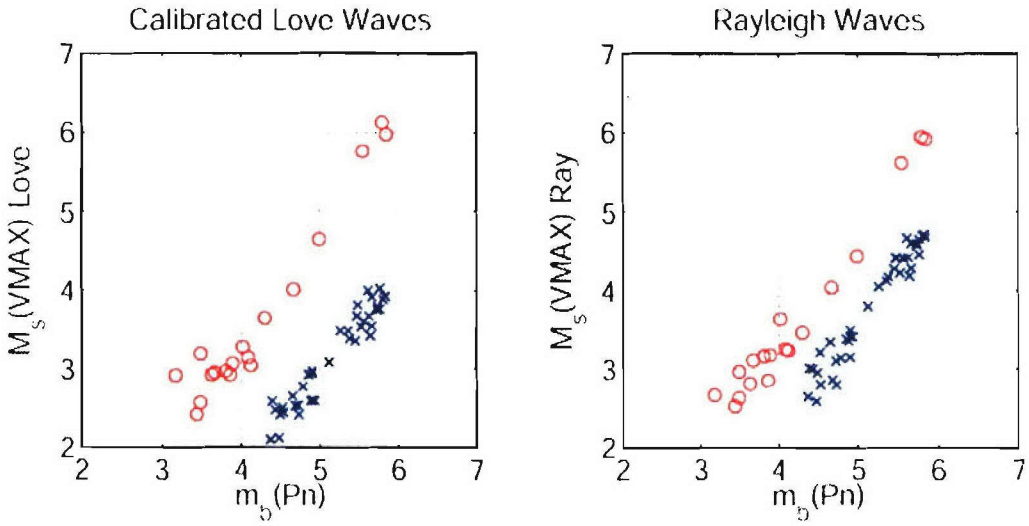


**Figure 5.14. Discrimination results for Love (left) and Rayleigh (right) waves. The Love-wave results were calibrated to the Rayleigh-waves from earthquakes by subtracting 0.24 m.u. from the magnitude values.**

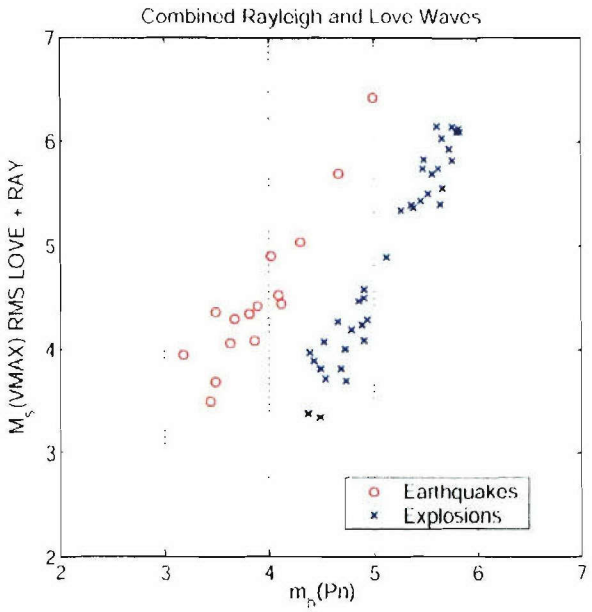


**Figure 5.15. Discrimination results for explosions and earthquakes using a combined Rayleigh and Love-wave magnitude relation (Eq. 5.4).**

## SYNTHETICS

Previously, I observed that Love wave $M_s$(VMAX) for NTS explosions was typically 0.4 m.u. smaller than Rayleigh $M_s$(VMAX). This observation led me to wonder how often earthquakes would have the same relationships between the two magnitudes.

So, I generated synthetics for earthquakes with strike-slip, normal, and oblique-slip mechanisms. The synthetics were generated at azimuths ranging from 0:10:170 degrees and at depths of 1,10, 30, and 50 km. I then estimated $M_s$(VMAX) for the Love and Rayleigh waves.

The results are shown in Figure 5.16. In each of the subplots, I present the x-axis as the Love wave $M_s$(VMAX) and the y-axis is the Rayleigh-wave $M_s$(VMAX). The data points are classified by color as different depths. Different data points at each depth represent a different source-to-station back azimuth. The shaded region represents events that have Love-wave $M_s$(VMAX) at least 0.4 m.u. less than Rayleigh-wave $M_s$(VMAX).

These results suggest that the majority of earthquakes fall outside that shaded region. The only instances where events fall into the shaded region is when we are approaching a null in the Love wave radiation pattern. These results are for a single station. For practical applications, if we can find at least two stations with both Love and Rayleigh waves for $M_s$(VMAX) estimation, it might be possible discriminate earthquakes and explosions w/o worrying about $m_b$ relationships. That hypothesis assumes that other test sites have similar or smaller tectonic release as NTS.

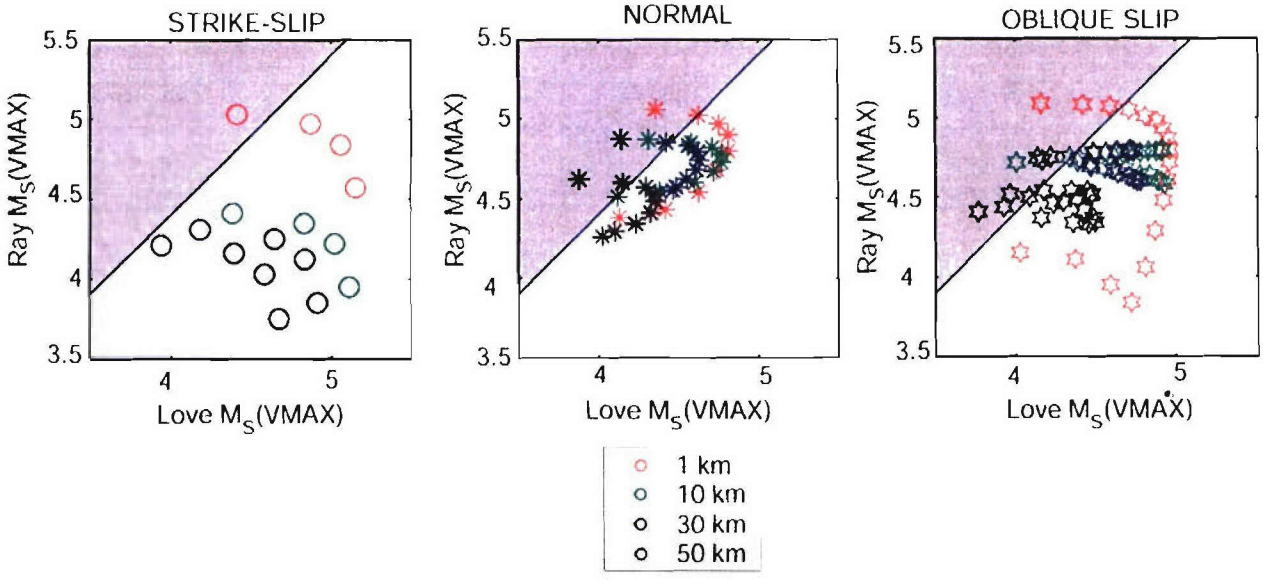


**Figure 5.16. A comparison of Rayleigh and Love $M_s$(VMAX) estimates for different focal mechanisms at different back azimuths and depths.**

## CONCLUSIONS AND FUTURE RECOMMENDATIONS

This pilot study applied the Russell (2005) surface wave magnitude formula and $M_s$(VMAX) analysis to Love and Rayleigh waves from explosions and earthquakes on or near the Nevada Test Site. The results suggest that:

a. The Love wave $M_s$(VMAX) estimates for earthquakes are larger than Rayleigh-wave estimates (0.24 m.u.),
b. The Love wave $M_s$(VMAX) estimates for explosions are smaller than Rayleigh-wave estimates (0.40 m.u.),
c. The variances for the Love wave estimates for both earthquakes and explosions are larger than for Rayleigh waves,
d. Application of the $M_s$(VMAX) technique to Love waves from explosions may be limited to $m_b > 4.3$, and
e. $M_s$:$m_b$ earthquake and explosion population separation is larger for Love waves due to the phenomenology differences of surface wave generation from explosions.

Certainly, combining the Love and Rayleigh-wave magnitudes could be used to increase confidence in the final decision on special events. While its application seems to be limited for explosions with $m_b < 4.3$, additional studies (both observational and synthetic) are needed to determine if earthquakes can generate a situation where the Love and Rayleigh $M_s$ estimates are drastically different—other than single stations sitting on a radiation null. Also, the earthquakes used in this study all occurred in the western United States and were shallow. Additional studies should determine the effects of depth on the independent Love and Rayleigh-wave magnitudes.

## REFERENCES


Bonner, J. L., D. Russell, D. Harkrider, D. Reiter, and R. Herrmann, (in review). Development of a Time-Domain, Variable-Period Surface Wave Magnitude Measurement Procedure for Application at Regional and Teleseismic Distances, Part II: Application and $M_s$—$m_b$ Performance, submitted revisions to *Bull. Seism. Soc. Am.*

Russell, D.R. (2005). Development of a time-domain, variable-period surface wave magnitude measurement procedure for application at regional and teleseismic distances. Part I—Theory. Submitted to *the Bull. Seism. Soc. Am.*

von Seggern, D. (1977). Amplitude distance relation for 20-Second Rayleigh waves, *Bull. Seism. Soc. Am.*, **67**, 405-411.

Toksöz, M.N., D. G. Harkrider, and A. Ben-Menahem (1965). Determination of source parameters by amplitude equalization of seismic surface waves, *J. Geophys. Res.*, 907-922.

Woods, B. (1994). Regional surface wave magnitude and moment determination methods applied to nuclear explosions at the Nevada Test Site: implications for yield estimation and seismic discrimination. Cal. Tech Ph.D. Dissertation.